International Journal of Photoenergy

Radiation Effects in Solar Cells and Optoelectronic Devices

Guest Editors: Aleksandra Vasic, Predrag Osmokrovic, Nenad Marjanovic, and Momčilo Pejović

Radiation Effects in Solar Cells and Optoelectronic Devices

International Journal of Photoenergy

Radiation Effects in Solar Cells and Optoelectronic Devices

Guest Editors: Aleksandra Vasic, Predrag Osmokrovic, Nenad Marjanovic, and Momčilo Pejović

Editorial Board

Contents

Hindawi Publishing Corporation
International Journal of Photoenergy
Volume 2013, Article ID 171753, 3 pages
http://dx.doi.org/10.1155/2013/171753

Editorial
Radiation Effects in Solar Cells and Optoelectronic Devices

Aleksandra Vasic,[1] Predrag Osmokrovic,[2] Nenad Marjanovic,[3] and Momčilo Pejović[4]

[1] *Faculty of Mechanical Engineering, University of Belgrade, Kraljice Marije 16, 11000 Belgrade, Serbia*
[2] *Faculty of Electrical Engineering, University of Belgrade, Bulevar kralja Aleksandra 73, 11000 Belgrade, Serbia*
[3] *CSEM Centre Suisse d'Electronique et de Microtechnique SAEntwicklungszentrum für Polytronics, Tramstrasse 99, 4132 Muttenz, Switzerland*
[4] *Faculty of Electronic Engineering, University of Niš, Aleksandra Medvedeva 14, 18000 Niš, Serbia*

Correspondence should be addressed to Aleksandra Vasic; avasic@mas.bg.ac.rs

Received 25 August 2013; Accepted 25 August 2013

Beside the diversity of the device technologies used for designing the solar cells and various optoelectronic devices, there are a variety of radiation environments in which they are used (natural space and atmospheric, as well as military and civil nuclear environments, etc.). Reliability of electrical devices in a radiation environment is very important, and extensive studies concerning the development of semiconductor devices that can operate normally in such conditions have been seriously undertaken. Possible degradation of the electrical performance of optoelectronic devices in general, induced by irradiation, means that very strict conditions for their application must be predetermined for the worst case scenario. Performance failure in such conditions could have negative impact on both the financial and environmental aspects of the device application.

The lifetime of the semiconducting device is restricted by the degree of radiation damage that the device receives. This is an important factor that affects the performance of various devices in practical applications. The permanent damage in the materials is caused by collisions of the incident radiation particles with the atoms in the crystalline lattice, which are displaced from their positions. These defects degrade the transport properties of the material and particularly the minority carrier lifetime. This lifetime decrease produces degradation of the parameters of the device ultimately leading to an increase of the noise level. The interaction between vacancies, self-interstitials, impurities, and dopants in the basic material leads to the formation of undesirable point defects such as recombination and compensator centers which affect performance of the solar cells and other optoelectronic devices, especially in space. Introduction of radiation-induced recombination centers reduces the minority carrier lifetime in the base layer of the p-n junction increasing series resistance. After very high doses of radiation series resistance of the base layer could be so high that most of the power generated by the device such as solar cell is dissipated by its own internal resistance.

On the other hand, γ radiation damage is induced by the ionization and excitation of the atoms within the junction space charge region of a junction device such as solar cell. The presence of impurity atoms that are either added to the base material as donors, or during the manufacturing process, has indicated the possibility that some of the produced electrons might be trapped by those atoms between the valence and conduction band. As a consequence, the output of the optoelectronic device exposed to γ radiation is also reduced. Therefore, from the technological point of view, it is important to study the variations induced by irradiation of semiconductor junction characteristic parameters (ideality factor, saturation current, etc.) that affect the performance of the solar cells, photodiodes, phototransistors, and other photonic devices.

This special issue reveals recent developments in the vastly undertaken investigations concerning radiation effects in various optoelectronic devices (solar cells, photodiodes, phototransistors, insulating layers, memories, dosimeters, etc.). Each paper was reviewed by at least two reviewers

(mostly three) and presents the most recent breakthroughs in this interesting field.

Many fundamental and practical problems were discussed in the received and accepted papers, ranging from solar cells, photodiodes, phototransistors, insulating films, memories, and so forth. Various experimental techniques, numerical analysis, and theoretical discussions were presented in order to reveal current problems, and to offer adequate solutions. Behavior of the solar cells, photodiodes, and photodetectors exposed to gamma and neutron irradiation was discussed in D. Nikolic et al.'s and B. Simic et al.'s papers, respectively. After thorough investigations, the authors concluded that although neutron irradiation in all samples caused degradation of their structure and deterioration of the output characteristics, solar panels have proved to be most resistant to the effects of neutrons. Also, results obtained from gamma irradiation showed the degradation of the I-V characteristics, but following annealing process improved these characteristics. Due to their amplifying action, the phototransistors are the most sensitive to radiation effects. On the other hand, the solar panels are the least sensitive to gamma radiation.

Another vast group of electrical devices such as resistors were considered in the I. Kostic et al.'s paper. The temperature dependence has been treated without taking the thermal source into consideration, which means that, in the cosmic radiation conditions, this dependence could be reached by the collision energy transfer between particle from cosmic radiation and the observed component. A novel approach was proposed for thermal testing of the resistors. It was found that thermography can be used as noncontact method because it gives temperature distribution in more than a couple points and because in the short time a set of measurements can be done.

Radiation effects in insulating films were also investigated. In L. Timotijevic et al.'s paper Monte Carlo simulation of proton beam effects on five insulating materials, commonly encountered in modern day electronic components: silicon dioxide, silicon nitride, aluminum nitride, alumina, and polycarbonate were discussed. It was found that nonionizing energy loss of high-energy protons is low, and they traverse the films without much atomic displacement. However, for the lower part of the investigated proton energy range (from 10 keV to 1 MeV), substantial ionization losses and NIEL are to be expected. Ionization and displacement damage produced by protons could influence the properties of these insulators and compromise their reliability within complex structures and devices.

A newly discovered class of materials, Cooper-pair insulators, based on InO_x films, with distinct structural properties and unique physical mechanism of electrical current conduction were investigated in S. Milosavljevic et al.'s paper. The study suggests that radiation-induced changes in InO_x films exposed to ion beams could significantly alter their current-voltage characteristics, and that a transition to a metallic state is possible, due to radiation-induced perturbation of the fine-tuned granular structure. Furthermore, incident and displaced ions can break up enough Cooper pairs in InO_x films to cause dissolution of this specific insulating state. Since Cooper-pair insulators are recently used in resistive random-access memories, investigation of effects of radiation environment on different memory devices is of considerable relevance. In I. Fetahovic et al.'s paper, different types of commercially available memory chips were exposed to indirect ionizing radiation by changing radiation dose intensity. The effect of direct ionizing radiation on semiconductor memory behavior has been analyzed by using Monte Carlo simulation method. Obtained results showed that gamma radiation causes decrease in threshold voltage, being proportional to the absorbed dose of radiation. Monte Carlo simulations of radiation interaction with material proved to be significant and can be a good estimation tool in probing semiconductor memory behavior in radiation environment.

Another type of commonly used memories, such as flash memories exposed to radiation, was investigated in B. Cavric et al.'s paper. This topic is up-to-date since the high degree of components miniaturization integrated into the flash memory causes the extreme sensitivity of this memory type on the ionizing radiation effects. The effects of ionizing radiation may cause changes in stored data, or even the physical destruction of the components. The obtained results indicate that the sensitivity to gamma rays depends primarily on the thickness of the dielectric layers of cells, which is about the same for all tested memories, since they belong to the same generation of technology. Partial recovery of errors caused by radiation, in a few weeks at room temperature, was observed in all the four types of memory.

One group of semiconducting devices that are by their function always exposed to radiation, dosimeters, were the topic of M. Pejovic et al.'s paper. Specifically, radiation-sensitive p-channel MOSFETs (also known as RADFETs) have recently been developed for applications in space, nuclear industry research, and radiotherapy, so sensitivity of p-channel MOSFET to X and gamma irradiation is of great interest. Results have shown that the response is greater when RADFETs are irradiated with X-rays. It was concluded that this is a consequence of the dominant influence of photoelectric effect in X-ray cases in comparison to Compton's effect in gamma-ray cases. Another significant conclusion was that a satisfactory response of these RADFETs could be achieved for lower doses especially in X-ray cases, which would enable their efficient application for measuring low doses order of several mGy used in diagnostic and interventional radiology.

All of the presented papers give a substantial insight into the state of the art concerning this important interdisciplinary field. Since very comprehensive comparative analysis of measurement results has been performed in order to determine the reliability of optoelectronic devices in radiation environment, the editorial team expects that these papers would inspire further investigations and possible breakthroughs in this important area.

Acknowledgments

We would like to thank all contributing authors, reviewers, and Editorial Board of the International Journal of Photoenergy for their support and efforts to make this special

issue possible. Also, the support of Safi Hosni, Editorial Office, Hindawi Publishing Corporation, was invaluable for preparing this issue, for which we are thankful.

Aleksandra Vasic
Predrag Osmokrovic
Nenad Marjanovic
Momčilo Pejović

Hindawi Publishing Corporation
International Journal of Photoenergy
Volume 2013, Article ID 236823, 8 pages
http://dx.doi.org/10.1155/2013/236823

Research Article

Effects of Ion Beam Irradiation on Nanoscale InO_x Cooper-Pair Insulators

Srdjan Milosavljević,[1] Djordje Lazarević,[2] Koviljka Stanković,[3] Milić Pejović,[4] and Miloš Vujisić[3]

[1] *Institute of Electrical Engineering "Nikola Tesla", 11000 Belgrade, Serbia*
[2] *Institute of Nuclear Sciencies "Vinca", 11000 Belgrade, Serbia*
[3] *Faculty of Electrical Engineering, University of Belgrade, 11000 Belgrade, Serbia*
[4] *Faculty of Electronic Engineering, University of Niš, 18000 Niš, Serbia*

Correspondence should be addressed to Miloš Vujisić; vujsa@ikomline.net

Received 7 April 2013; Accepted 25 May 2013

Academic Editor: Momčilo Pejović

This paper examines the effects of irradiating indium oxide films of nanoscale thickness by ion beams, when these films are in the Cooper-pair insulator state. Radiation effects are predicted on the basis of Monte Carlo simulations of ion transport. Results of numerical experiments are interpreted within the theoretical model of a Cooper-pair insulator. The study suggests that radiation-induced changes in InO_x films exposed to ion beams could significantly alter their current-voltage characteristics and that a transition to a metallic state is possible, due to radiation-induced perturbation of the fine-tuned granular structure. Furthermore, incident and displaced ions can break up enough Cooper pairs in InO_x films to cause dissolution of this specific insulating state.

1. Introduction

Cooper-pair insulators (CPIs) are a newly discovered class of materials, with distinct structural properties and a unique physical mechanism of electrical current conduction. The Cooper-pair insulating phase appears only at very low temperatures, in materials that are otherwise superconducting. The superconductor-insulator transition (SIT) has been studied extensively in the recent years, and a fairly accurate understanding of this process has been acquired [1–6].

During the past decade, a lot of efforts have also been invested in designing resistive random-access memories (RRAMs). The cells of these new memories are expected to have a high on-to-off current ratio, dependent on a large change of ohmic resistance, such as the one that occurs during an SIT. CPIs are, therefore, one of the promising materials for future resistive memories.

Like many other memories, CPI-based RRAMs would also be used in various radiation environments, for example, in radiology and nuclear medicine departments, at nuclear facilities, or aboard space satellites [7, 8]. Consequently, the issue of radiation effects in materials which behave as Cooper-pair insulators is of considerable relevance.

This paper investigates the effects of ion beam irradiation on the properties of nanoscale indium oxide films in the Cooper-pair insulator state, by using numerical simulation of ion transport.

2. Theoretical Foundations

The Cooper-pair insulators are materials that exhibit superconducting behavior, but under specific conditions (regarding film thickness, bias voltage, applied magnetic field, and presence of magnetic impurities) they become insulators with thermally activated Cooper pairs as charge carriers [1–4]. Such behavior has been observed in films of indium oxide with nanoscale thickness [5, 6, 9, 10]. The insulating phase has a granular structure of superconducting islands (regions of localized Cooper pairs) distributed throughout a matrix of normal nonsuperconducting material [11–13]. When the conditions are right, the grouping of Cooper

pairs into superconducting islands occurs spontaneously in the material, due to increased disorder. This process is akin to the Anderson localization, which is an absence of diffusion of waves (including quantum waves assigned to particles) in a disordered medium, provided that the degree of randomness of impurities or defects is sufficiently large. One such effect of disorder on electronic systems is the localization of electrons, which transforms an otherwise metallic system into an insulator [1]. The phenomenon of superconducting materials turning into insulators is therefore often regarded as a disorder-driven superconductor-insulator transition [13–17].

A two-dimensional Josephson junction array (2D JJA) is used to model the granular structure of a CPI [2, 18]. A 2D JJA consists of small superconducting islands, each coupled to the nearest neighboring islands by the Josephson weak links. A weak link that forms over the section of non-superconducting material between superconducting islands constitutes a Josephson junction. Each junction is characterized by the following Josephson coupling energy:

$$E_J = \frac{\hbar I_c}{2e}, \tag{1}$$

where I_c is the critical current of the junction, e is the elementary charge, and $\hbar = h/2\pi$ is the reduced Planck constant. Two more energies that characterize each junction are the charging energies E_c and E_{c0}, related to inter-island capacitance and capacitance to the ground (substrate), respectively. The inter-island charging energy E_c is the energy needed for a Cooper pair to be transferred between neighboring islands.

Investigations of the conditions under which indium oxide acts as either a superconductor or an insulator at temperatures below 1 K have shown that, in terms of the JJA model, the Cooper-pair insulating phase emerges only when the degree of disorder makes the charging energies larger than the coupling energy ($E_c, E_{c0} > E_J$), while the superconducting gap still exceeds the interisland charging energy ($\Delta > E_c$) [6, 9].

Cooper pairs spatially confined to a single superconducting island in a JJA exhibit *local* coherence of the wave function phase. When an external voltage is applied to the ends of a JJA, wave function phase synchronization of all Cooper pairs in the JJA occurs. This *global* phase coherence gives rise to a collective current state. The DC Josephson current that runs through the JJA couples the phases of adjacent junctions, so as to provide minimal power dissipation in the array. This establishes a global phase-synchronized state, and the transport of current occurs through simultaneous thermal activation of Cooper pairs throughout the whole array [2, 3]. Due to this activation conduction, resistance of a Cooper-pair insulator follows an Arrhenius-like temperature dependence. This also means that the low-bias ($V \ll \Delta_c/e$) current-voltage dependence in the temperature interval $E_c < k_B T < \Delta_c$ is exponential:

$$I = I_c \exp\left(-\frac{(\Delta_c - eV)^2}{2\Delta_c k_B T}\right), \tag{2}$$

where I_c is the critical current of a Josephson junction in the 2D array, k_B is the Boltzmann constant, T is the absolute temperature, and Δ_c is the collective Coulomb barrier of the array. For the 2D JJA, this barrier is given as follows:

$$\Delta_c = E_c \ln \frac{L}{d}, \tag{3}$$

where L is the characteristic linear size of the array (e.g., film thickness) and d is the size of an elemental cell in it [2].

3. Monte Carlo Simulations of Ion Beam Transport

Monte Carlo simulations of ion transport through InO_x films of varying thickness (5 to 15 nm) were performed in the TRIM module of the SRIM software package [19]. Oxygen content was varied from $x = 0.95$ to $x = 1.05$ to reflect the amorphous structure of indium oxide films used in previous experimental studies [5, 6, 9, 10].

Simulations were conducted with ions chosen to represent certain well-known radiation fields, such as those encountered in the space environment (hydrogen, helium, and lead) [20, 21] or beams commonly used in ion implantation processes (phosphorus, boron, and arsenic). Simulations were restricted to monoenergetic unidirectional beams, incident perpendicularly on the film's surface. Beam energy was varied across typical energy ranges of the considered ion species.

SRIM has been proved to provide results in significant agreement with experiments [19]. Its continuous upgrades during the past decade have made it a foremost tool for numerical analysis of interaction of ions with matter and validation of theoretical predictions [22–24]. Transport of ions in matter (TRIM) not only calculates the range of ions in matter, but it also details many other aspects of the damage done to the target during the ion beam slowing-down process, such as cascades of displaced target atoms. It makes calculations for one ion at a time, in order to make precise evaluations of the physics of each encounter between the ion and a target atom. The accuracy of a simulation run is determined by the number of ions, that is, histories followed. A calculation for 1000 incident ions will give better than 10% accuracy [19].

The fact that TRIM calculations assume target temperature to be absolute zero makes it an appropriate tool for modeling radiation effects in the Cooper-pair insulating state, which exists only at very low temperatures anyway, so that thermal diffusion and annealing of displaced atoms in the film can be neglected. Another approximation inherent in TRIM is that there is no buildup of radiation damage in the target; that is, for each new incident ion, the film is assumed to contain no damage produced by the previous ions. Any assessment of the degree of radiation damage in the film is therefore an underestimation of the damage that a real ion beam would have caused.

Ionization energy losses calculated by TRIM were taken as an estimate of the extent of the Cooper-pair dissociation in superconducting islands within the granular structure of InO_x films. Assessment of pair dissociation can be performed by comparing ionization potentials of indium and oxygen

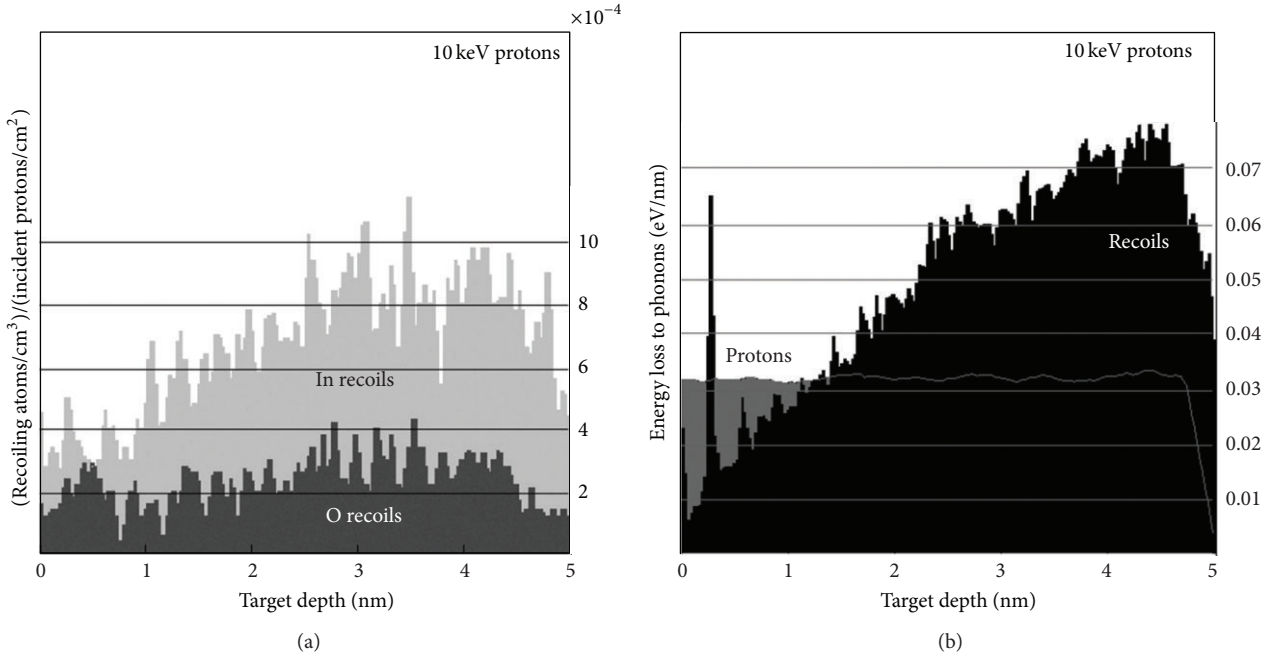

FIGURE 1: Results of irradiating a 5 nm thick InO_x film by a beam of 10^5 protons with 10 keV energy. (a) Distribution of the concentration of the displaced indium and oxygen atoms (recoils) per unit proton fluence. (b) Energy loss to phononic excitations per unit depth by protons and recoils.

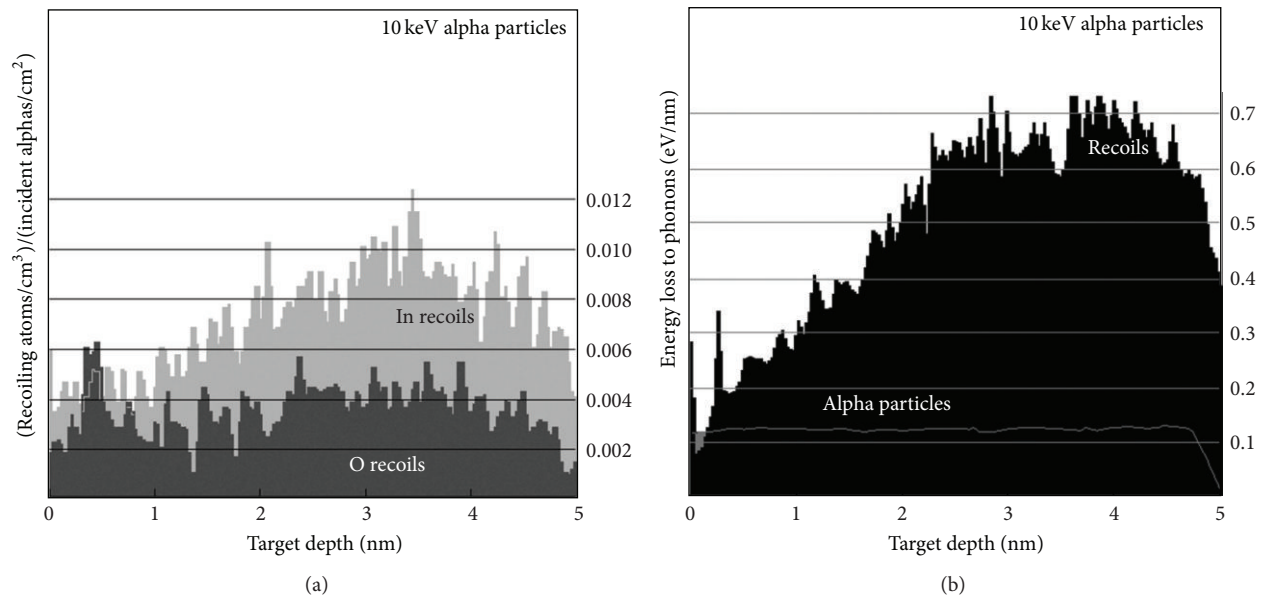

FIGURE 2: Results of irradiating a 5 nm thick InO_x film by a beam of 10^4 alpha particles with 10 keV energy. (a) Distribution of the concentration of the displaced indium and oxygen atoms (recoils) per unit alpha particle fluence. (b) Energy loss to phononic excitations per unit depth by alphas and recoils.

atoms with the depairing energy (i.e., the energy for breaking up a Cooper pair) in indium oxide. First ionization energies of indium and oxygen are 5.786 eV and 13.618 eV, respectively. The energy for breaking up a Cooper pair at absolute zero can be assessed as $2\Delta \sim 3.5k_BT_C$, which for InO, with the critical temperature of $T_C \approx 3.3$ K, yields the value of ≈0.001 eV.

4. Results and Discussion

Plots in Figures 1, 2, 3, 4, and 5 demonstrate some of the most relevant results obtained from simulations. These plots show the distributions of ionizing events (commensurate to the Cooper-pair dissociations) and nonionizing events

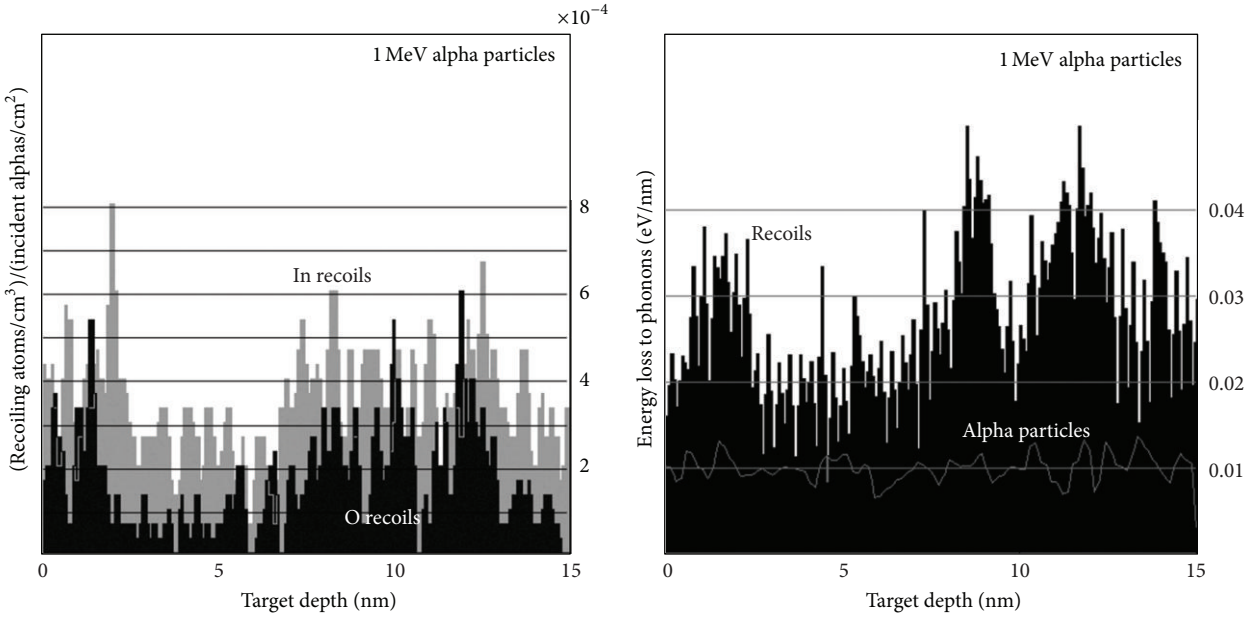

FIGURE 3: Results of irradiating a 15 nm thick InO_x film by a beam of 10^4 alpha particles with 1 MeV energy. (a) Distribution of the concentration of the displaced indium and oxygen atoms (recoils) per unit alpha particle fluence. (b) Energy loss to phononic excitations per unit depth by alphas and recoils.

(phononic excitations and atomic displacements) within InO_x films.

Distributions of displaced indium and oxygen atoms in a 5 nm thick InO_x film irradiated by a beam of 10^5 protons with 10 keV energy are shown in Figure 1(a). Energy losses to phononic excitations for the same irradiation conditions are shown in Figure 1(b).

For comparison with proton results, Figure 2 presents atomic displacements and energy losses to phonons in a 5 nm thick InO_x film irradiated by a beam of 10 keV alpha particles (10^4 histories). Figure 3, on the other hand, shows the results for high-energy alphas (1 MeV) in a 15 nm thick InO_x film.

Results for 0.1 MeV iron ions, one of the few heavy-ion species with considerable fluences in the primary cosmic rays that reach the Earth's atmosphere, are presented in Figure 4 for three different thicknesses of the InO_x film: 5 nm, 10 nm, and 15 nm.

Finally, plots in Figure 5 offer a comparison of the effects caused by different ion species (phosphorus, boron, and arsenic) with the same beam energy (0.1 MeV) in a 15 nm thick InO_x film.

Since the investigated InO_x films are less than 15 nm in thickness, they are immune to the passage of high-energy ions. Both ionizing and nonionizing energy losses of high-energy ions are low, and they traverse the thin InO_x films without deflection or notable ionization, producing only slight effects [25–30].

The selected results presented in Figures 1–5 suggest, however, that for certain ion species there exist energy ranges in which a great number of atom displacements, phonon excitations, and ionization events would occur in irradiated InO_x films.

The number of atomic displacements is in direct proportion to the fluence of incident radiation, that is, the number of particle histories followed in the Monte Carlo simulation. Space charge created by the displaced ions that finally take interstitial positions could affect the size of the Josephson junction-charging energy E_c, which then changes the collective Coulomb barrier Δ_c. The change in the I-V curve of an indium oxide film, resulting from the radiation-induced change of E_c, is illustrated in Figure 6. The curves in this figure were obtained from expressions (2) and (3) for three different values of E_c, with $L = 15$ nm, $d = 1$ nm, $I_c = 10\,\mu$A, and $T = 0.3$ K.

The Cooper-pair insulating state depends critically on the value of E_c, existing only when $E_c > E_J$. If the radiation damage produced by ion beams is large enough to disrupt this condition, InO thin film may revert to the ordinary metallic state.

Ionization energy losses by incident ions and recoils, observed in simulations, indicate that appreciable breaking of Cooper pairs in superconducting islands is possible. Decrease of Cooper-pair concentration could destroy the insulating state during irradiation. With other conditions unchanged, this effect is expected to be transient. Once the InO_x film is no longer exposed to ions, Cooper pairs may reform, and the insulating state could be restored.

Results of the simulations also indicate that one part of ion beam energy is converted to phononic excitations. Energy losses to phonons increase the effective temperature

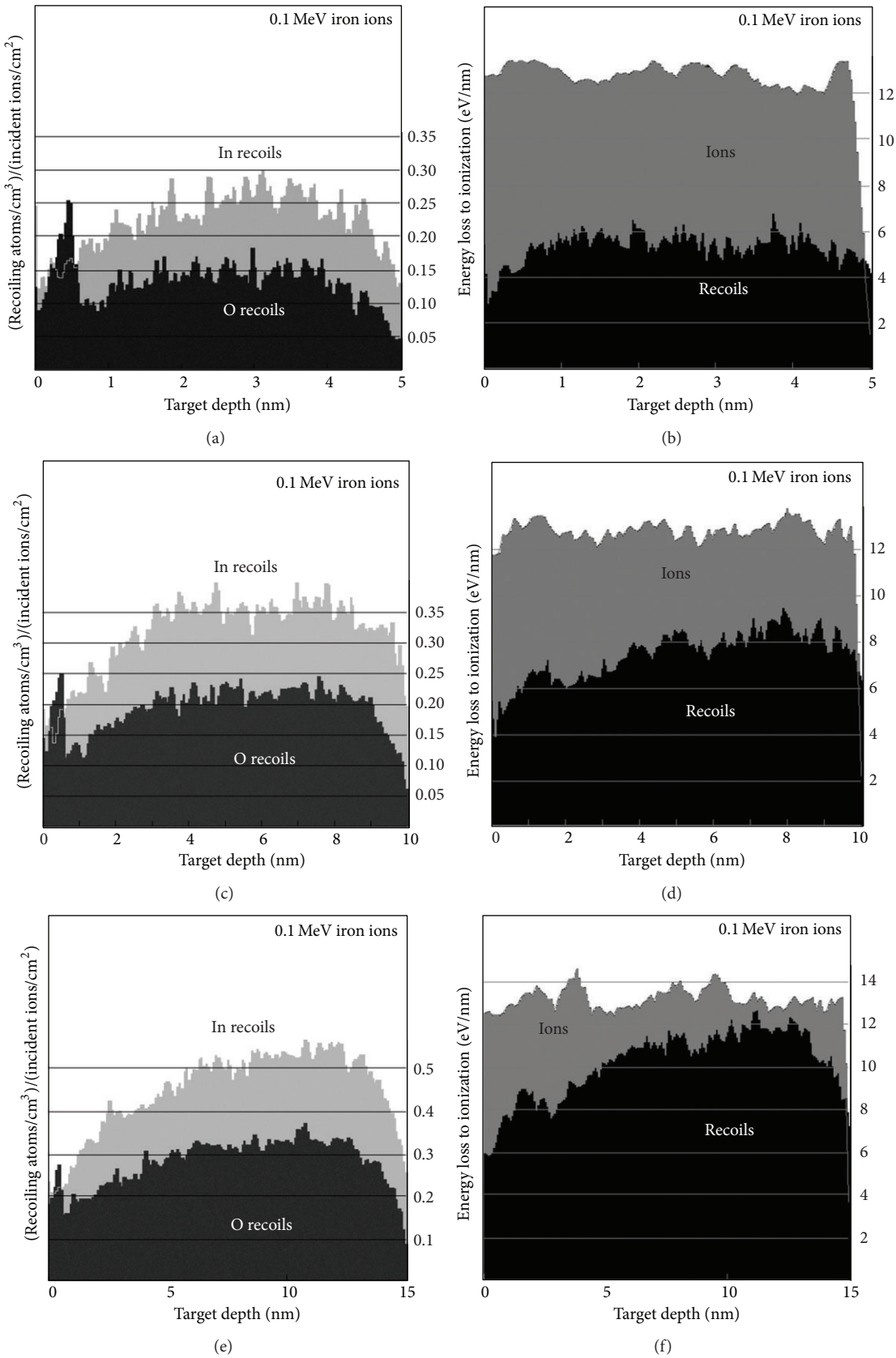

Figure 4: Results for 10^3 iron ions with 0.1 MeV energy. Distribution of the concentration of the recoils per unit ion fluence and ionization energy losses per unit depth for various thicknesses of the InO_x film: 5 nm (a and b), 10 nm (c and d), and 15 nm (e and f).

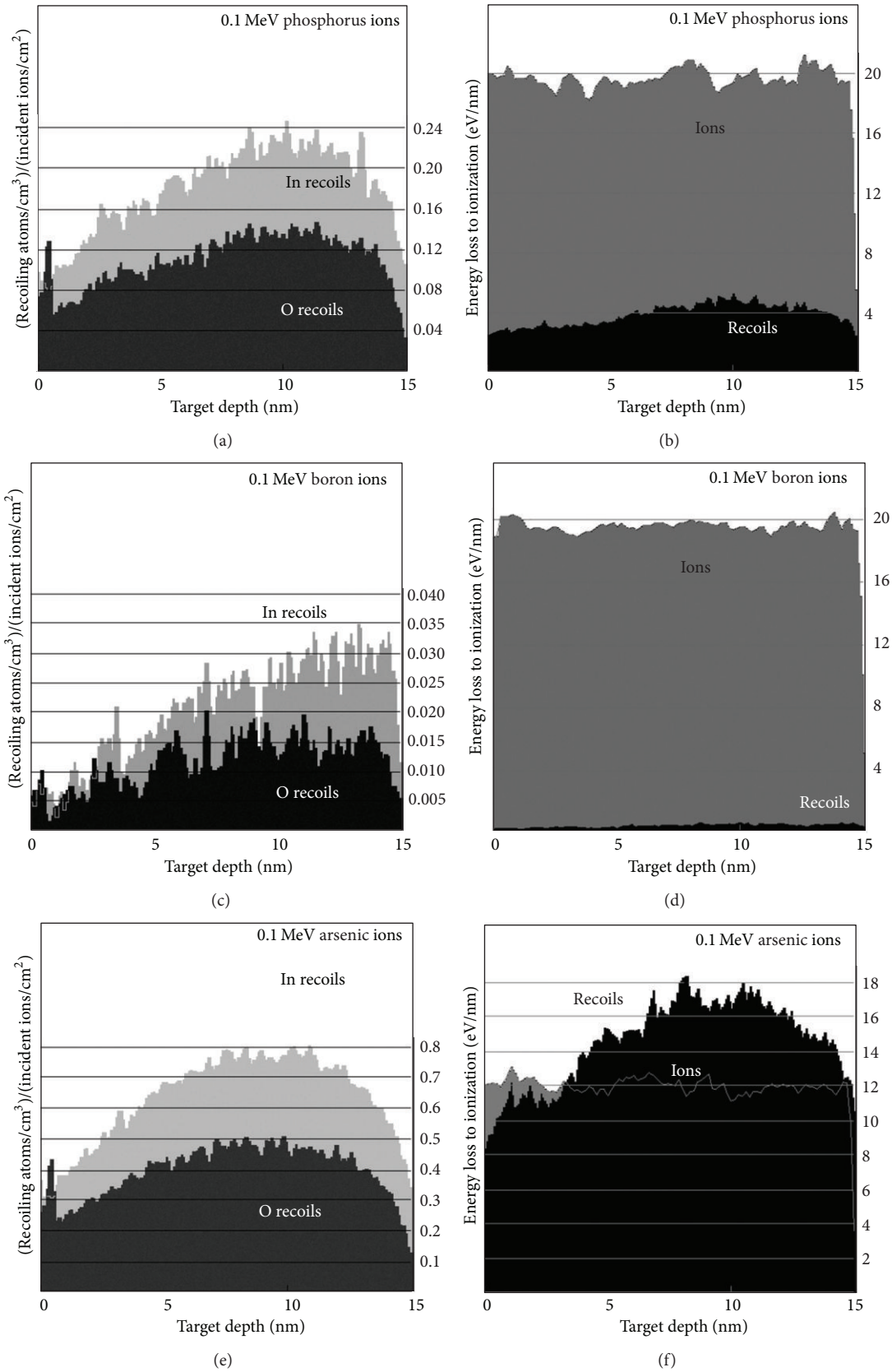

FIGURE 5: Distribution of the concentration of the recoils per unit ion fluence and ionization energy losses per unit depth in a 15 nm thick InO_x film for a 0.1 MeV incident beam of 10^3 phosphorus ions (a and b), boron ions (c and d), and arsenic ions (e and f).

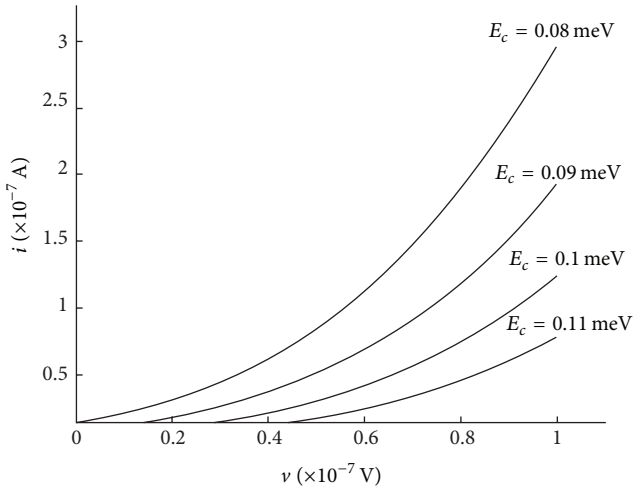

FIGURE 6: InO_x film I-V curves for three values of the Josephson junction-charging energy E_c. The change in E_c is brought about by the space charge of the displaced In and O ions (recoils) which become interstitials in the irradiated film.

of the InO_x film. Eventually, film temperature could become large enough for the Cooper-pair insulating phase to collapse ($T > \Delta_c/k_B$), or even for the superconducting state to become unsustainable ($T > \Delta/k_B$).

5. Conclusion

Although the investigated nanoscale indium oxide CPI films are immune to the passage of high-energy ions, simulations of ion transport reveal that significant ionization, phononic excitation, and production of displaced atoms can be expected for certain energies, fluences, and types of ions. Indium and oxygen recoils that occupy interstitial positions affect the film's current-voltage characteristics. Moreover, conditions for the Cooper-pair insulating state to persist in InO_x may be disrupted by the ion beam irradiation, through the decrease of the charging energy (between superconducting islands in the 2D Josephson junction array that represents the material in the CPI phase), by the breaking of Cooper pairs in the islands, or by the increase of the film's temperature due to energy losses to phonons.

Acknowledgment

The Ministry of Education and Science of the Republic of Serbia supported this work under Contract no. 171007.

References

[1] B. Sacépé, T. Dubouchet, C. Chapelier et al., "Localization of preformed Cooper pairs in disordered superconductors," *Nature Physics*, vol. 7, no. 3, pp. 239–244, 2011.

[2] M. V. Fistul, V. M. Vinokur, and T. I. Baturina, "Collective cooper-pair transport in the insulating state of josephson-junction arrays," *Physical Review Letters*, vol. 100, no. 8, Article ID 086805, 2008.

[3] G. Sambandamurthy, L. W. Engel, A. Johansson, E. Peled, and D. Shahar, "Experimental evidence for a collective insulating state in two-dimensional superconductors," *Physical Review Letters*, vol. 94, no. 1, Article ID 017003, 2005.

[4] P. Nikolić and Z. Tesanovic, "Cooper pair insulators and theory of correlated superconductors," *Physical Review B*, vol. 83, Article ID 064501, 6 pages, 2011.

[5] M. D. Stewart Jr., A. Yin, J. M. Xu, and J. M. Valles Jr., "Superconducting pair correlations in an amorphous insulating nanohoneycomb film," *Science*, vol. 318, no. 5854, pp. 1273–1275, 2007.

[6] T. I. Baturina, A. Y. Mironov, V. M. Vinokur, M. R. Baklanov, and C. Strunk, "Localized superconductivity in the quantum-critical region of the disorder-driven superconductor-insulator transition in TiN thin films," *Physical Review Letters*, vol. 99, no. 25, Article ID 257003, 2007.

[7] P. A. Mangrulkar, S. P. Kamble, M. M. Joshi, J. S. Meshram, N. K. Labhsetwar, and S. S. Rayalu, "Photocatalytic degradation of phenolics by N-doped mesoporous titania under solar radiation," *International Journal of Photoenergy*, vol. 2012, Article ID 780562, 10 pages, 2012.

[8] C. Wang and J. Yao, "Decolorization of methylene blue with TiO_2 sol via UV irradiation photocatalytic degradation," *International Journal of Photoenergy*, vol. 2010, Article ID 643182, 6 pages, 2010.

[9] G. Sambandamurthy, L. W. Engel, A. Johansson, and D. Shahar, "Superconductivity-related insulating behavior," *Physical Review Letters*, vol. 92, no. 10, pp. 107005–1, 2004.

[10] E. Bielejec, J. Ruan, and W. Wu, "Hard correlation gap observed in quench-condensed ultrathin beryllium," *Physical Review Letters*, vol. 87, no. 3, Article ID 036801, pp. 368011–368014, 2001.

[11] B. Sacépé, C. Chapelier, T. I. Baturina, V. M. Vinokur, M. R. Baklanov, and M. Sanquer, "Disorder-induced inhomogeneities of the superconducting state close to the superconductor-insulator transition," *Physical Review Letters*, vol. 101, no. 15, Article ID 157006, 2008.

[12] Y. Dubi, Y. Meir, and Y. Avishai, "Theory of the magnetoresistance of disordered superconducting films," *Physical Review B*, vol. 73, no. 5, Article ID 054509, 2006.

[13] Y. Dubi, Y. Meir, and Y. Avishai, "Nature of the superconductor-insulator transition in disordered superconductors," *Nature*, vol. 449, no. 7164, pp. 876–880, 2007.

[14] M. V. Feigei'man, L. B. Ioffe, V. E. Kravtsov, and E. A. Yuzbashyan, "Eigenfunction fractality and pseudogap state near the superconductor-insulator transition," *Physical Review Letters*, vol. 98, no. 2, Article ID 027001, 2007.

[15] V. M. Galitski, G. Refael, M. P. A. Fisher, and T. Senthil, "Vortices and quasiparticles near the superconductor-insulator transition in thin films," *Physical Review Letters*, vol. 95, no. 7, Article ID 077002, 2005.

[16] V. L. Pokrovsky, G. M. Falco, and T. Nattermann, "Phase diagram of electron systems near the superconductor-insulator transition," *Physical Review Letters*, vol. 105, no. 26, Article ID 267001, 2010.

[17] Y. Imry, M. Strongin, and C. C. Homes, "An inhomogeneous Josephson phase in thin-film and high-Tc superconductors," *Physica C*, vol. 468, no. 4, pp. 288–293, 2008.

[18] N. M. Chtchelkatchev, V. M. Vinokur, and T. I. Baturina, "Hierarchical energy relaxation in mesoscopic tunnel junctions: effect of a nonequilibrium environment on low-temperature transport," *Physical Review Letters*, vol. 103, no. 24, Article ID 247003, 2009.

[19] J. F. Ziegler, J. P. Biersack, and M. D. Ziegler, "SRIM (The Stopping and Range of Ions in Matter)," http://www.srim.org/.

[20] J. L. Barth, C. S. Dyer, and E. G. Stassinopoulos, "Space, atmospheric, and terrestrial radiation environments," *IEEE Transactions on Nuclear Science*, vol. 50, no. 3, pp. 466–482, 2003.

[21] M. A. Xapsos, J. L. Barth, E. G. Stassinopoulos et al., "Characterizing solar proton energy spectra for radiation effects applications," *IEEE Transactions on Nuclear Science*, vol. 47, no. 6, pp. 2218–2223, 2000.

[22] J. H. Warner, S. R. Messenger, R. J. Walters, and G. P. Summers, "Displacement damage correlation of proton and silicon ion radiation in GaAs," *IEEE Transactions on Nuclear Science*, vol. 52, no. 6, pp. 2678–2682, 2005.

[23] A. A. E. Stevens, W. M. M. Kessels, M. C. M. van de Sanden, and H. C. W. Beijerinck, "Amorphous silicon layer characteristics during 70-2000 eV Ar +-ion bombardment of Si(100)," *Journal of Vacuum Science and Technology A*, vol. 24, no. 5, pp. 1933–1940, 2006.

[24] M. Vujisić, K. Stanković, N. Marjanović, and P. Osmokrović, "Simulated effects of proton and ion beam irradiation on titanium dioxide memristors," *IEEE Transactions on Nuclear Science*, vol. 57, no. 4, pp. 1798–1804, 2010.

[25] D. Nikolić, A. Vasić, I. Fetahović, K. Stanković, and P. Osmokrović, "Photodiode behavior in radiation environment," *Scientific Publications of the State University of Novi Pazar Series A*, vol. 3, no. 1, pp. 27–34, 2011.

[26] R. Radosavljević and A. Vasić, "Effects of radiation on solar cells as photovoltaic generators," *Nuclear Technology & Radiation Protection*, vol. 27, no. 1, pp. 28–32, 2012.

[27] M. Vujisić, N. Marjanović, I. Fetahović, K. Stanković, and P. Osmokrović, "Influence of radiation on titanium dioxide mermistors," *Scientific Publications of the State University of Novi Pazar Series ANo*, vol. 4, no. 1, pp. 75–82, 2012.

[28] K. D. Stanković, "Influence of the plain-parallel electrode surface dimensions on the type a measurement uncertainty of GM counter," *Nuclear Technology and Radiation Protection*, vol. 26, no. 1, pp. 39–44, 2011.

[29] C. Dolicanin, K. Stanković, D. Dolicanin, and B. Loncar, "Statistisal treatment of nuclear counting results," *Nuclear Technology & Radiation Protection*, vol. 26, no. 2, pp. 164–170, 2011.

[30] M. Zdravkovic, A. Vasić, R. Radosavljević, M. Vujisić, and P. Osmokrović, "Influence of radiation on the properties of solar cells," *Nuclear Technology & Radiation Protection*, vol. 26, no. 2, pp. 158–163, 2011.

Hindawi Publishing Corporation
International Journal of Photoenergy
Volume 2013, Article ID 128410, 9 pages
http://dx.doi.org/10.1155/2013/128410

Research Article

Simulation of Proton Beam Effects in Thin Insulating Films

Ljubinko Timotijevic,[1] Irfan Fetahovic,[2] Djordje Lazarevic,[3] and Milos Vujisic[1]

[1] *Faculty of Electrical Engineering, University of Belgrade, 11060 Belgrade, Serbia*
[2] *State University of Novi Pazar, 36300 Novi Pazar, Serbia*
[3] *Institute of Nuclear Sciences "Vinca", 11000 Belgrade, Serbia*

Correspondence should be addressed to Milos Vujisic; vujsa@ikomline.net

Received 15 April 2013; Accepted 28 May 2013

Academic Editor: Predrag Osmokrovic

Effects of exposing several insulators, commonly used for various purposes in integrated circuits, to beams of protons have been investigated. Materials considered include silicon dioxide, silicon nitride, aluminium nitride, alumina, and polycarbonate (Lexan). The passage of proton beams through ultrathin layers of these materials has been modeled by Monte Carlo simulations of particle transport. Parameters that have been varied in simulations include proton energy and insulating layer thickness. Materials are compared according to both ionizing and nonionizing effects produced by the passage of protons.

1. Introduction

Insulating layers are needed in various kinds of microelectronic components. Roles of these insulating layers vary from surface passivation of chips to more specific functions, such as lateral insulation of components in planar technology, capacitor dielectrics, or tunnel oxides in flash memory cells. Depending on their purposes within structures and devices, insulating layers are made out of different materials and with various thicknesses. Since many devices are expected to be operated in radiation environments, it is essential that radiation effects in insulators they comprise are investigated. Actual irradiation at accelerator facilities can be costly and time consuming, which is why radiation hardness of materials and components is often tested through simulations of radiation transport.

The present study investigates effects of proton beams on five insulating materials, commonly encountered in modern day electronic components: silicon dioxide, silicon nitride, aluminium nitride, alumina, and polycarbonate. Radiation effects are predicted and compared on the basis of Monte Carlo simulations of proton transport through ultrathin layers of these insulators.

2. Radiation Effects in Insulators

Insulators are a broad class of materials. They include crystals, amorphous materials, and organics (polymers). The response of insulators to irradiation is determined by their structural properties and electronic configuration [1, 2].

Interaction of incoming particles with matter results in two major effects: ionization energy loss and nonionizing energy loss (NIEL). Interactions of incoming particles which result in electronic excitation or ionization of atoms are referred to as ionization energy loss. In NIEL processes, the energy imparted by the incident particles results in atomic displacements or in collisions where the primary knock-on atom (PKA) remains in its lattice position, in which case the energy is converted to lattice vibrations (phonons). Displaced atoms can also undergo both electronic and displacement energy losses to dissipate their energy inside the medium.

Secondary electrons created by ionization energy losses affect electrical properties of crystalline insulators in a transient manner, except if these electrons get trapped at electrically active point defects in the crystal lattice. Point defects that serve as charge-carrier traps or donors, arise in irradiated insulators as a result of atomic displacements, that

is, of NIEL. Polymer insulators exhibit radiation effects that are specific to that kind of materials. They include chain scission and cross-linking, both of which can significantly alter insulator's physical properties.

A heavy charged particle can transfer only a small fraction of its energy in a single electronic collision, and its deflection in the collision is negligible. It therefore has an almost straight trajectory in matter, losing energy continuously in small amounts through collisions with atomic electrons, leaving ionized and excited atoms along its path. Only occasionally does it undergo a substantial deflection, due to elastic scattering from an atomic nucleus [1–4].

For charged particles, such as protons, ionization, and electronic excitation, energy losses are represented by the electronic stopping power (also called collision stopping power, which is a misnomer, since all interactions can be considered collisions) of the material through which they propagate. Stopping power of a medium for a charged particle is the average linear rate of energy loss of the particle in the medium. It is, therefore, equal to the unrestricted linear energy transfer (LET). Several semiempirical stopping power formulas have been devised. The SRIM code, used for simulating proton transport in the present paper, implements the so-called ZBL stopping, which is based on the model given by Ziegler, Biersack, and Littmark.

Displacement damage can occur in crystal insulators when the energy transferred to lattice atoms exceeds the threshold displacement energy (E_d). Irradiation of materials with electrons and light ions introduces predominantly isolated interstitial atoms and vacancies (Frenkel pairs) and small clusters of these point defects, because of the low average recoil atom energies (0.1–1 keV). Energetic heavy ion irradiations, on the other hand, produce energetic displacement cascades that can lead to direct formation of defect clusters within isolated displacement cascades, due to more energetic average recoil atom energies (>10 keV) [5, 6].

The effects of irradiation on the electrical parameters of many materials have been found to display a simple, often linear, relationship with NIEL. NIEL is the rate at which energy is lost to nonionizing events. It is a direct analog of stopping power for ionization events. The units of NIEL are typically MeV/cm, or MeV cm^2/g if mass NIEL is considered. The calculation of NIEL requires information regarding the differential cross section for atomic displacements ($d\sigma/d\Omega$), the average recoil energy of the target atoms (E_r), and a term which partitions the energy into ionizing and nonionizing events, called the Lindhard partition factor (L). NIEL can be written as an integral over solid angle as follows:

$$\mathrm{NIEL}\,(E) = \frac{N_A}{A}\int_{\theta_{\min}}^{\pi} \frac{d\sigma\,(\theta, E)}{d\Omega} T\,(\theta, E)\, L\,(T\,(\theta, E))\, d\Omega, \quad (1)$$

where the N_A is Avogadro's number, A is the atomic mass, and $\theta_{\min}$ is the scattering angle for which the recoil energy equals the threshold for atomic displacement. For protons having nonrelativistic energy, the Rutherford differential cross section can be used for elastic scattering at atomic nuclei [7–11].

3. Results of Simulations

Monte Carlo simulations of proton transport through thin layers of insulators were performed in the TRIM module of the SRIM software package [12]. Simulations used monoenergetic unidirectional beams, incident perpendicularly on the film's surface. Proton energies were varied from 10 keV to 10 MeV. At each value of proton energy, the thickness of the insulating film was increased until the whole beam was stopped within it. Film thickness in that case exceeded the maximum range of both protons and any secondary charged particles, which corresponds to a maximum radiation effect in the insulator. Each simulation run followed 10^4 proton histories.

Results in Figures 1–5 present the most illustrative examples of proton beam effects in the studied insulators for the investigated proton energy range. Vacancy depth distribution plots, LET versus depth plots, and NIEL versus depth plots were obtained from SRIM outputs, following the procedure outlined in [13].

The rate of vacancy formation can be converted into NIEL using the modified Kinchin-Pease relationship between the number of atomic displacements N_d and the nonionizing energy E_n as follows:

$$N_d = 0.8\frac{E_n}{2E_d}, \quad (2)$$

where E_d is the threshold energy for atomic displacement. Equation (2) applies for $E_n > 2.5E_d$ [13–15].

Distributions of atomic vacancies, created within the insulating films by the NIEL of both protons and recoils, are shown in total (curves denoted by "Total vacancies" in the graphs), but also for each kind of displaced atom separately (e.g., curves denoted by "Silicon vacancies" or "Oxygen vacancies"). Curves of total vacancy concentration along the depth of the insulating film are, naturally, always the top ones in these graphs.

4. Analysis of the Results

Thin insulating films investigated herein are immune to the passage of protons with energies exceeding 10 MeV. Simulation results (omitted from this paper) have shown that proton beams with 10 MeV energy experience inconsiderable broadening (fanning) for the considered range of insulating film thickness (from 0.4 μm to 20 μm). For these high energy protons, NIEL is also negligible, while LET is at least one order of magnitude lower than for 1 MeV protons.

Of the four investigated insulators, protons went to larger penetration depths in silicon dioxide and lexan than in the other two materials. In SiO_2, there is a somewhat greater concentration of silicon vacancies than oxygen ones, despite the 2 : 1 stoichiometric ratio of oxygen to silicon atoms, which is attributed to the threshold displacement energy of Si being considerably lower ($E_{d\mathrm{Si}} = 15$ eV, $E_{d\mathrm{O}} = 28$ eV). Ionizing energy losses (LET) generally dominate NIEL by 1 to 3 orders of magnitude. This difference becomes larger as the energy of the proton beam is increased, which means that it subsides

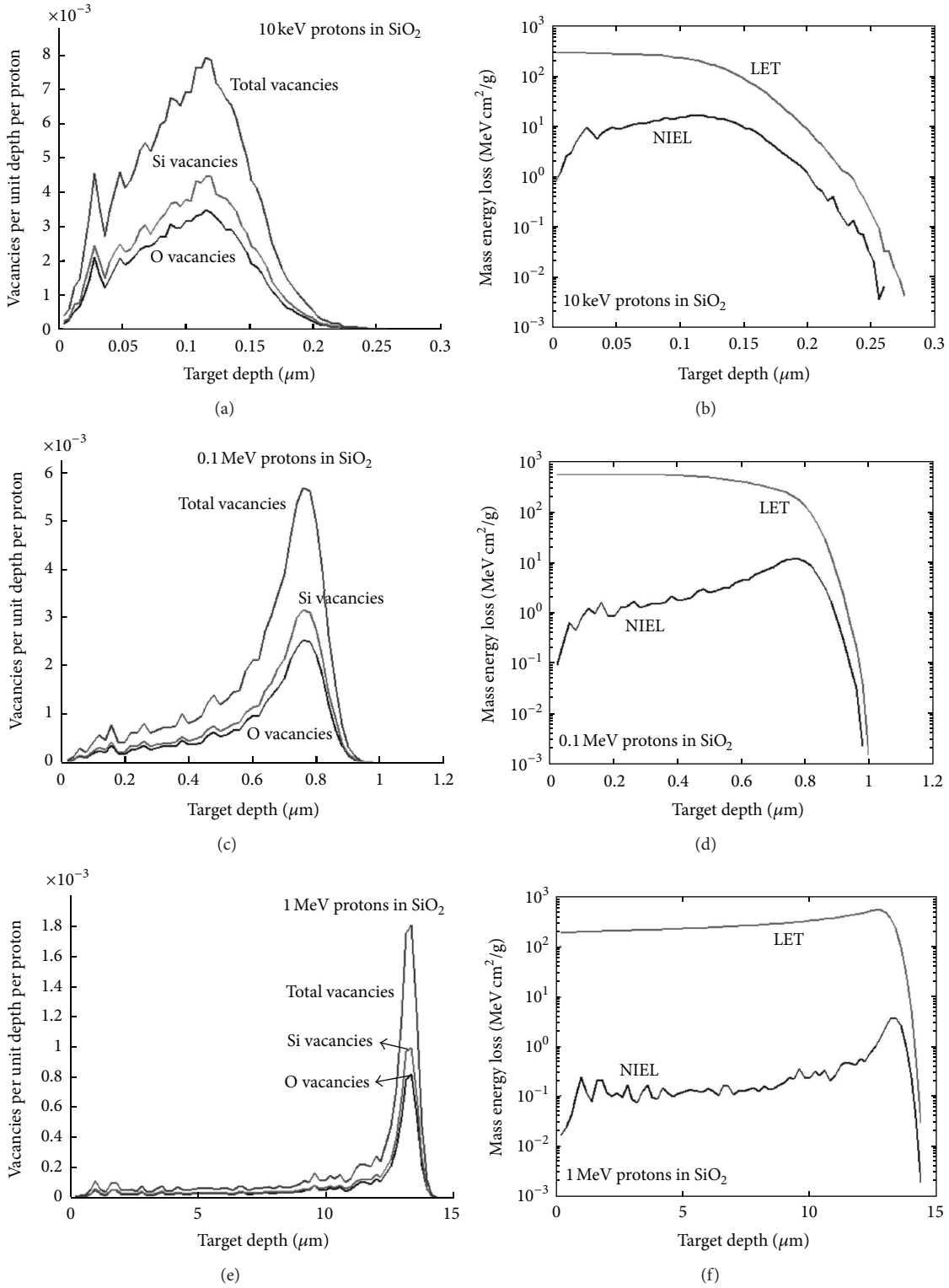

Figure 1: Plots of vacancy concentrations and mass energy losses (LET and NIEL divided by material density) along the depth of a silicon dioxide (SiO_2) insulating film. Results were obtained from simulations of 10^4 proton histories, which included subcascades of recoiling atoms.

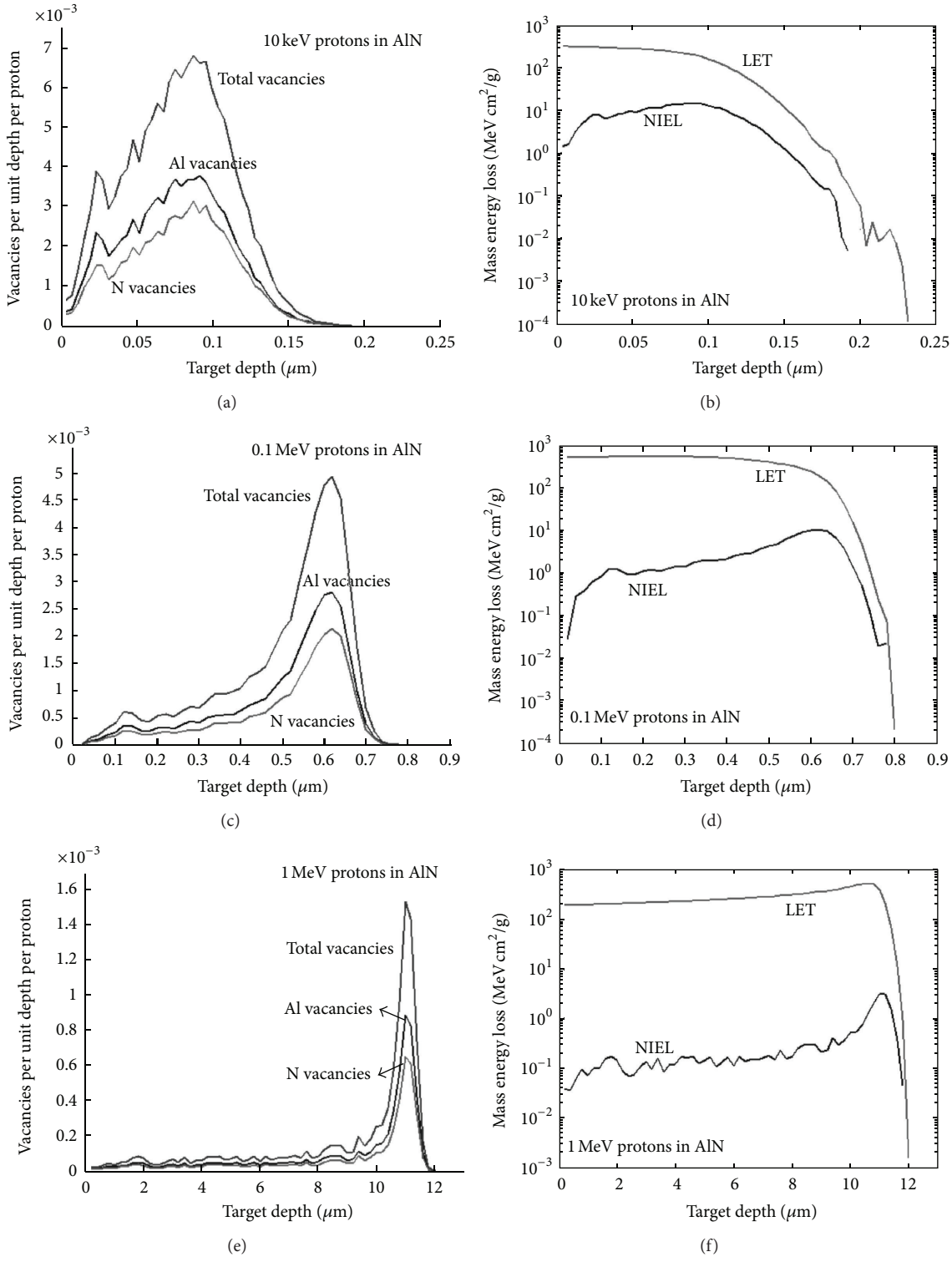

Figure 2: Plots of vacancy concentrations and mass energy losses (LET and NIEL divided by material density) along the depth of an aluminium nitride (AlN) insulating film. Results were obtained from simulations of 10^4 proton histories, which included subcascades of recoiling atoms.

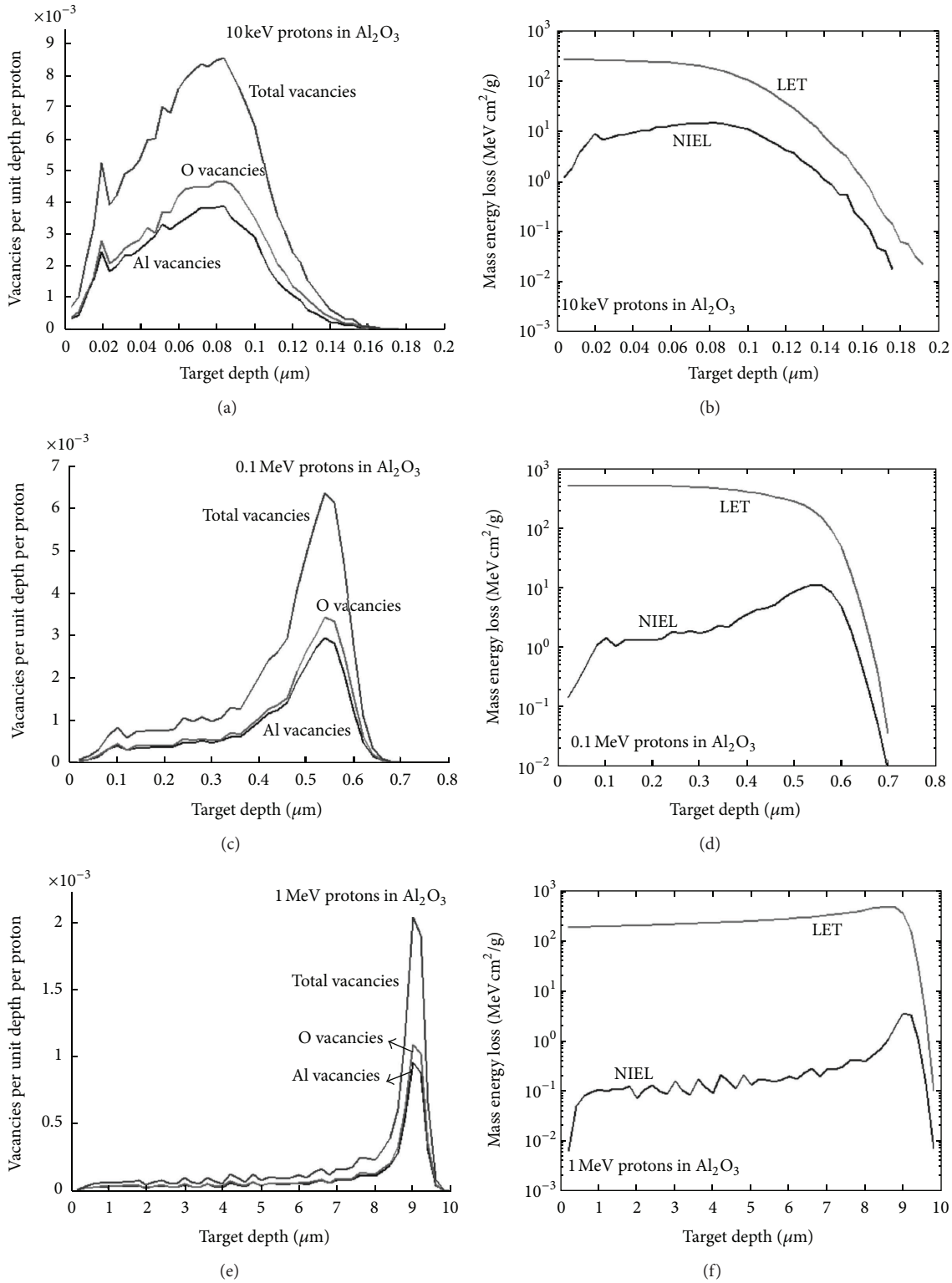

Figure 3: Plots of vacancy concentrations and mass energy losses (LET and NIEL divided by material density) along the depth of an alumina (Al_2O_3) insulating film. Results were obtained from simulations of 10^4 proton histories, which included subcascades of recoiling atoms.

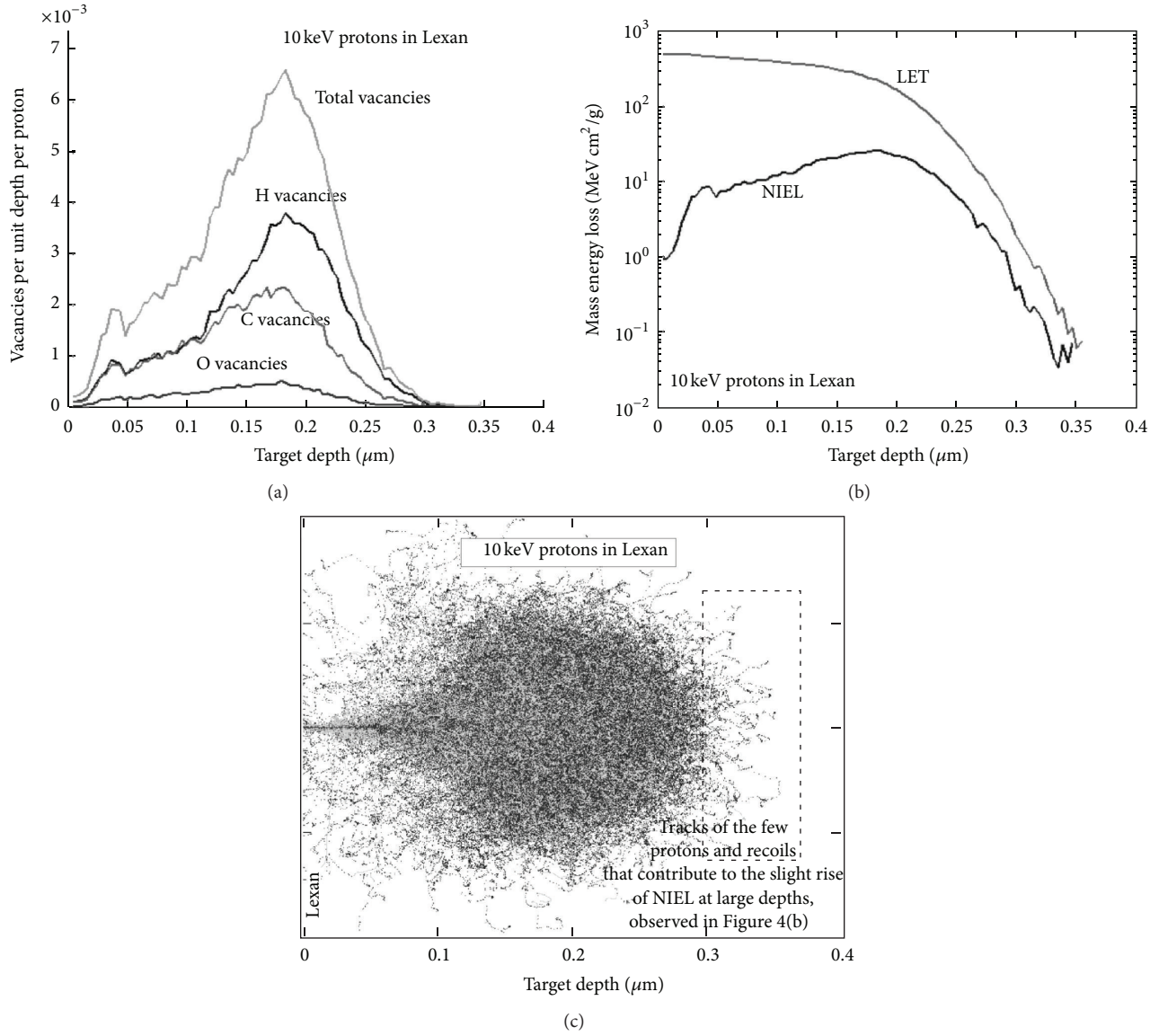

FIGURE 4: Plots of (a) vacancy concentrations and (b) mass energy losses (LET and NIEL divided by material density) along the depth of a 0.4 μm thick lexan (polycarbonate) film. (c) Tracks of protons and recoiling atoms. Results were obtained from simulations of 10^4 proton histories, for a 10 keV incident proton beam.

towards the ends of proton tracks, where nuclear elastic scatterings that give rise to atomic displacements become more probable than electronic collisional events.

The slight increase of NIEL seen at the rightmost part of the lower curve in Figure 4(b) is due to the few protons that reach penetration depths close to 0.35 μm, larger than the mean beam range, and also due to the recoils (mainly hydrogen) that these protons displace. Although the number of such protons is small, they arrive at these large depths without losing much of the original energy in electronic collisions, as most other protons from the beam do. The resulting rise of the NIEL curve is small, but still noticeable in the logarithmic scale. Tracks of protons and recoils that contribute to this rise of NIEL are marked in Figure 4(c).

The energy loss versus depth plot begins to take the classic shape of a Bragg curve only at proton energies >0.5 MeV. As proton energy is increased from ~100 keV, it is first the NIEL curve that starts exhibiting a peak near the maximum penetration depth, as seen in Figures 1(d), 2(d), and 3(d). Around 1 MeV proton energy, both LET and NIEL curves peak toward the end of the penetration depth, giving shape to the Bragg peak, observed much more clearly when the scale of the mass energy loss axis is linear, and not logarithmic. This is illustrated by the plot in Figure 6 for 1 MeV protons in SiO_2.

If one cascade creates more than 8000 recoil atoms, SRIM discards the atoms beyond 8000, which causes certain inaccuracy in vacancy calculations. During our simulations, this happened for protons with energies higher than ~1 MeV

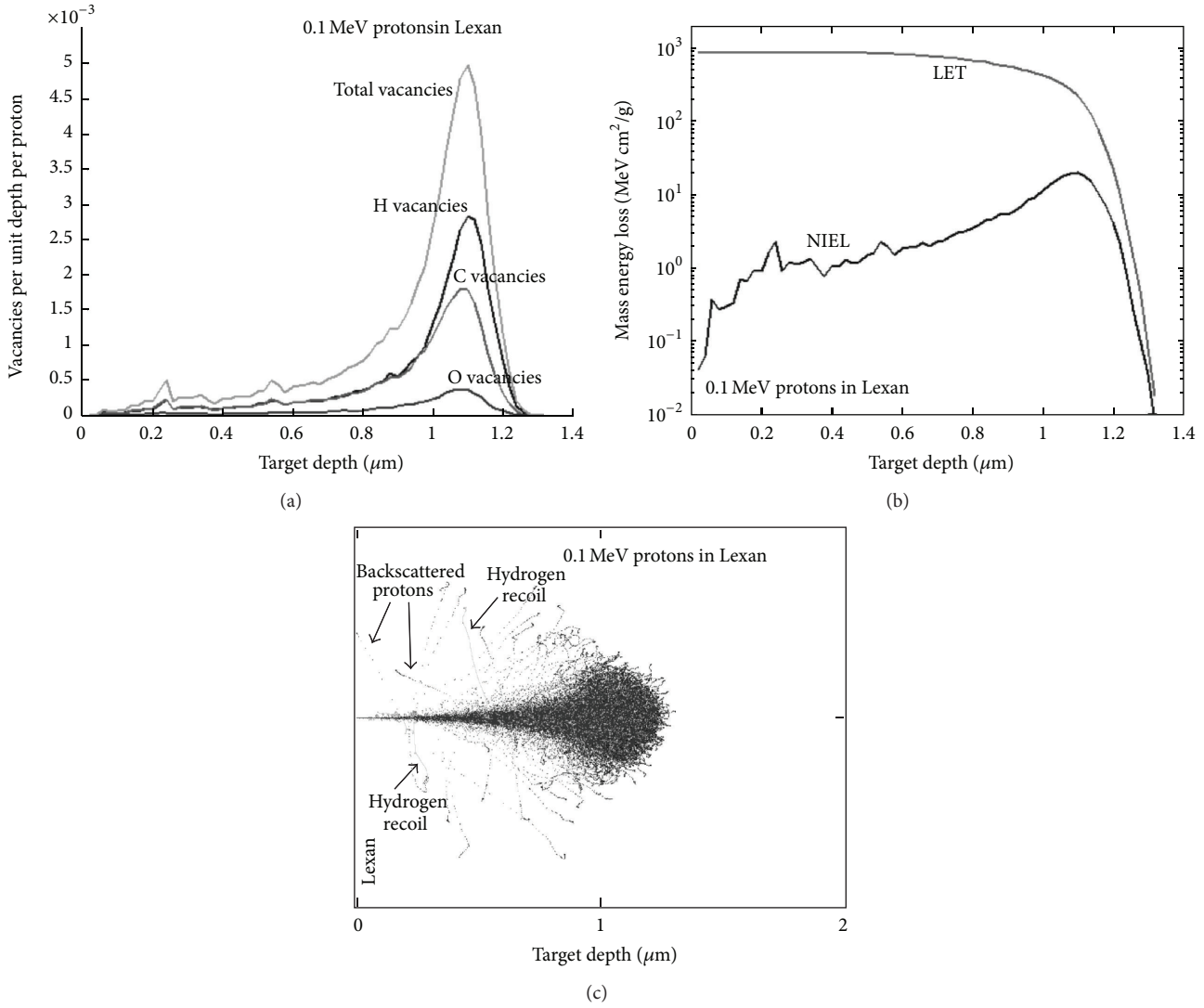

Figure 5: Plots of (a) vacancy concentrations and (b) mass energy losses (LET and NIEL divided by material density) along the depth of a 0.2 μm thick lexan (polycarbonate) film. (c) Tracks of protons and recoiling atoms. Results were obtained from simulations of 10^4 proton histories, for a 0.1 MeV incident proton beam.

in lexan films. In a hydrogen-rich medium such as lexan, high energy incident protons give rise to a large number of energetic hydrogen knockons, which results in a multitude of highly branched cascades.

Figure 5(c) clearly demonstrates large-angle backscattering of protons and long tracks of energetic hydrogen recoils in lexan.

Chemical structure unit of polycarbonate is presented in Figure 7. It contains 14 atoms of hydrogen, 16 of carbon, and 3 of oxygen. The stoichiometric ratio of the three elements, along with their threshold displacement energies ($E_{d\mathrm{H}}$ = 10 eV, $E_{d\mathrm{C}} = E_{d\mathrm{O}}$ = 28 eV), accounts for the observed ratios of vacancy concentration curves seen in Figures 4(a) and 5(a).

Secondary electrons, produced by protons through ionization energy losses, further interact with polymer macromolecules, causing their ionization and excitation. Relaxation of excited molecules and locally formed ionization clusters results in a formation of large amounts of free radicals. Highly reactive free radicals cause destruction of polymer chains, by either chain scission (random rupturing of bonds) or cross-linking (formation of large three-dimensional molecular networks). As a result of chain scission, low-molecular-weight fragments, gas evolution, and unsaturated bonds may appear [16].

Many important physical and chemical properties of polymers can be modified by irradiation. Among these are molecular weight, chain length, entanglement, polydispersity, branching, and chain termination. These structural changes also affect the electrical insulating properties of polycarbonate films [17, 18].

Radiation effects in thin insulating layers are relevant due to the increasing miniaturization of electronic components. Miniaturization makes these components sensitive to primary and secondary cosmic rays, which also present one of

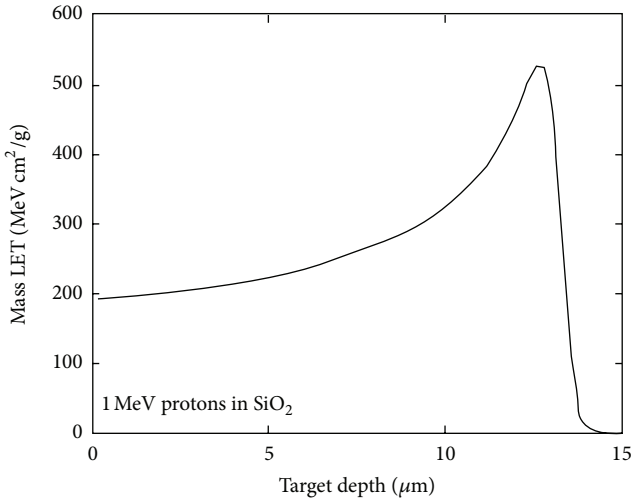

Figure 6: Plot of the mass LET for 1 MeV protons along the depth of a 15 μm thick silicon dioxide film. The scale of the energy loss axis is linear, in contrast to Figure 1(f) where it is logarithmic.

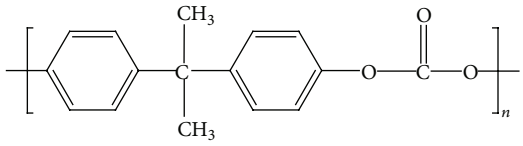

Figure 7: Chemical structure unit of polycarbonate, containing 14 atoms of hydrogen, 16 of carbon, and 3 of oxygen.

the most severe obstacles for a widespread use of photovoltaic cells [19–22].

5. Conclusion

Monte Carlo simulations of proton transport through thin films of SiO_2, AlN, Al_2O_3 and polycarbonate have shown that the investigated films are immune to the passage of protons with energies higher than ~10 MeV. Nonionizing energy loss of these high energy protons is low, and they traverse the films without much atomic displacement. In the lower part of the investigated proton energy range (from 10 keV to 1 MeV), however, substantial ionization losses and NIEL are to be expected. Ionization and displacement damage produced by protons could influence the properties of these insulators and compromise their reliability within complex structures and devices. Point defects, some of which are charge-carrier donors, arise in irradiated insulators as a result of atomic displacements. Highly reactive free radicals that can appear in irradiated lexan cause chain scission and/or cross-linking, which then affects the insulating properties of polycarbonate films.

Acknowledgment

The Ministry of Education and Science of the Republic of Serbia supported this work under Contract 171007.

References

[1] A. G. Holmes-Siedle and L. Adams, *Handbook of Radiation Effects*, Oxford University Press, 2nd edition, 2002.

[2] J. R. Schwank, M. R. Shaneyfelt, D. M. Fleetwood et al., "Radiation effects in MOS oxides," *IEEE Transactions on Nuclear Science*, vol. 55, no. 4, pp. 1833–1853, 2008.

[3] S. Stanković, B. Iričanin, D. Nikolić et al., "MSV signal processing system for neutron-gamma discrimination in a mixed field," *Nuclear Technology & Radiation Protection*, vol. 27, no. 2, pp. 165–170, 2012.

[4] I. Knezevic, N. Zdjelarevic, M. Obrenovic, and M. Vujisic, "Absorbed dose assessment in particle-beam irradiated metal-oxide and metal-nonmetal memristors," *Nuclear Technology & Radiation Protection*, vol. 27, no. 3, pp. 290–296, 2012.

[5] P. Sigmund, *Stopping of Heavy Ions*, vol. 4 of *Springer Tracts of Modern Physics*, Springer, Berlin, Germany, 2004.

[6] J. H. Warner, S. R. Messenger, R. J. Walters, and G. P. Summers, "Displacement damage correlation of proton and silicon ion radiation in GaAs," *IEEE Transactions on Nuclear Science*, vol. 52, no. 6, pp. 2678–2682, 2005.

[7] H. García, S. Dueñas, H. Castán et al., "Irradiation effect on dielectric properties of hafnium and gadolinium oxide gate dielectrics," *Journal of Vacuum Science and Technology B*, vol. 27, no. 1, pp. 416–420, 2009.

[8] C. Leroy and P.-G. Rancoita, "Particle interaction and displacement damage in silicon devices operated in radiation environments," *Reports on Progress in Physics*, vol. 70, no. 4, pp. 493–625, 2007.

[9] R. Radosavljević and A. Vasić, "Effects of radiation on solar cells as photovoltaic generators," *Nuclear Technology & Radiation Protection*, vol. 27, no. 1, pp. 28–32, 2012.

[10] Đ. Lazarević, M. Vujisić, K. Stanković, E. Dolićanin, and P. Osmokrović, "Radiation hardness of indium oxide films in the cooper-pair insulator state," *Nuclear Technology & Radiation Protection*, vol. 27, no. 1, pp. 40–43, 2012.

[11] E. Dolićanin, "Gamma ray effects on flash memory cell arrays," *Nuclear Technology & Radiation Protection*, vol. 27, no. 3, pp. 284–289, 2012.

[12] J. F. Ziegler, J. P. Biersack, and M. D. Ziegler, "SRIM—The Stopping and Range of Ions in Matter," http://www.srim.org.

[13] S. R. Messenger, E. A. Burke, G. P. Summers et al., "Nonionizing Energy Loss (NIEL) for heavy ions," *IEEE Transactions on Nuclear Science*, vol. 46, pp. 1595–1602, 1999.

[14] D. Nikolić, A. Vasić, I. Fetahović, K. Stanković, and P. Osmokrović, "Photodiode behavior in radiation environment," *Applied Mathematics, Informatics & Mechanics*, vol. 3, no. 1, pp. 27–34, 2011.

[15] M. Vujisić, N. Marjanović, I. Fetahović, K. Stanković, and P. Osmokrović, "Influence of radiation on titanium dioxide mermistors," *Applied Mathematics, Informatics & Mechanics*, vol. 4, no. 1, pp. 75–82, 2012.

[16] "Polymer durability and radiation effects," in *Proceedings of the Acs Symposium*, M. C. Celina and R. A. Assink, Eds., series 978, 2007.

[17] M. P. Petkov, K. G. Lynn, K. P. Rodbell, W. Volksen, and R. D. Miller, "Radiation effects in low dielectric constant methylsilsesquioxane films," *IEEE Transactions on Nuclear Science*, vol. 49, no. 6, pp. 2724–2728, 2002.

[18] T. Iwahashi, T. Tamagawa, A. Hayato et al., "Heavy ion and proton irradiation of gas electron multipliers with liquid crystal

polymer insulator: evaluation tests for use in space," *IEEE Transactions on Nuclear Science*, vol. 58, no. 5, pp. 2401–2406, 2011.

[19] X. L. Han, H. Ni, K. Zhao, Y.-C. Kong, H. K. Wong, and S. Q. Zhao, "Load-resistance- and voltage-tunable photovoltaic effect in tilting manganite films," *International Journal of Photoenergy*, vol. 2011, Article ID 314085, 2011.

[20] Z. Hu, B. Jiao, J. Zhang, X. Zhang, and Y. Zhao, "Indium-doped zinc oxide thin films as effective anodes of organic photovoltaic devices," *International Journal of Photoenergy*, vol. 2011, Article ID 158065, 5 pages, 2011.

[21] T. T. Chow, G. N. Tiwari, and C. Menezo, "Hybrid Solar: a review on photovoltaic and thermal power integration," *International Journal of Photoenergy*, vol. 2012, Article ID 307287, 17 pages, 2012.

[22] P. Ooshaksaraei, K. Sopian, R. Zulkifli, M. A. Alghoul, and S. H. Zaidi, "Characterization of a bifacial photovoltaic panel integrated with external diffuse and semimirror type reflectors," *International Journal of Photoenergy*, vol. 2013, Article ID 465837, 7 pages, 2013.

Hindawi Publishing Corporation
International Journal of Photoenergy
Volume 2013, Article ID 802789, 5 pages
http://dx.doi.org/10.1155/2013/802789

Research Article

Thermal Characterization of the Overload Carbon Resistors

Ivana Kostić,[1] Ljubiša Tomić,[1] Aleksandar Kovačević,[1] and Saša Nikolić[2]

[1] *Technical Test Center, Vojvode Stepe 445, 11000 Belgrade, Serbia*
[2] *Faculty of Electrical Engineering, University of Niš, Aleksandra Medvedeva 14, 18000 Niš, Serbia*

Correspondence should be addressed to Ivana Kostić; kostic.ici@gmail.com

Received 10 May 2013; Accepted 17 June 2013

Academic Editor: Momčilo Pejović

In many applications, the electronic component is not continuously but only intermittently overloaded (e.g., inrush current, short circuit, or discharging interference). With this paper, we provide insight into carbon resistors that have to hold out a rarely occurring transient overload. Using simple electrical circuit, the resistor is overheating with higher current than declared, and dissipation is observed by a thermal camera.

1. Introduction

The electronic designers must be sure that the correct device is chosen on the basis of both electrical and thermal performances. Many companies have established their own standards and testing techniques based on their experience, but often this information is not enough. It is necessary to know the operating life of electronic components affected by temperature and voltage stress. Measurement and temperature control are becoming increasingly important especially since device and electronic board sizes are shrinking.

Temperature measurement is not easy but is necessary since it is the only measurable parameter for the quality of the thermal design [1]. Every electronic component requires dedicated approaches according to its specific functionality.

One of the most frequently used electronic components is resistor. Resistor can be connected in various networks where it acts as voltage dropper, voltage divider, or current limiter. Resistors reduce the voltage or current signal passing through them. A higher voltage makes the electrons move faster through resistor and it warms up the resistor. As a result, energy is turned into heat. Typical values for this parameter are 1/16 W, 1/10 W, 1/8 W, 1/4 W, 1/2 W, 1 W, 2 W, 2.5 W, 3 W, or higher to 100 W or even 300 W. For the thermal problem, given that energy is not the only restriction parameter, the temperature will increase faster reducing the size of the resistor because the power dissipation capability is directly proportional to size. Also, a system that will reduce the temperature rise of electronic parts and equipment is necessary [2].

2. Experimental Setup

Measurements were performed by heating the resistor by electric current. The propagation of the heat is a physical process and depends on the thermal properties of materials, size of the area, and length of the wire. Because of the small area of the resistor, contact methods can easily change the value of surface temperature. So this method is worthless for this kind of measurements [3]. Most of the light is radiated at infrared (IR) wavelengths, but at sufficiently high temperatures there is a considerable amount of light also at visible wavelengths. This amount of radiated heat energy has $\sim T^4$ dependency assuming that it is by natural convection [4, 5].

In this experiment, it is not important to know the exact temperature of the resistor, but rather how fast temperature rises and its influence on resistor. The process is observed by an infrared camera. In this case, we used FLIR SC 620 camera, manufactured by FLIR Systems. With an operational range of 7.5 μm–13 μm band at temperatures between 0°C and +500°C, it is equipped with a 45° lens and enables capturing structures by FPA (focal plane array) microbolometer set to a rate of 120 frames per second. The major technical specifications of the camera used in this study are listed in Table 1. The readout

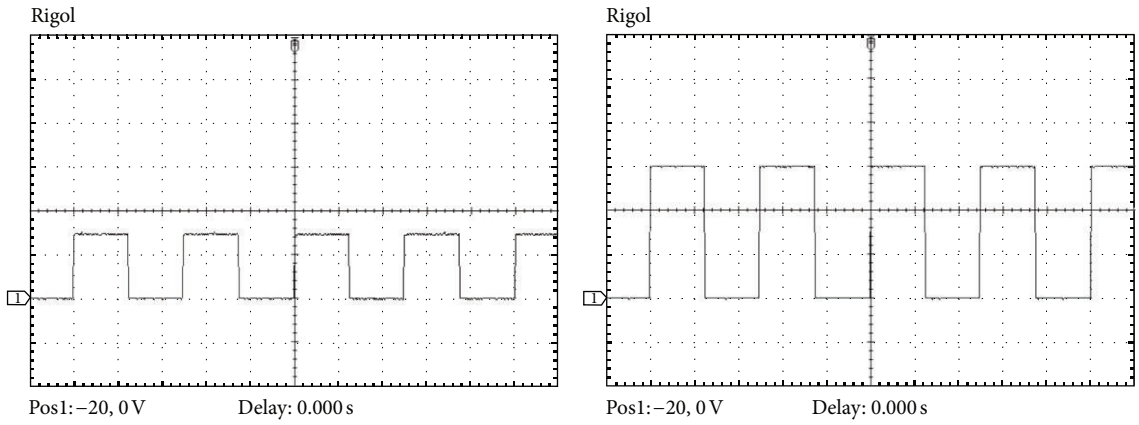

(a) Input signal 15 V (b) Input signal 30 V

Figure 1: Characteristics of input signals.

Table 1: Technical specifications of FLIR SC 620 infrared camera.

Field of view (FOV)	45° × 34°
Minimum focus distance	0.2 m
Spectral range	7.5 μm–13 μm
Accuracy	2°C or 2% of reading
Spatial resolution	0.65 mrad
IR resolution	640 × 480 pixels
Image frequency	30/60/120 Hz
Temperature range	−40°C to +1500°C
Thermal sensitivity	40 mK at 30°C
Focus	Automatic or manual
Laser pointer	Semiconductor AlGaInP diode laser, Class 2

Table 2: Thermal characteristics of MOSFET BD 135.

Characteristics	Symbol	Max	Unit
Thermal resistance, junction to case	θ_{JC}	10	°C/W
Thermal resistance, junction to ambient	θ_{JA}	100	°C/W

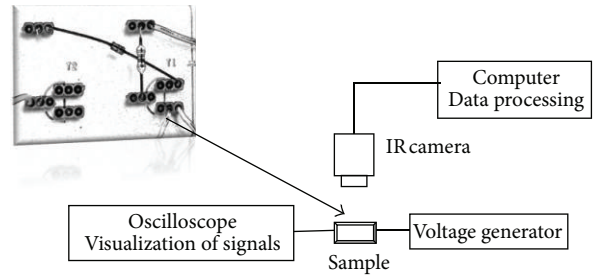

Figure 2: A schematic illustration of the experimental setup.

temperature is proportional to the IR flux coming from the scene. The main components of the signal are the thermal radiation emitted by the object (assumed to be an opaque grey body), the thermal radiation emitted by the heater, and the background radiation reflected from the object surface.

Test circuit board is very simple because of thermal spreading. The heat generated from a localized hot spot will eventually reach thermal equilibrium with its environment to minimize temperature gradients. The temperature distribution is completely different on an isolated resistor than in circuit with couple resistors. It consists of MOSFET BD135 that controls input signal as it is shown in Figure 1 and 75 Ohm carbon resistor of 1/4 W which simulates electronic circuit with pulse excitation. In this case, MOSFET has a role of voltage regulator [6]. Resistor has a ceramic substrate which normally holds the resistor together during and after firing, so the resistor can be fired at least twice as it is tried in this experiment. It is calculated from the input signals that the maximum reached power can be 3 W and 12 W which is more than declared. Thermal characteristics of MOSFET BD135, which is used in this experiment, are given in Table 2 [7].

MOSFET is connected to a source supplying 15 V or 30 V. Voltage through resistor (shown in Figure 1) is monitored by Rigol oscilloscope.

Using a thermal camera and an oscilloscope to observe the voltage and current through the resistor, we can gain an understanding of how a hot spot develops on the surface of the resistor. Data recording began by turning on the thermal camera and starting its Researcher software on computer (Figure 2).

The main interest of this experiment is temperature change, so we set up emission of the resistor to $\varepsilon = 0.96$, distance to 0.1 m, and temperature reflectance to 8°C.

Observed heat is higher than preferred value ranges and carbon resistor is discoloured soon (Figure 3). Five minutes after heating, we checked resistance and it has not changed; it was within the margin of the error (error is 5% as the manufacturer declared).

Also, after we had stopped the heating, we checked the resistance when the thermal camera showed a temperature of 100°C and it was within the limits of error. Heat dissipation

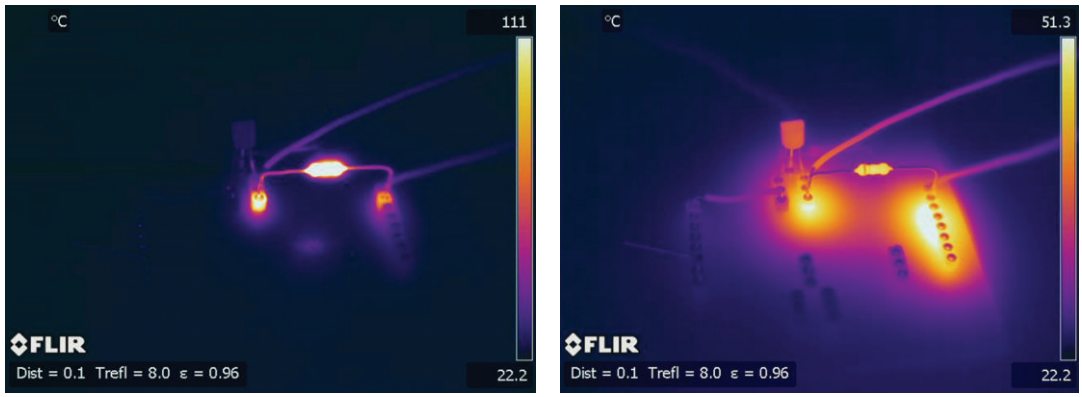

(a) Recorded sequence thermogram (INS0240.SEQ, 53rd frame), during pulse excitation

(b) Recorded sequence (INS0240.SEQ, 1500th frame), thermogram after pulse excitation

Figure 3: Thermogram of the resistor in electronic circuit with pulse excitation.

is high and the resistor does not lose its resistance, but it has an influence on the board and on the other components at the board. After pulse excitation, when surface temperature of resistor was near 50°C, we noticed that resistor was cooling faster than some points of the board [8–10].

The process of heating is very fast because the resistors were heating by current 10 times higher than it is declared. Temperature was changing very fast, so it was necessary to use fast thermal camera for measurements [8]. Because of the small dimension of a resistor, it is impossible to measure temperature transition by contact methods. Each test runs for 1-2 minutes after turning on the test circuit. Resistor temperature profiles were monitored from 3 different aspects as it is shown in Figure 4.

3. Results and Discussion

In Figure 5(a), steady-state condition is reached in a short time after 10–15 seconds. It is shown that the maximum temperature is reached in the centre of the resistor as it was expected (red curve) [9–11]. Red and green curves represent temperature profiles taken from LI02 and LI04 lines as it is shown in Figure 4(a). Internal parameters of the resistor lead to changes in maximum generated power [12, 13]. It is important to study the variation of power from a technological point of view. In recent papers, the efficiency and properties in terms of various conditions have been observed [14, 15].

Line LI01 in Figure 4(b) represents temperature profile of the resistor taken from one frame as proof of different heat distribution as it is shown in Figure 5(b).

During testing, we wanted to know the temperature profile for the resistor in DC current circuit (Figure 6). Temperature profile is observed at lines in Figure 4(a) (LI02 and LI04) during excitation.

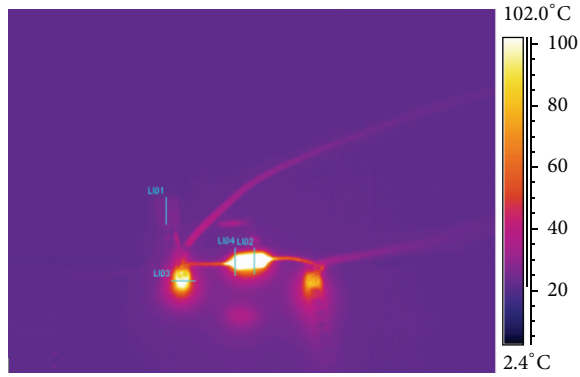

(a) Temperature in function of time for resistor in DC electronic circuit: temperature profile from LI02 and LI04 lines (INS0234.SEQ, 2004th frame)

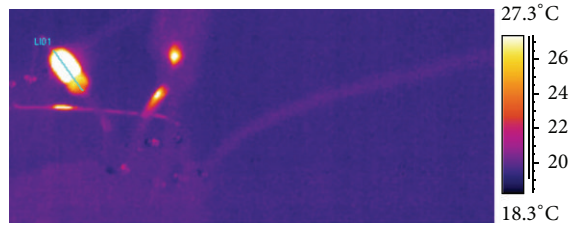

(b) Temperature in function of time for resistor in electronic circuit with pulse excitation: temperature profile from LI01 line (NEW 0010.SEQ, 640th frame)

Figure 4: Thermograms for resistor in DC electronic circuit and in electronic circuit with pulse excitation.

4. Conclusion

The limiting temperatures are those which the constituents can withstand before they oxidize, melt, or change value. The idea that there is a nonuniform distribution of temperature is demonstrated. The resistors used in this test showed excellent flame resistance. It is shown that thermography can be used during addition testing. Thermography can be used as noncontact method because it gives temperature distribution in more than a couple of points and because, in the short time, a set of measurements can be done. Because of the small area of the resistor, contact methods can easily change value of

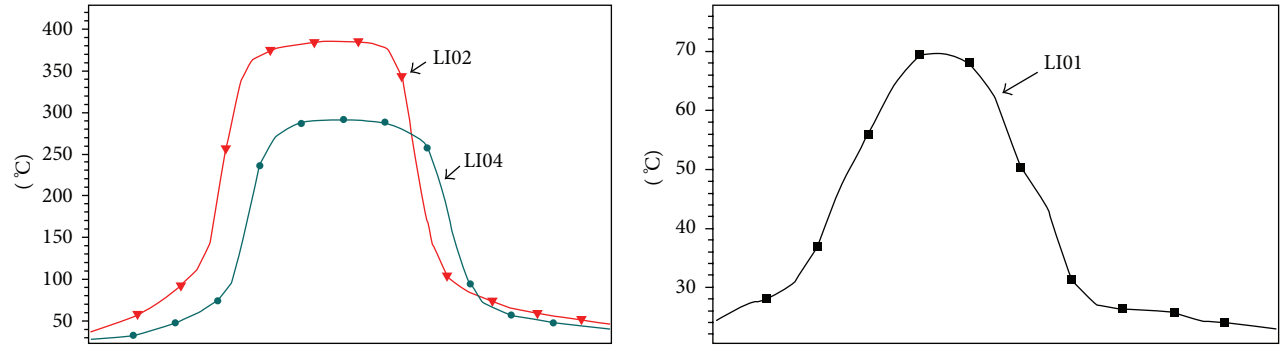

(a) Resistor temperature profile for LI02 and LI04 lines from the beginning to the end of excitation in electronic circuit with pulse excitation (INS0240.SEQ, 53rd frame)

(b) Resistor temperature profile for LI01 line during excitation (NEW 0010.SEQ, 640th frame)

Figure 5: Resistor temperature profile from different aspects.

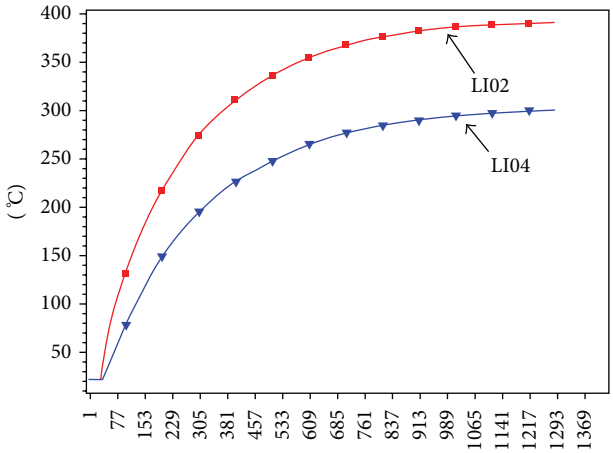

Figure 6: Temperature in function of time for resistor in DC current circuit (INS0234.SEQ, from 1st to 1000th frame).

surface temperature. So this method is worthless for this kind of measurements.

Also, it has been noticed that the resistor was cooling faster than some points of the board. Heat conduction of the resistor has an influence on the board and on the other components at the board which can be damaged, which can be the subject of the next research. The system must be considered by many aspects and that is why it is necessary to have cooling system or to pay more attention to construction of board.

Acknowledgment

The Ministry of Education, Science and Technological Development of Serbia supported this work under Contract III 43009.

References

[1] Cornell Aeronautical Laboratory, *Guide Manual of Cooling Methods For Electronic Equipment*, vol. 25, Bureau of ships Navy Department, Washington, DC, USA, 1957.

[2] F. Windrich, "Carbon contacts and resistors in printed circuit boards—a practical overview," in *Proceedings of the 1st Electronics Systemintegration Technology Conference (ESTC '06)*, pp. 788–793, Dresden, Germany, September 2006.

[3] C. J. Hallier, *Handbook of Nondestructive Evaluation*, The McGraw-Hill Companies, New York, NY, USA, 2003.

[4] A. E. Aliev, M. H. Lima, E. M. Silverman, and R. H. Baughman, "Thermal conductivity of multi-walled carbon nanotube sheets: radiation losses and quenching of phonon modes," *Nanotechnology*, vol. 21, no. 3, Article ID 035709, 2010.

[5] L. Sainiemi, K. Grigoras, I. Kassamakov et al., "Fabrication of thermal microbridge actuators and characterization of their electrical and mechanical responses," *Sensors and Actuators A*, vol. 149, no. 2, pp. 305–314, 2009.

[6] V. D. Vukić, "Minimum dropout voltage on a serial PNP transistor of a moderately loaded voltage regulator in a gamma radiation field," *Nuclear Technology & Radiation Protection*, vol. 27, no. 4, pp. 333–340, 2012.

[7] "Plastic medium power silicon NPN transistor," *Semiconductor Component Industries*, 2005, http://www.onsemi.com/.

[8] X. P. Maldague, *Theory and Practice of Infrared Technology for Nondestructive Testing*, John Wiley & Sons, New York, NY, USA, 2001.

[9] L. T. J. Elazar and B. Milanović, "Maximal temperature difference determination in pulse infrared thermography by fitting experimental results with numerical simulation curve," in *Book of the Abstract III International School and Conference on Photonics*, Photonica, Belgrade, Serbia, 2011.

[10] Lj. Tomić and M. Milinović, "Experimental research of limits for thermal modulation transfer function," *Thermal Science*, vol. 13, no. 4, pp. 119–128, 2009.

[11] "Thermalmanagement in surface-mounted resistor applications," Document Number 28844, 2011, http://www.vishay.com/.

[12] R. L. Radosavljević and A. I. Vasić, "Effects of radiation on solar cells as photovoltaic generators," *Nuclear Technology & Radiation Protection*, vol. 27, no. 1, pp. 28–32, 2012.

[13] M. R. Zdravković, A. I. Vasić, R. L. Radosavljević, M. L. Vujisić, and P. V. Osmokrović, "Influence of radiation on the properties of solar cells," *Nuclear Technology & Radiation Protection*, vol. 47, no. 2, pp. 152–154, 2011.

[14] T. T. Chow, G. N. Tiwari, and C. Menezo, "Hybrid solar: a review on photovoltaic and thermal power integration," *International*

Journal of Photoenergy, vol. 2012, Article ID 307287, 17 pages, 2012.

[15] M. Herman, M. Jankovec, and M. Topič, "Optimal I-V curve scan time of solar cells and modules in light of irradiancelevel," *International Journal of Photoenergy*, vol. 2012, Article ID 151452, 11 pages, 2012.

Hindawi Publishing Corporation
International Journal of Photoenergy
Volume 2013, Article ID 158403, 6 pages
http://dx.doi.org/10.1155/2013/158403

Research Article

Sensitivity of P-Channel MOSFET to X- and Gamma-Ray Irradiation

Milić Pejović,[1] Olivera Ciraj-Bjelac,[2] Milojko Kovačević,[2] Zoran Rajović,[3] and Gvozden Ilić[3]

[1] *Faculty of Electronic Engineering, University of Niš, Aleksandra Medvedeva 14, 18000 Niš, Serbia*
[2] *Vinča Institute of Nuclear Sciences, University of Belgrade, P.O. Box 522, 11001 Belgrade, Serbia*
[3] *Electric Power Industry of Serbia, 11000 Belgrade, Serbia*

Correspondence should be addressed to Milić Pejović; milic.pejovic@elfak.ni.ac.rs

Received 17 April 2013; Accepted 16 June 2013

Academic Editor: Predrag Osmokrovic

Investigation of Al-gate p-channel MOSFETs sensitivity following irradiation using 200 and 280 kV X-ray beams as well as gamma-ray irradiation of ^{60}Co in the dose range from 1 to 5 Gy was performed in this paper. The response followed on the basis of threshold voltage shift and was studied as a function of absorbed dose. It was shown that the most significant change in threshold voltage was in the case of MOSFET irradiation in X-ray fields of 200 kV and when the gate voltage was +5 V. For practical applications in dosimetry, the sensitivity of the investigated MOSFETs was also satisfactory for X-ray tube voltage of 280 kV and for gamma rays. Possible processes in gate oxide caused by radiation and its impact on the response of MOSFETs were also analyzed in this paper.

1. Introduction

Since the introduction of the space-charge dosimeter concept [1], radiation sensitive p-channel MOSFETs (also known as RADFETs) have been developed for applications such as space, nuclear industry and research, and radiotherapy [1–4]. Other types of dosimeters that are commonly used or are being developed for these applications include thermoluminescent dosimeters (TLDs), semiconductor diodes, and optically stimulated luminescence dosimeters (OSDLs). A comprehensive review of radiation dosimetry issues and devices can be found in [5]. The RADFET advantages over other dosimetric systems include immediate, nondestructive readout of dosimetric information, small size, low-power consumption, electric interfaces fully compatible with microprocessors, high-dose range, and very competitive price. The RADFET disadvantages are in a need for calibration in different radiation fields, relatively low resolution (starting from about 10^{-2} Gy), and nonreusability. The concept of RADFETs is based on converting threshold voltage shift, ΔV_T, induced by radiation into radiation dose D. Their behavior during irradiation is the result of complex contribution of energy-dependent processes: (1) electron-hole generation, (2) electron-hole recombination, (3) hole transport, (4) deep hole trapping, and (5) radiation-induced interface traps and positive oxide trapped charge. These processes induce threshold voltage shift ΔV_T [2]. Usually a RADFET is operated in an integral mode, where the dose is determined from the threshold voltage, before and after it is irradiated. As in the case of many detectors, they need to be calibrated to an accurate dosimetric reference, such as an ionizing chamber traceable to an accurate dosimetry calibration laboratory. The calibration factor relates the threshold voltage shift of RADFET dosimeters to the dose which is received.

The aim of this work was to investigate the sensitivity of RADFET to X-rays in kilovoltages as well as gamma rays from ^{60}Co. Also analysis of possible processes in gate oxide caused by irradiation and their impact on the sensitivity of RADFETs was conducted.

2. Materials and Methods

The RADFETs of Tyndall National Institute (earlier National Microelectronics Research Centre or NMRC for short), Cork, Ireland, have been used for analyses. Devices represent p-channel MOSFETs fabricated in Al-gate process. A single RADFET has a 1 μm thick gate oxide, grown at 1000°C in dry

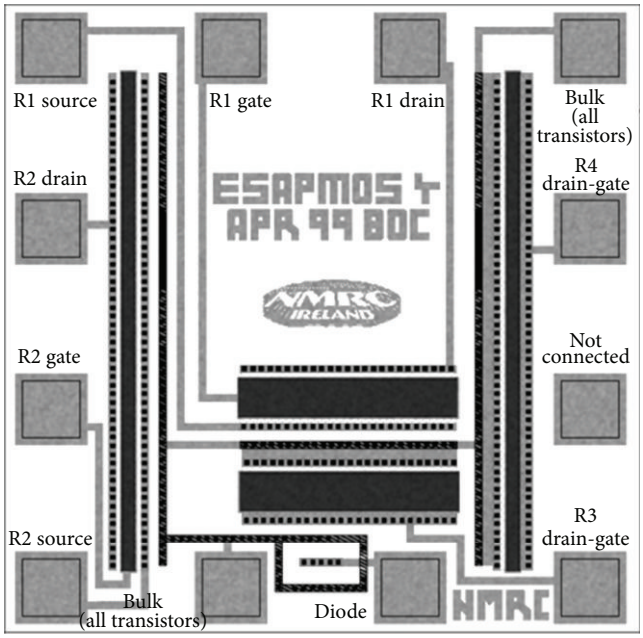

Figure 1: Diagram of a single RADFET used in this study.

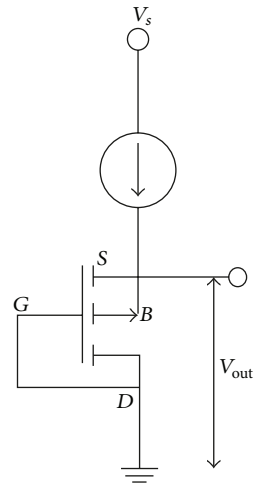

Figure 2: Electronic scheme for reader circuit measurement.

oxygen, and annealed for 15 min at 1000°C in nitrogen. The postmetalization annealing was performed at 400°C in forming gas for 60 min. Figure 1 shows a layout of a single chip. The size of the chip is $1 \times 1\,\text{mm}^2$, and there are two 300/50 and two 690/15 devices in the chip, which represent the width and length given in micrometers of the RADFETs channels, respectively. The first 300/50 device (R1) has four terminals, which are bulk, drain, gate, and source. The first 690/15 device (R2) has the same structure. The bulk connections for R1 and R2 transistors are joined together and connected to the bond pad, which thus represents the bulk connection for both transistors. In both second 300/50 (R3) device and the second 690/15 (R4) device, the gate and the drain are physically tied, and the source and the bulk are also connected. This means that R3 and R4 are two terminal devices, which enables their use in the reader circuit configuration (reader circuit configuration is explained further on in the text).

RADFETs were divided into three groups. The first RADFET group was irradiated using 200 kV (90 keV) X-rays. The second was irradiated by 280 kV (140 keV) X-rays, and the third group was irradiated by gamma rays with energies of 1.17 MeV and 1.33 MeV which derive from ^{60}Co. The irradiation was performed at the Secondary Standard Dosimetry Laboratory of the Vinča Institute of Nuclear Sciences, Vinča, Belgrade, Serbia. All measurements were conducted in a climate-controlled laboratory environment with ambient temperature of 20 ± 0.2°C. The air kerma at the reference point was measured with a calibrated vented $0.6\,\text{cm}^3$ ionization chamber (Model 30012, PTW, Freiburg, Germany) and electrometer Unidos (PTW, Freiburg, Germany). The calibration of the chamber in terms of air kerma for all radiation qualities had been performed at the Secondary Standards Dosimetry Laboratory of the International Atomic Energy Agency (Vienna, Austria), to provide traceability to BIPM (Bureau International des Poids et Mesures, the standards body that ensures worldwide uniformity of measurements and their traceability to the international system of units (SI)). The irradiation was carried out with the beam perpendicular to the gate oxide plane. The RADFETs were irradiated in the range of absorbed doses from 1 to 5 Gy in low-field mode (with zero voltages, $V_{\text{irr}} = 0$, on the gate, that is all terminals shorted together) and high-field mode (with a positive bias, $V_{\text{irr}} = +5\,\text{V}$ applied on the gate). It was emphasized that the low-field mode during irradiation could be particularly useful considering that no additional power supplies are required during irradiation, while on the other hand high-field mode increases the sensitivity and improves the linearity of the response. The threshold voltage was measured immediately after each irradiation in order to minimize drift effect.

In order to detect the absorbed dose, threshold voltage before irradiation V_{T0} and threshold voltage after irradiation V_T were determined. Threshold voltage shift ΔV_T can be expressed as $\Delta V_T = V_T - V_{T0} = AD^n$ [6], where A is the constant, n is the degree of linearity, and D is the absorbed dose. Two methods were used for determining threshold voltage. One of the methods is based on determining threshold voltage from the transfer characteristics of RADFETs in saturation, that is, as an intersection between V_G axis and extrapolation of linear region of $I_D^{1/2}$-V_G characteristics [7], where I_D is drain current and V_G is the gate voltage. The second method is based on determining threshold voltage at a fixed point of the transfer I-V characteristics using so-called reader circuit configuration (Figure 2) [8]. In this configuration the gate and the drain are connected together, as well as the bulk and the source. In this arrangement a RADFET is treated as two terminal devices. Through the channel a steady current I_D is established (in our case 10 μA), and the voltage V_{out} which corresponds to this current is then measured. This voltage represents threshold voltage [8]. Reader circuit configuration is commonly used with MOSFET dosimeters

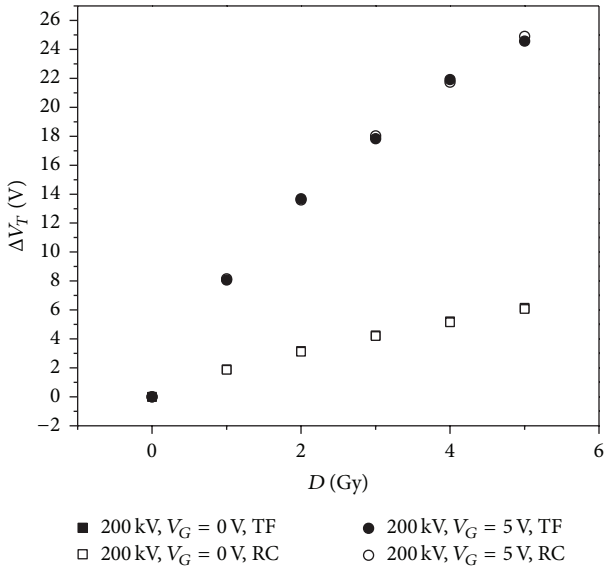

Figure 3: Extrapolated (TF) and reader circuit (RC) ΔV_T during 200 kV X-ray irradiation with zero and +5 V gate bias.

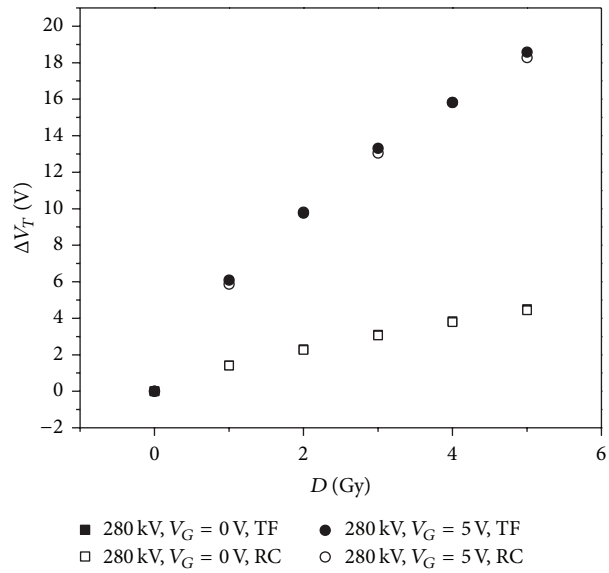

Figure 4: Extrapolated (TF) and reader circuit (RC) ΔV_T during 280 kV X-ray irradiation with zero and +5 V gate bias.

since it provides a quick V_T measurement and thus minimizes the temperature sensitivity of the reading.

Transfer characteristics were obtained by a Keithley 4200 Semiconductor Characterization System (SCS). The system is equipped with three medium-power source measuring units (4200 SMU) for I-V characterization. The source measuring units have four voltage ranges (200 mV, 2 V, 20 V, and 200 V) and three current ranges (100 μA, 100 mA, and 1 A). One of the source measuring units is equipped with a preamplifier to measure very weak currents (of the order of 1 pA).

3. Results and Discussion

Previous research into RADFETs, which are considered in this paper, was mostly based on their response to gamma irradiation for doses ranging from several tenths to several hundreds of Gy [8–14]. Our recent research [15] showed that these RADFETs are also sensitive to gamma-ray doses from 0.1 to 1 Gy. Also, our recently conducted research [16, 17] showed the possibility of reusing the RADFETs, when after the first irradiation by gamma-rays annealing is carried out at room and elevated temperature. Results shown in this paper represent a continuation of the research into widening the application of these RADFETs for cases when X-rays are used, predominantly in radiotherapy and interventional radiology.

Figures 3 and 4 show both extrapolated and reader circuit ΔV_T during X-ray irradiation of 200 kV and 280 kV, respectively. These figures show values of ΔV_T for cases when RADFET dosimeters were irradiated in low-field mode ($V_{\text{irr}} = 0$) and high-field mode ($V_{\text{irr}} = +5$ V). The agreement between extrapolated and reader circuit ΔV_T is satisfactory (less than 1%) in all cases, justifying the use of the reader circuit configuration in practical applications. It can be seen that lower X-ray energies lead to a greater change in ΔV_T for the same irradiation dose. Similar behavior is detected in

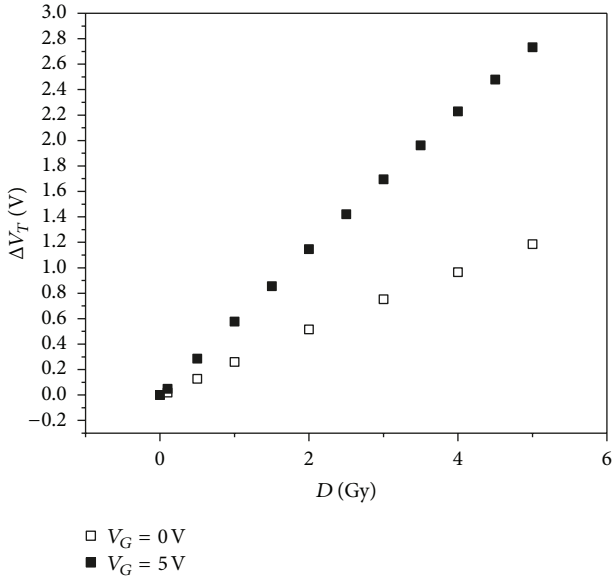

Figure 5: ΔV_T during gamma-ray irradiation with zero and +5 V gate bias.

TN-502RDI MOSFET (Thomson and Nielson Electronic Ltd, Ottawa, Canada) [18].

Also, the increase in electric field during RADFET dosimeter irradiation (Figures 3 and 4) leads to a significant change in ΔV_T value. Similar response of these RADFETs had been detected in gamma-ray irradiation cases for doses from several tenths to several hundreds of Gy [10–12].

Figure 5 presents the values of ΔV_T for gamma-ray irradiation doses up to 5 Gy when RADFETs were in a low-field mode ($V_{\text{irr}} = 0$) and also in high-field mode ($V_{\text{irr}} = +5$ V). One can notice that the behavior is the same as in the case when they are irradiated by X-rays (Figures 3 and 4);

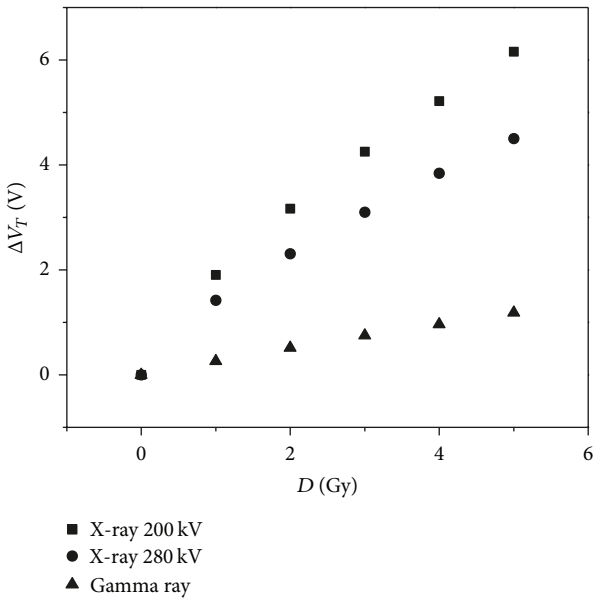

Figure 6: ΔV_T during 200 kV and 280 kV X-ray as well as gamma-ray irradiation with zero gate bias.

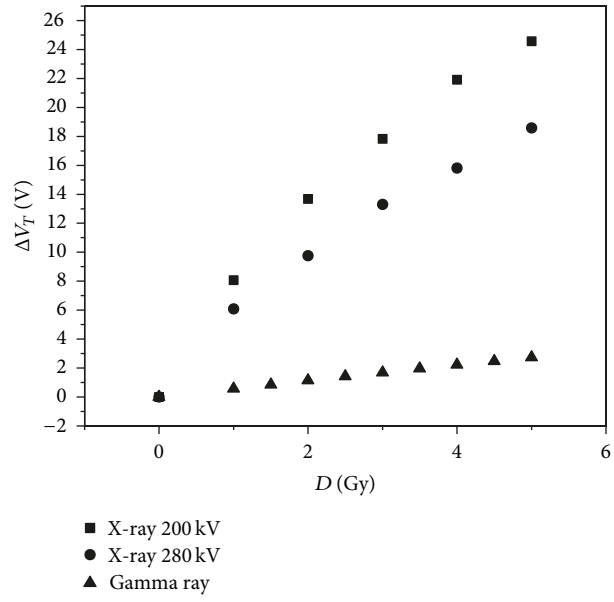

Figure 7: ΔV_T during 200 kV and 280 kV X-ray as well as gamma-ray irradiation with +5 V gate bias.

however, the increase in ΔV_T with the increase in dose is significantly lower. This shows that RADFETs response to gamma rays is significantly lower than their response to X-rays. This can clearly be seen in Figures 6 and 7 where collective values of ΔV_T as a function of dose D for $V_{\text{irr}} = 0$ and $V_{\text{irr}} = +5$ V and for both gamma and X-ray irradiation are presented. Significantly lower RADFETs response during irradiation by gamma rays than by X-rays is a consequence of different photon energies which interact with atoms in the material. Namely, X-ray photons with energies of 90 and 140 keV lead to atom ionization by photoelectric effect, and also this process is more dominant for lower photon energies (in our case this was for energies of 90 keV).

Gamma-ray photons with energies of 1.17 and 1.33 MeV lead to atom ionization by Compton's effect. Since the probability for atom ionization by photoelectric effect is significantly higher than that by Compton's effect, during X-ray irradiation a larger number of positive trap charge is formed during X-ray irradiation than during gamma-ray irradiation which directly effects the change in ΔV_T values. Moreover, ΔV_T represents the sum of threshold voltage shift $\Delta V_{\text{ot}} = q\Delta N_{\text{ot}}/C_{\text{ox}}$ caused by the presence of positive oxide trap charge and threshold voltage shift $\Delta V_{\text{it}} = q\Delta N_{\text{it}}/C_{\text{ox}}$ caused by the presence of interface traps [19], where C_{ox} is the capacitance per unit array, q is the absolute value of electron charge, and ΔN_{ot} and ΔN_{it} are the change in areal density of positive oxide trapped charge and areal density of interface traps, respectively. ΔN_{ot} and ΔN_{it} were determined from the subthreshold I-V curves using the midgap technique of McWhoter and Winokur [20]. It was shown that for doses up to 5 Gy during irradiation by both X-rays and gamma rays $\Delta N_{\text{ot}} \gg \Delta N_{\text{it}}$; that is, positive oxide trapped charge ($\Delta V_{\text{ot}}/\Delta V_T > 90\%$) has the dominant influence on threshold voltage shift.

ΔN_{ot} during X-ray irradiation by energies of 90 and 140 keV as well as during gamma irradiation is presented in Figures 8 and 9. As it can be seen from the figures lower irradiation energy leads to a higher generation of positive oxide trapped charge. Also, applied voltage on the gate during irradiation (high-field mode) generates a greater density of this charge, increasing the value of ΔV_T, that is, the sensitivity of RADFETs. Namely, it was shown [21] that during irradiation E'_γ centers are formed, which represent a weak Si–Si bond in the oxide caused by an oxygen atom vacancy between two Si atoms, each back-bonded to three oxygen atoms [22]. The E'_γ center acts as a hole trap, and it is predominantly responsible for the increase in oxide trapped charge during irradiation [23]. The number of created positive oxide trapped charge rises with the number of holes which have avoided electron recombination. In the case of irradiation in low-field mode ($V_{\text{irr}} = 0$) the electric field in the oxide is only due to the work function difference between the gate and the substrate of RADFETs (zero bias conditions are equal to gate bias of 0.3 V), so the probability for electron-hole recombination is higher than that in the case when RADFETs are in high-field mode ($V_{\text{irr}} = +5$ V). During irradiation in high-field mode the large number of holes will escape the initial recombination, which therefore further increases the probability for their capture at E'_γ centers and consequently increases in positive oxide trapped charge. This is in agreement with results shown in Figures 8 and 9.

4. Conclusion

The sensitivity of p-channel MOSFETs fabricated in Al-gate technology process (also known as RADFETs) with 1 μm thick gate oxide to kilovoltage X-ray and gamma-ray irradiation with dose range from 1 to 5 Gy was studied.

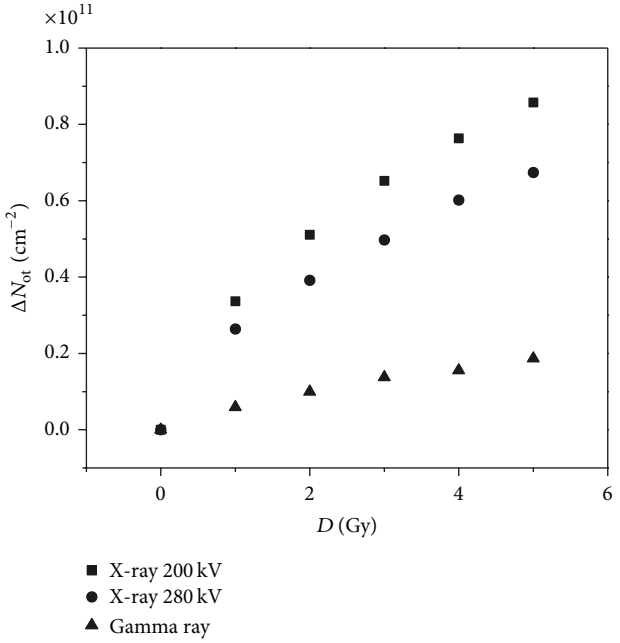

Figure 8: ΔN_{ot} during 200 kV and 280 kV X-ray as well as gamma-ray irradiation with zero gate bias.

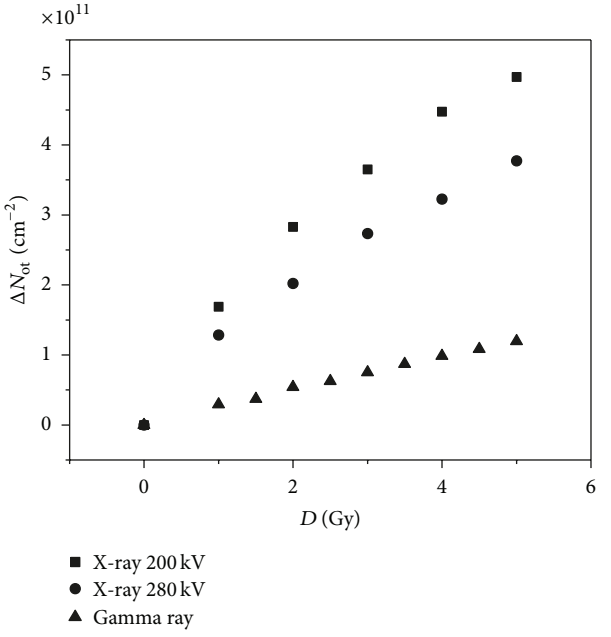

Figure 9: ΔN_{ot} during 200 kV and 280 kV X-ray as well as gamma-ray irradiation with +5 V gate bias.

The sensitivity was characterized by the threshold voltage shift determined from transfer characteristics in saturation and reader circuit measurements. Results have shown that the response is greater when RADFETs are irradiated by X-rays. It was concluded that this is a consequence of the dominant influence of photoelectric effect in X-ray cases in comparison to Compton's effect in gamma-ray cases. In order to optimize RADFETs fabrication process, the analysis of defects formed during irradiation was performed. It was shown that positive oxide trapped charge which is formed by trapping holes at E'_γ centers has the dominant effect on threshold voltage shift. The centers are formed during irradiation and their number increases with the decrease in photon energies. According to the results it can be concluded that a satisfactory response of these RADFETs could be achieved for significantly lower doses especially in X-ray cases, which would enable their efficient application for measuring low doses order of several mGy used in diagnostic and interventional radiology. Taking this into consideration our further research will focus on the application of RADFETs for measuring low doses for a wide range of X-rays.

Acknowledgment

The work presented in this paper has been supported by the Ministry of Education and Science of Republic of Serbia under Contract no. 177007.

References

[1] A. Holmes Siedle, "The space charge dosimeter: general principles of a new method of radiation detection," *Nuclear Instruments and Methods*, vol. 121, no. 1, pp. 169–179, 1974.

[2] A. Holmes-Siedle and L. Adams, "RADFET: a review of the use of metal-oxide-silicon devices as integrating dosimeters," *Radiation Physics and Chemistry*, vol. 28, no. 2, pp. 235–244, 1986.

[3] A. Kelleher, N. McDonnell, B. O'Neill, L. Adams, and W. Lane, "The effect of gate-oxide process variations on the long-term fading of PMOS dosimeters," *Sensors and Actuators A*, vol. 37-38, pp. 370–374, 1993.

[4] D. J. Gladstone, X. Q. Lu, J. L. Humm, H. F. Bowman, and L. M. Chin, "A miniature MOSFET radiation dosimeter probe," *Medical Physics*, vol. 21, no. 11, pp. 1721–1728, 1994.

[5] G. F. Knoll, *Radiation Detection and Measurement*, John Wiley & Sons, New York, NY, USA, 1989.

[6] M. M. Pejović, M. M. Pejović, and A. B. Jaksic, "Contribution of fixed oxide traps to sensitivity of pMOS dosimeters during gamma ray irradiation and annealing at room and elevated temperature," *Sensors and Actuators A*, vol. 174, no. 1, pp. 85–90, 2012.

[7] L. J. Asensio, M. A. Carvajal, J. A. López-Villanueva, M. Vilches, A. M. Lallena, and A. J. Palma, "Evaluation of a low-cost commercial mosfet as radiation dosimeter," *Sensors and Actuators A*, vol. 125, no. 2, pp. 288–295, 2006.

[8] A. Kelleher, M. O'Sullivin, J. Ryan, B. O'Neal, and W. Lane, "Development of the radiation sensitivity of pMOS dosimeters," *IEEE Transactions on Nuclear Science*, vol. 39, no. 3, pp. 342–346, 1992.

[9] A. Kelleher, N. McDonnell, B. O'Neill, W. Lane, and L. Adams, "Investigation into the re-use of PMOS dosimeters," *IEEE Transactions on Nuclear Science*, vol. 41, no. 3, pp. 445–451, 1994.

[10] A. Jaksic, G. Ristic, M. Pejović, A. Mohammadzadeh, C. Sudre, and W. Lane, "Gamma-ray irradiation and post-irradiation responses of high dose range RADFETs," *IEEE Transactions on Nuclear Science*, vol. 49, no. 3, pp. 1356–1363, 2002.

[11] A. Haran, A. Jakšić, N. Refaeli, A. Eliyahu, D. David, and J. Barak, "Temperature effects and long term fading of implanted

and unimplanted gate oxide RADFETs," *IEEE Transactions on Nuclear Science*, vol. 51, no. 5, pp. 2917–2921, 2004.

[12] M. M. Pejović, M. M. Pejović, and A. B. Jakšić, "Radiation-sensitive fieldeffect transistor response to gamma-ray irradiation," *Nuclear Technology and Radiation Protection*, vol. 26, no. 1, pp. 25–31, 2011.

[13] M. M. Pejović, S. M. Pejović, E. Ć. Dolićanin, and D. Lazarević, "Gamma-ray irradiation and post-irradiation at room and elevated temperature response of pMOS dosimeters with thick gate oxides," *Nuclear Technology and Radiation Protection*, vol. 26, no. 3, pp. 261–265, 2011.

[14] M. M. Pejović, M. M. Pejović, and A. B. Jaksic, "Contribution of fixed oxide traps to sensitivity of pMOS dosimeters during gamma ray irradiation and annealing at room and elevated temperature," *Sensors and Actuators A*, vol. 174, no. 1, pp. 85–90, 2012.

[15] S. Pejović, P. Bosnjakovic, O. Ciraj-Bjelac, and M. Pejović, "Characteristics of a pMOS suitable for use in radiotherapy," *Applied Radiation and Isotopes*, vol. 77, pp. 44–49, 2013.

[16] M. M. Pejović, M. M. Pejović, A. B. Jaksic, K. D. Stankovic, and S. A. Markovic, "Successive gamma-ray irradiation and corresponding post-irradiation annealing of pMOS dosimeters," *Nuclear Technology and Radiation Protection*, vol. 27, no. 4, pp. 341–345, 2012.

[17] M. M. Pejović, M. M. Pejović, and A. B. Jaksic, "Response of pMOS dosimeters on gamma-ray irradiation during its re-use," *Radiation Protection Dosimetry*, 2013.

[18] C. Ehringfeld, S. Schmid, K. Poljanc, Ch. Kirisits, H. Aiginger, and D. Georg, "Application of commercial MOSFET detectors for in vivo dosimetry in the therapeutic X-ray range from 80 kV to 250 kV," *Physics in Medicine and Biology*, vol. 50, no. 2, pp. 289–303, 2005.

[19] M. Nenoi, Ed., *Current Topics in Ionizing Radiation Research*, InTech, Rijeka, Croatia, 2012.

[20] P. J. McWhorter and P. S. Winokur, "Simple technique for separating the effects of interface traps and trapped-oxide charge in metal-oxide-semiconductor transistors," *Applied Physics Letters*, vol. 48, no. 2, pp. 133–135, 1986.

[21] A. J. Lelis, H. E. Boesch, T. R. Oldham, and F. B. McLean, "Reversibility of trapped hole annealing," *IEEE Transactions on Nuclear Science*, vol. 35, no. 6, pp. 1186–1191, 1988.

[22] F. J. Feigl, W. B. Fowler, and K. L. Yip, "Oxygen vacancy model for the E'_γ center in SiO_2," *Solid State Communications*, vol. 14, no. 3, pp. 225–229, 1974.

[23] P. M. Lenahan and P. V. Dressendorfer, "Hole traps and trivalent silicon centers in metal/oxide/silicon devices," *Journal of Applied Physics*, vol. 55, no. 10, pp. 3495–3499, 1984.

Hindawi Publishing Corporation
International Journal of Photoenergy
Volume 2013, Article ID 158792, 7 pages
http://dx.doi.org/10.1155/2013/158792

Research Article

Radiation Hardness of Flash Memory Fabricated in Deep-Submicron Technology

Bojan Cavrić,[1] Edin Dolićanin,[2] Predrag Petronijević,[2] Milić Pejović,[3] and Koviljka Stanković[2]

[1] *Life Robinson Private Hospital, Hospital Road, P.O. Box 37, Randfontein 1760, South Africa*
[2] *Faculty of Electrical Engineering, University of Belgrade, Bulevar Kralja Aleksandra 73, 11000 Belgrade, Serbia*
[3] *Faculty of Electronic Engineering, University of Niš, Aleksandra Medvedeva 14, 18000 Niš, Serbia*

Correspondence should be addressed to Koviljka Stanković; kstankovic@etf.rs

Received 5 April 2013; Accepted 25 May 2013

Academic Editor: Momčilo Pejović

This paper discusses the current problem of the electronic memory reliability in terms of the ionizing radiation effects. The topic is actual since the high degree of components' miniaturization integrated into the flash memory causes the extreme sensitivity of this memory type to the ionizing radiation effects. The effects of ionizing radiation may cause changes in stored data, or even the physical destruction of the components. At the end, the experimentally and numerically obtained effects of radiation on specific flash memories are shown and discussed. The results obtained by laboratory and numerical experiments showed good agreement with each other and with the theoretically expected results.

1. Introduction

The miniaturization of electronic components includes their production by using extremely thin layers that build a composite-packaged structure capable of performing complex functions. This way of creating electronic devices makes them very irresistible to ionizing radiation in the conditions under which they operate, and in this respect, the radiation hardness of memory components is especially important [1].

The aim of the paper is to investigate, theoretically, experimentally, and numerically, the radiation hardness of flash memory. Flash memory plays an important role in the control of solar cells in cosmic application, since they are main components of devices which control all operations of solar cells in the space. In this way, the flash memory devices are exposed to intense primary cosmic radiation, so the prediction of their applicability limits is the main task of the research.

Flash memory was developed by the Japanese researcher Fujio Masuoka (1984) in the laboratories of the company Toshiba. Flash memory has an easy reprogramming ability obtained by improving EEPROM memory architecture. Flash memory bases its work on a modified MOSFET transistor with induced channel which has an insulated gate between the common gate and substrate [2, 3] (Figure 1).

The operating mode of the transistor with an interrupted gate contact is determined by the preceding amount of charge that existed on the gate. This analysis is the result of the idea of the construction of a new type of the memory cell in the form of a transistor with two gates, which, besides the normal gate with a galvanic contact, also has an isolated inner gate. Based on the n-MOSFET with an isolated gate, the EPROM memory is built, after which the EEPROM memory follows, and at the end, there is flash memory.

2. Numerical Simulation of the Radiation Interaction with Materials by Using Monte-Carlo Method

The Monte-Carlo method is a numerical method for solving complex, mathematical, statistical, and physical problems using random selection of samples. The main goal of this method is the formation of a stochastic model which should

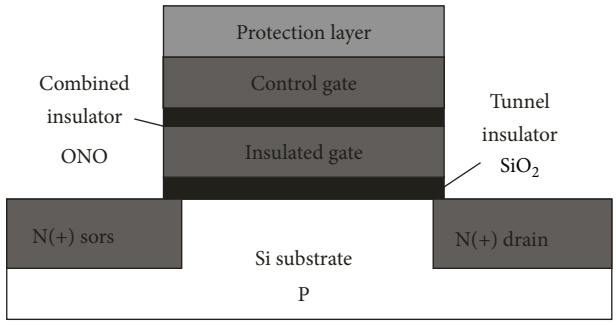

Figure 1: The structure of the memory cells with control (external) and insulated gate.

be consistent with the real problem or represents its direct simulation.

The basic assumption for the application of the Monte-Carlo method is the possibility of generating a sequence of random numbers, that is, a sequence of independent random variables on the interval $(0, 1)$. Starting from the sequence of random numbers, it is possible to generate a sequence of random distribution [4].

The simulation of passing the particles, electrons, positrons, and photons, is based on the stochastic nature of the collision processes. Between two successive collisions, a particle exceeds a random path determined by the total macroscopic cross-section and distribution density. At each collision, the particle loses energy and the energy loss is determined from the corresponding distribution density. After the collision, the particle changes its direction compared to the direction before the collision, and the angle of deviation is a random value which is selected by the angular distribution [5, 6]. On its path, the particle loses energy at the value in which considered the particle is absorbed, or with some energy leaves the medium. All collisions on the path of the particle belong to its history. By repeating the history for many times, the spatial and energy distribution of particles in the medium is obtained. The absorbed energy in the medium changes the properties of the substance and the resulting changes affect the particle passage of the "following" history because the temperature and density of the substance are changing, and in the nuclear reactions, even the isotopic composition of the substance is changed. A simple Monte-Carlo algorithm assumes that all processes are described mathematically, the transition probabilities of the particles are prepared from the previous to the next state of the phase space, an efficient algorithm of random selection of probabilities is prepared, that is an available quick and reliable model which describes the complex geometry space, and, finally, the used computer must have a reliable generator of pseudorandom numbers. When all these conditions are fulfilled, the algorithm can be translated into a computer program and simulated particles passage.

The input information required for the Monte-Carlo simulation includes

(1) dimensions of the source and the distance from the detector;

(2) dimensions of the detector housing and the sensitive and nonsensitive zones of the detector;

(3) elemental composition and density of materials through which photons and particles pass;

(4) attenuation coefficient of photons for all materials;

(5) sections for different photon interactions in the detector material as a function of energy and dispersive angle;

(6) information of the transport of electrons and positrons through the detector material.

The results of Monte-Carlo calculations agree with the measured values for the corresponding configuration, in the best case about ±5%. The uncertainty of the experimental value is typically less than ±5%, so these discrepancies must be attributed to the systematic errors or uncertainty of calculations [7].

3. Experiment

Experimental setting is applied to the determination of the gamma rays effect on the flash memories, which are the dominant types of long-term memory, and these memories are used in many applications that require electronic parts that work in terms of radiation.

The interaction of radiation with insulators that surround the floating gate (FG) damages the properties of memory cells, increases the possibility of losing the stored content, and damages the performance or lacks performance functionality [8, 9]. The scope of the gamma radiation effects on the sequence of flash memory cells depends primarily on the absorbed dose. Therefore, these effects are called effects of total ionized dose (TID). The functionality of flash memories which are exposed to radiation decreases with the accumulation of TID [10].

The experiment explores the effects of gamma radiation on the cell sequence of four different flash memories. The memories are produced by different manufacturers, and all of them are currently available on market. The obtained results are interpreted in terms of the interaction of gamma rays with the internal structure of memory cells. The tested samples of memory are also compared with the data obtained after gamma radiation.

For the purposes of the performed experiment, NOR memories from different manufacturers were subjected to radiation. Conclusions made from the analysis of experimental results are also valid for NAND flash memories. Therefore, the results are related to the effects of radiation which appear at the level of FG cells, regardless of the specific sequence architecture.

The research was conducted on four types of flash memory, with a capacity of 512 Kbit, including Numonyx M25P05-A (marked as Type 1), Atmel AT25F512B (marked as Type 2), SST SST25VF512 (marked as Type 3), and Macronix MX25L5211E (marked as Type 4). Type 1 memory has TSS0P8 packaging, while the other three have SOIC package.

All the tested memory chips are programmed by the scheme called "chessboard," with alternately switching on/off

Figure 2: Standard Co-60 radiation field used in the Laboratory for Radiation Protection at the Institute of Nuclear Sciences "Vinča."

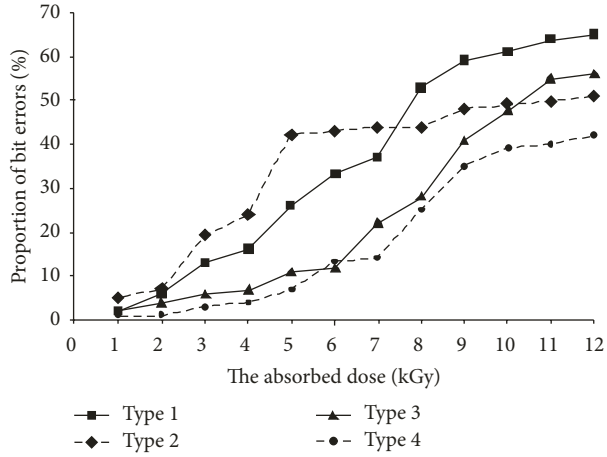

Figure 3: Registered percentage of bit errors depending on the absorbed dose for the four analyzed types of flash memory.

the cells (alternately writing 1 and 0) before radiation, while chip connections remain nonpolarized during the radiation. In this way, the influence of gamma radiation on the memory cells and the ability to keep the stored data is examined.

Radiation was carried out on Co-60 in the Laboratory for Radiation Protection of the Institute of Nuclear Sciences "Vinča" in Belgrade, Serbia. The unit of radiation field is determined by the value of absorbed dose in air at different distances from the source of radiation. The absorbed dose of memory samples is determined by changing the position of the sample in the field during radiation. The absorbed dose in silicon is calculated from the absorbed dose in the air by setting the energy absorption coefficient for the average energy of Co-60, which is exposed to the effects of gamma rays, to the value of 1.25 MeV. All measurements were performed at room temperature. Figure 2 shows the photography of the standard radiation field used in the Laboratory for Radiation Protection at the Institute of Nuclear Sciences "Vinča."

Five samples of four different types of memory were subjected to gamma rays. The absorbed dose ranged from 1 kGy to 12 kGy, with a rise of 1 kGy. The presented results were obtained by averaging all the experimental results for all the five samples. The measurement uncertainty of obtained results was about 10% for all the samples.

4. Results and Discussion

To perform the experiments, NOR memories from different manufacturers were selected. Conclusions are also applicable to the NAND memories because they are related to the effects of radiation on the cell level with a floating gate, regardless of the architecture of the memory matrix.

4.1. TID Effects (Exposure to Gamma Rays). Four types of flash memory programmed in "chessboard" scheme, in which adjacent cells are alternately in "on" and "off" states before radiation, have been analyzed. During radiation, the pins of chips were free. In this way, the influence of gamma rays on the ability to hold the stored data (retention) of tested memory, that is the ability of flash memory to preserve the written content in the absence of the power supply, is examined. The radiation field at the cobalt unit is characterized by values of the intensity of the absorbed dose in air at different distances from the Co-60 source.

The results presented in Figure 3 were obtained as average values for groups of 5 chips with the measurement uncertainty of results about 10% for all the groups of chips.

The graph in Figure 3 shows the percentage change in bit errors (i.e., the ratio of the bits number and the disturbance compared to the original written state and the total number of bits, which is 512000) with an increasing absorbed dose, up to a dose of about 9 kGy, after which the saturation of the errors percentage occurs. In the memory of Type 2, a slightly steeper increase in the number of bit errors occurred in a lower dose range than in the other three memories. Specifically, the saturation of Type 2 has occurred at a dose of about 5 kGy. The memory of Type 1 showed the highest percentage of bit errors (65%) at the maximum dose (12 kGy), while the memory of Type 4 had the lowest number of errors (42%) at the maximum dose. Saturation is the least pronounced in the memory of Type 3, which means that with this type of memory errors could be increased at doses greater than 12 kGy.

The graph in Figure 4 shows the results of recovery for the examined four types of flash memories at room temperature after exposure to a maximum dose of 12 kGy. The percentage of bit errors was measured once a week for nine weeks after radiation.

In all the four types of memory, the temperate recovery of the initially written content is observed. By the end of 9 weeks, Type 4 memory had the lowest percentage of the remaining errors (17%), while the maximum bit errors remained in the memory of Type 2 (32%).

4.2. Damages Caused by Displacement (Simulation of the Ions Passage). For the numerical simulation of the radiation effects on the films of superinsulators, the Monte-Carlo method is used, based on the stochastic nature of the interactions of radiation with the structural units of the material environment through which the radiation passes. In real

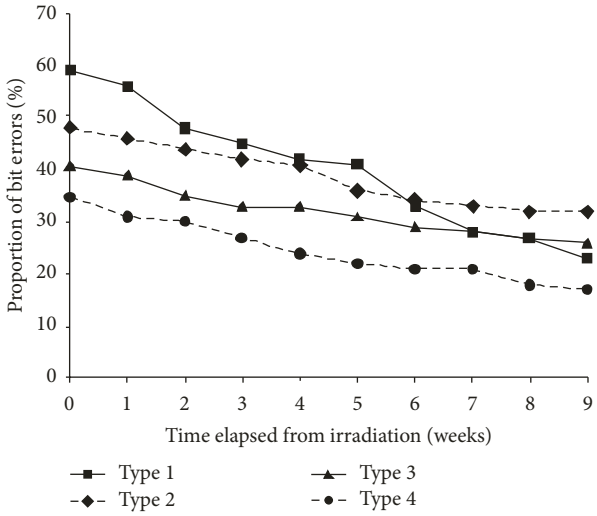

Figure 4: Recovery of the four tested types of flash memory at room temperature for nine weeks after exposure to a maximum dose of 12 kGy.

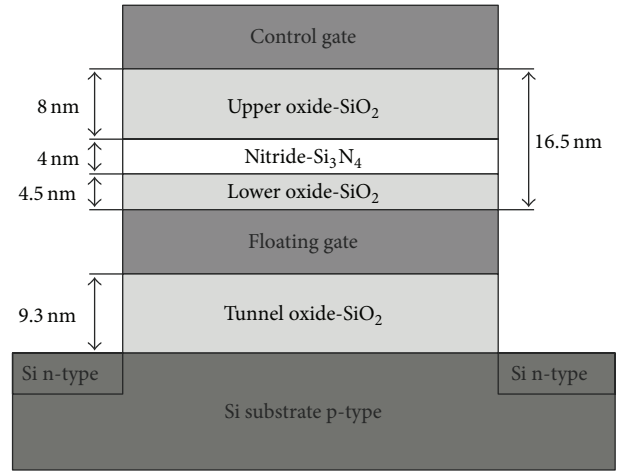

Figure 5: Model of the flash memory cell used in the numerical simulation of the ions passage.

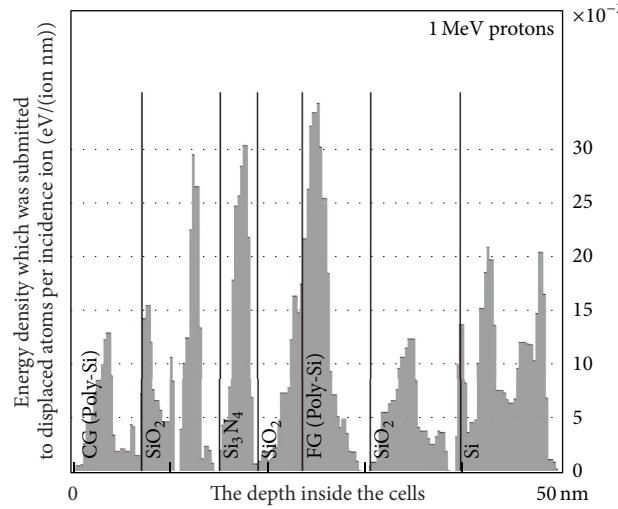

Figure 6: Energy density of incident protons per unit of depth which is submitted to atoms displaced in the layers of the flash cell (expressed per incident proton) for 1 MeV protons.

physical experiments, the measurements uncertainty is evaluated and calculated when the experiment ends. Numerical simulations of the same physical process with Monte-Carlo methods can be performed with predetermined uncertainty, following an adequate number of primary particles of radiation, as well as secondary particles produced in the material.

Monte-Carlo simulations of ion beams passing through the material in the superinsulator state are implemented in the TRIM module of the software package SRIM [11]. This program allows the calculation of the energy loss of incident radiation through ionization, photon excitation of grid, and displacement of atom material [12].

An ion beam in the simulations was chosen to match the radiation field in which the electronic components often are ions of hydrogen, helium, lead, then phosphorus, boron, and arsenic. SRIM limits calculations on the monoenergetic beams, but for repeated simulations, energy of each ion species is varied due to the range of values represented in practice.

A simulation of the ions passage is designed to compare the radiation damage by displacing atoms in the dielectric ONO and tunnel oxide. The dimensions of the layers used in the simulations are given in Figure 5 and taken from [13].

ONO dielectric is presented in the form of a three-layered structure with upper and lower oxide (SiO_2) and Si_3N_4 layer between them. Simulations were performed with the ion beam, which normally falls on the upper surface of the cells (control gate).

The simulation results are presented in Figures 6, 7, and 8; the unit is on the x-axis, which corresponds to a depth within the flash cell. The incident beam in all cases is simulated with 10^4 ions.

Comparing the results in Figures 6 and 7(a), it can be concluded that due to nanometre dimensions, flash memory cells are much less sensitive to the proton effects with MeV energies than the protons with energies in the keV field. The energy density of incident protons per unit of depth, which is delivered to atoms displaced in the layers of the flash cell, is much lower for 1 MeV than for 10 keV protons.

The high degree of the flash cell immunity to the effects of particle radiation in MeV energy field is expressed by the results for 2 MeV alpha particles given in Figure 8.

The divergence of an alpha particle beam is negligible throughout the entire structure of the cell. Displaced atoms are spatially concentrated, with an almost straight-line path of alpha particles, and the number of lateral branches, in which the secondary displacement occurs, is small (Figure 8(a)). Except on the separated surface of the nitride layer and lower oxide in ONO dielectric, the energy loss of alpha particles due to the displacement of atoms is almost negligible. The results

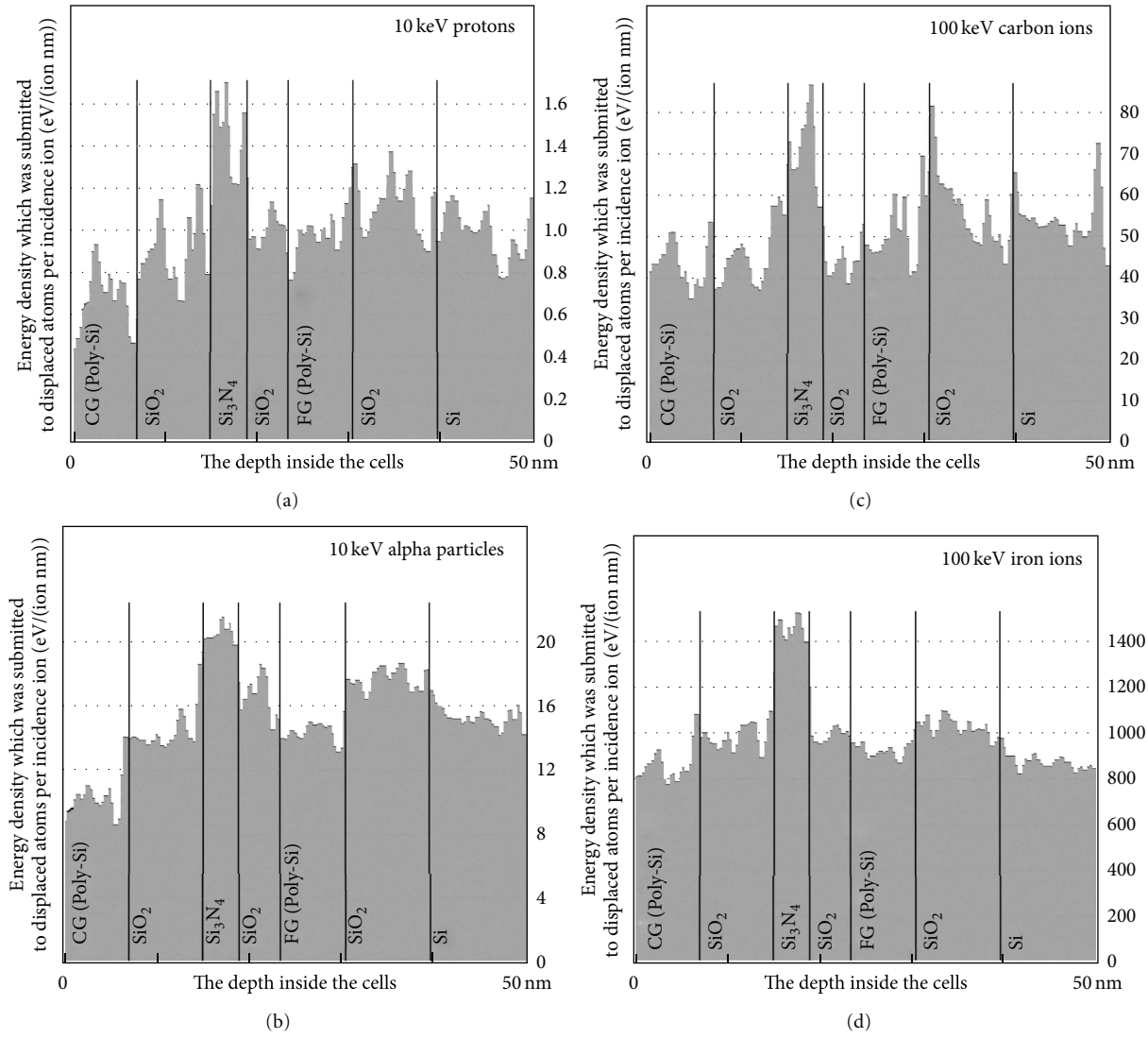

Figure 7: Density of ion energy (per unit of depth), which was submitted to atoms displaced in the layers of the flash cell (expressed per incident ion) for (a) 10 keV protons, (b) 10 keV α particles, (c) 100 keV ions of C, and (d) 100 keV ions of Fe.

in Figures 8(b) and 8(c) show that the density of vacancies produced by the incident beam are much lower for 2 MeV than for 10 keV particles.

5. Conclusion

In the analysis of TID effects, the ability of keeping written data of the four models of flash memory after exposure to gamma rays is examined. The increase in the number of bit error rate with increasing the absorbed dose can be attributed to the effects of tunnel oxide radiation and oxide which separates the floating gate in the cell of flash memory. The theoretical analysis of these effects shows that under the influence of radiation, the value of the threshold voltage is reduced for programmed cells, while in the cells that have been erased, it is increased. This means that both states are subject to disturbance which is, while reading the memory, registered as bit errors. The percentage of bit errors did not differ much in the four tested types of memory, which indicates that the sensitivity to gamma rays depends primarily on the thickness of the dielectric layers of cells, which is about the same for all tested memories, since they belong to the same generation of technology.

Partial recovery of errors caused by radiation, in a few weeks at room temperature, was observed in all the four types of memory. This explains recovery with the gradual compensation of charge trapped in the tunnel oxide, with electrons tunneling from the substrate.

An analysis of the effects due to the displacement of atoms was performed using a numerical simulation of the

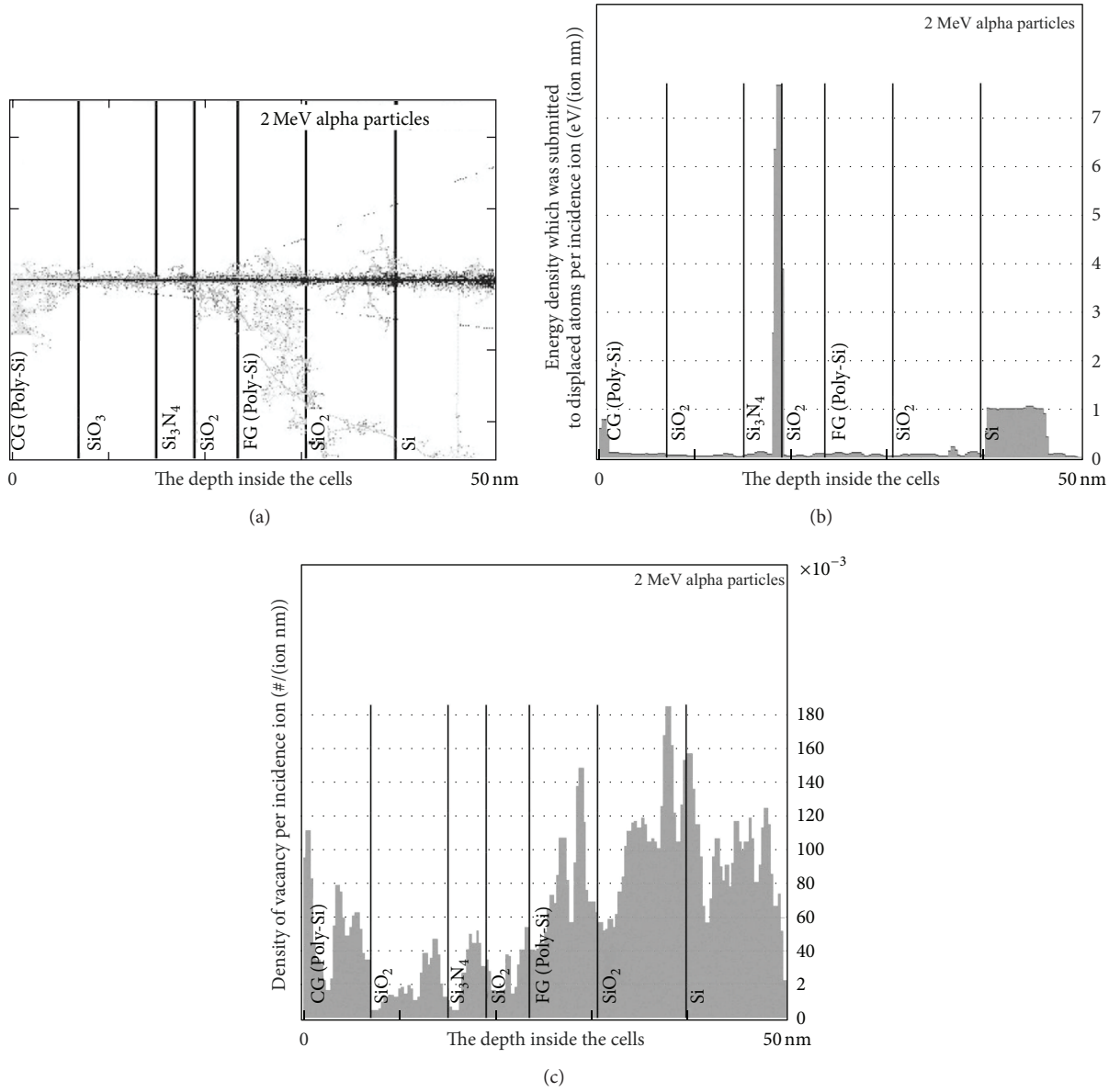

Figure 8: Results for the incident beam of 2 MeV: (a) traces of particles (dark traces correspond to alpha particles, while the lighter traces are the path of the displaced ions Si, O, and N), (b) energy density of alpha particles submitted to displaced atoms, and (c) density of vacancy caused by displacement of atoms.

ions passage through the cell of flash memory. Due to the low thickness, the layers of the flash memory cells are insensitive to ion energies greater than approximately 1 MeV. The simulation of radiation transport, however, shows that for a given type and energy of ions in some layers of the cells a considerable number of displaced atoms and vacancies occur. Damages caused by such displacement, which occur in the structure of flash cells, can affect the whole range of its parameters (threshold voltage, leakage current, access time, and time of writing data), as well as preventing the reprogramming of the cell. Some types of errors may occur even for devices that are not biased during the time that heavy ions strike occurs. Error detection and correction may be a viable way to recognize this type of failure mechanism, but it is also necessary to understand how and why the errors are generated within the device, as well as whether internal errors in the memory controller will affect their operation in the space.

Acknowledgment

The Ministry of Education, Science and Technological Development of the Republic of Serbia supported this work under Contract 171007.

References

[1] M. Vujisić, K. Stanković, E. Dolićanin, and P. Osmokrović, "Radiation hardness of COTS EPROMs and EEPROMs," *Radiation Effects and Defects in Solids: Incorporating Plasma Science and Plasma Technology*, vol. 165, no. 5, pp. 362–369, 2010.

[2] J. E. Velazquez-Perez and Y. G. Gurevich, "Charge-carrier transport in thin film solar cells: new formulation," *International Journal of Photoenergy*, vol. 2011, Article ID 976063, 2011.

[3] S. Sladić, S. Skok, and D. Nedeljković, "Efficiency considerations and application limits of single-phase active power filter with converters for photoenergy applications," *International Journal of Photoenergy*, vol. 2011, Article ID 643912, 2011.

[4] M. Vujisić, K. Stanković, and P. Osmokrović, "A statistical analysis of measurement results obtained from nonlinear physical laws," *Applied Mathematical Modelling*, vol. 35, no. 7, pp. 3128–3135, 2011.

[5] Holmes-Siedle and L. Adams, *Handbook of Radiation Effects*, Oxford Science Publication, Oxford, UK, 1993.

[6] G. C. Messenger and M. S. Ash, *The Effects of Radiation on Electronic Systems*, Van Nostrand Reinhold, New York, NY, USA, 2nd edition, 1991.

[7] K. D. Stanković, "Influence of the plain-parallel electrode surface dimensions on the type a measurement uncertainty of gm counter," *Nuclear Technology and Radiation Protection*, vol. 26, no. 1, pp. 39–44, 2011.

[8] M. Zdravković, A. Vasić, R. Radosavljević, M. Vujisić, and P. Osmokrović, "Influence of radiation on the properties of solar cells," *Nuclear Technology & Radiation Protection*, vol. 26, no. 2, pp. 158–163, 2011.

[9] R. Radosavljević and A. Vasić, "Effects of radiation on solar cells as photovoltaic generators," *Nuclear Technology & Radiation Protection*, vol. 27, no. 1, pp. 28–32, 2012.

[10] M. Vujisić, N. Marjanović, I. Fetahović, K. Stanković, and P. Osmokrović, "Influence of radiation on titanium dioxide mermistors," *Scientific Publications of the State University of Novi Pazar Series A: Applied Mathematics, Informatics & Mechanics*, vol. 4, no. 1, pp. 75–82, 2012.

[11] J. F. Ziegler, J. P. Biersack, and M. D. Ziegler, "SRIM (The Stopping and Range of Ions in Matter)," http://www.srim.org/.

[12] J. R. Srour, C. J. Marshall, and P. W. Marshall, "Review of displacement damage effects in silicon devices," *IEEE Transactions on Nuclear Science*, vol. 50, no. 3, pp. 653–670, 2003.

[13] A. Gasperin, A. Paccagnella, G. Ghidini, and A. Sebastiani, "Heavy ion irradiation effects on capacitors with SiO_2 and ONO as Dielectrics," *IEEE Transactions on Nuclear Science*, vol. 56, no. 4, pp. 2218–2224, 2009.

Hindawi Publishing Corporation
International Journal of Photoenergy
Volume 2013, Article ID 170269, 5 pages
http://dx.doi.org/10.1155/2013/170269

Research Article

Radiation Damage in Electronic Memory Devices

Irfan Fetahović,[1] Milić Pejović,[2] and Miloš Vujisić[3]

[1] *State University of Novi Pazar, 36300 Novi Pazar, Serbia*
[2] *Faculty of Electronic Engineering, University of Niš, 18000 Niš, Serbia*
[3] *Faculty of Electrical Engineering, University of Belgrade, 11120 Belgrade, Serbia*

Correspondence should be addressed to Irfan Fetahović; irfanfetahovic@gmail.com

Received 10 April 2013; Accepted 25 May 2013

Academic Editor: Predrag Osmokrovic

This paper investigates the behavior of semiconductor memories exposed to radiation in order to establish their applicability in a radiation environment. The experimental procedure has been used to test radiation hardness of commercial semiconductor memories. Different types of memory chips have been exposed to indirect ionizing radiation by changing radiation dose intensity. The effect of direct ionizing radiation on semiconductor memory behavior has been analyzed by using Monte Carlo simulation method. Obtained results show that gamma radiation causes decrease in threshold voltage, being proportional to the absorbed dose of radiation. Monte Carlo simulations of radiation interaction with material proved to be significant and can be a good estimation tool in probing semiconductor memory behavior in radiation environment.

1. Introduction

All devices used by mankind are constantly exposed to different kinds of radiation originating from natural sources, but also from artificial manmade sources. Increasing the level of integration of electronic components and miniaturization trends may have negative influence onto the component sensitivity to ionizing radiation. Radiation defects can also occur in a process of a very large scale integrated circuits fabrica tion, since the process often includes bombardment with high-energy ions and photons.

The aim of this paper is to examine the behavior of semiconductor memories exposed to radiation in order to establish their applicability in a radiation environment. The experimental procedure has been used to test radiation hardness of commercial semiconductor memories. Different types of memory chips have been exposed to indirect ionizing radiation by changing radiation dose intensity. The effect of direct ionizing radiation on semiconductor memory behavior has been analyzed by using Monte Carlo simulation method.

2. Radiation Effects in Basic Semiconductor Electronic Devices

Changes and disruptions of irradiated memory characteristics depend on type of radiation, speed of energy deposition in semiconductor device, and the type of material the semiconductor structure is made of. Radiation effects can be divided into transient and permanent, depending on time an irradiated device needs to recover from radiation and restore its functionality [1–4].

False signals and false logic states in digital electronic circuits are transient radiation effects. These effects do not cause destructive changes; they often disappear after a short period of time or can be removed by applying simple measures. Therefore, transient effects can induce a type of errors named after soft errors. The examples of transient effects are disruptions caused by high radiation dose (dose-rate effects) or by heavy charged particle passing through a component (single event upsets—SEU) [5, 6]. Permanent radiation effect, or hard error, is a change in semiconductor

structure after its component is being irradiated and cannot be easily resolved. Sometimes, these errors can be reversible after a long period of time. The examples of hard errors are latchup and snapback; they cannot be resolved without stopping the component [4, 5]. The component destruction is hard error because impaired functionality cannot be restored.

3. Radiation Damages in Semiconductor Memories

Semiconductor memories are often a limiting factor in applying a device in a radiation environment since they are most prone to damage when exposed to radiation, comparing to other semiconductor integrated circuits [5, 6].

Memory errors can occur under influence of a cosmic radiation or alpha particles emitted from memory chip package. Thorium and uranium isotopes' radiation, as well as radiation of alpha emitters, can lead to soft error occurrences in memories. These errors are often manifested as logic state disturbances of memory cells or disturbances in sense amplifiers; it is seldom a function disturbance of peripheral circuits in a memory chip. In cosmic applications, light and heavy ions can influence the semiconductor memories' characteristics, causing both soft and hard errors.

In different parts of memory chip, radiation can induce sudden occurrence of charged carriers—electrons and holes. These particles generate false currents that might disturb data written into the chip or influence data processing. These types of disturbances in memory are called soft errors, and when induced by radiation they are called transient upsets. Single event upsets (SEU), caused by heavy charged particle passing through memory, are very significant for radiation compatibility of semiconductor memories, since frequent occurrence of single event upsets has a negative impact on component's mean time to failure [6–8].

4. The Experiment

4.1. Gamma Radiation Experimental Procedure. Radiation effects on EPROM and EEPROM semiconductor memories have been tested by exposing samples to gamma radiation, the source of radiation being ^{60}Co.

The used components have not been exposed to the effects of neutron radiation since they belong to the group of MOS structures, where the effects of neutron radiation are significantly less comparing to gamma radiation.

All memory locations of the samples have been initially written into logic "1" state, since this state is more radiation sensitive than the logic "0" state. Testing has been performed in steps, by increasing absorbed dose of radiation within each step. During irradiation, some memory cells changed its logic state from "1" to "0," and the very process has been defined as an error. After irradiation, memory has been read, and the number of logic "0" state has been observed, being the same as the number of errors.

The experimental measurement results were collected with combined uncertainty lower than 10% [9, 10].

4.2. Simulation of Direct Ionizing Radiation Interaction with Semiconductor Memory. Monte Carlo simulations of interaction between direct ionizing radiation (protons and alpha particles) and MOS structure insulator layer have been performed in TRIM software, being part of SRIM 2008 programming package. TRIM is as open source software made for simulation of ions travelling through the material [11]. It is based on using a quantum mechanical treatment of ion-atom collisions [12, 13].

5. Results and Discussion

5.1. Indirect Ionizing Radiation Damage. Figures 1 and 2 show the average relative change in number of errors versus the absorbed dose of radiation, in irradiated EPROM and EEPROM samples, respectively. The number of errors is proportional to the absorbed dose for both EPROM and EEPROM memory samples. The first error in EPROM samples has been observed within the absorbed dose at 1110 Gy; the dose being greater than 1230 Gy, the number of error has become significantly larger. EEPROM memories proved to be more sensitive on gamma radiation, since the first error has been observed within radiation dose of 880 Gy.

In both EPROMs and EEPROMs, the floating gate is used to store charge and thus maintain a logical state. The stored charge determines the value of transistor threshold voltage, making the memory cell either "on" or "off" at readout.

Gamma radiation causes generation of electron-hole pairs in SiO_2 insulator of the gate. The number of generated pairs is directly proportional to the energy deposited in material, depending on the total absorbed dose of radiation [8, 14]. The part of generated pairs is recombined, depending on electric field strength. Being more mobile than the holes, electrons leave the insulator, influenced by the gate voltage. The generated holes slowly drift towards floating gate (FG). The fraction of holes becomes captured in trapping sites, forming positive radiation-induced charge in insulator. The remains of holes flow into the FG, reducing the number of electrons within it, thus influencing the logical state of a memory cell.

5.2. Direct Ionizing Radiation Damage. The calculation is made very efficient using statistical algorithms allowing the ion to make jumps between calculated collisions and then averaging the collision results over the intervening gap. The interaction of 50 keV protons and 30 keV alpha particles with 0.5 μm thick SiO_2 oxide layer has been simulated. The results are presented in Figures 3 and 4.

During inelastic scattering on electrons, the incident particle can transfer energy to the atom, raising it to a higher energy level (excitation), or it may transfer enough energy to remove an electron from the atom (ionization). A portion of energy transferred during each individual scattering of heavy charged particles on electrons is small compared to an entire kinetic energy of a particle, but the number of particle collisions per a unit path length is as high that the entire total energy loss is significant even in relatively thin material layers.

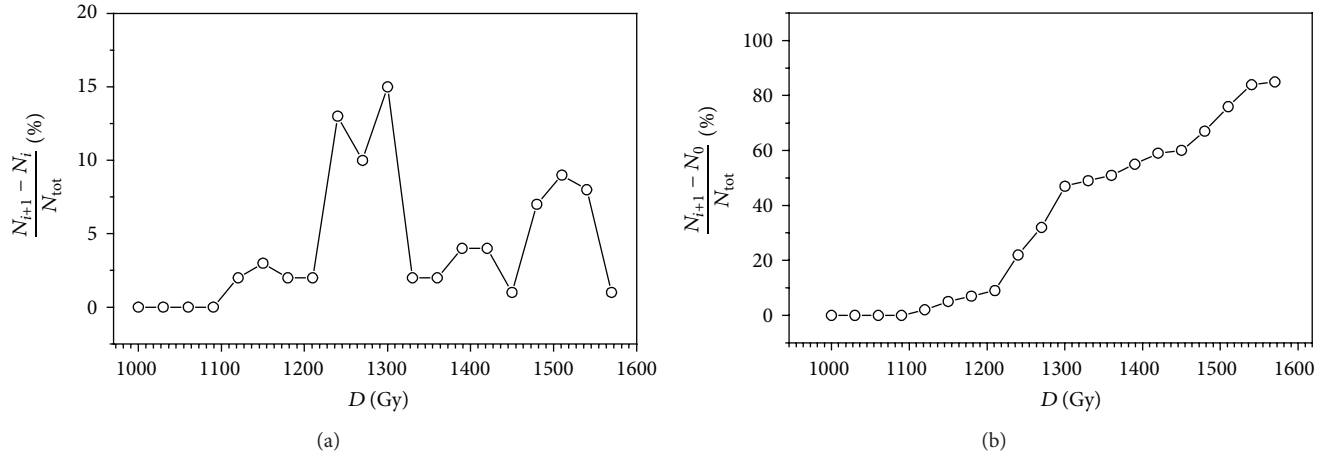

Figure 1: The average relative change in number of errors in irradiated EPROM samples (NM27C010) versus the absorbed dose of radiation: (a) differential; (b) cumulative (N_{tot} = 1,048,576 bit, $N_0 = 0$).

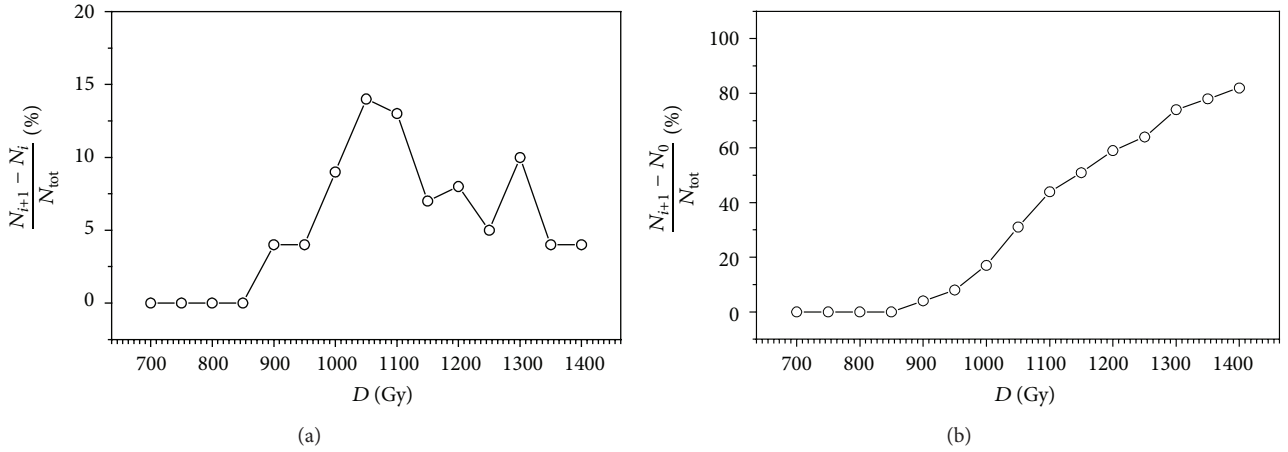

Figure 2: The average relative change in number of errors in irradiated EEPROM samples (NM93CS46) versus the absorbed dose of radiation: (a) differential; (b) cumulative (N_{tot} = 1024 bit, $N_0 = 0$).

The energy loss of heavy charged particles per a unit path length increases at the end of their path. At the very end of its path, when the particles have already lost the greatest part of their energy, the ones start to capture electrons, while a stopping power and specific ionization rapidly decrease [15]. Alpha particles are heavier than protons, and their energy is lower than the energy of protons, so a penetration depth of alpha particles in target SiO_2 layer is lower compared to the penetration depth of protons, as indicated in Figures 3(a) and 4(a).

Elastic scatterings on the nuclei lead to atom ejections from their positions in a crystal lattice, producing displacement damages. There is a silicon nucleus displacement when the energy of an incident particle (projectile) transferred to the nucleus in the elastic collision is higher than a threshold displacement energy E_d. Such ejected silicon atom is called *primary knock-on atom (PKA)*. An empty space in the crystal lattice produced by Si atom displacement is called a *vacancy*. When the displaced atom occupies a site among lattice nodes (interstitial site), the vacancy and the interstitial Si atom together represent *Frenkel pair* ($V + (\text{Si})_i$) [16]. Kinetic energy of the PKA being equal to the difference of the energy transferred to the atom in the elastic collision and the threshold displacement energy can be large enough so as the atom, before occupying its interstitial site, causes displacement of the entire set of other nearby nuclei that can themselves displace other nuclei, producing a collision cascade. Along its path, the recoil atoms lose their energy in two ways—by ionization and displacement of other nuclei. Figure 4(b) contains two distinct plots, one for electronic energy loss from the incident alpha particles and one for energy loss from displaced atoms. The ionization energy loss is greater within alpha particles than within recoil atoms. The electrons tend to absorb energy most efficiently from particles whose velocity is similar to their velocity. The alpha particles lose more energy to the target electrons since they move much faster than the recoil atoms.

Point defects in an insulator, produced as a result of displacement damages, can serve as the trapping sites for charge carriers. These imperfections may alter material properties of

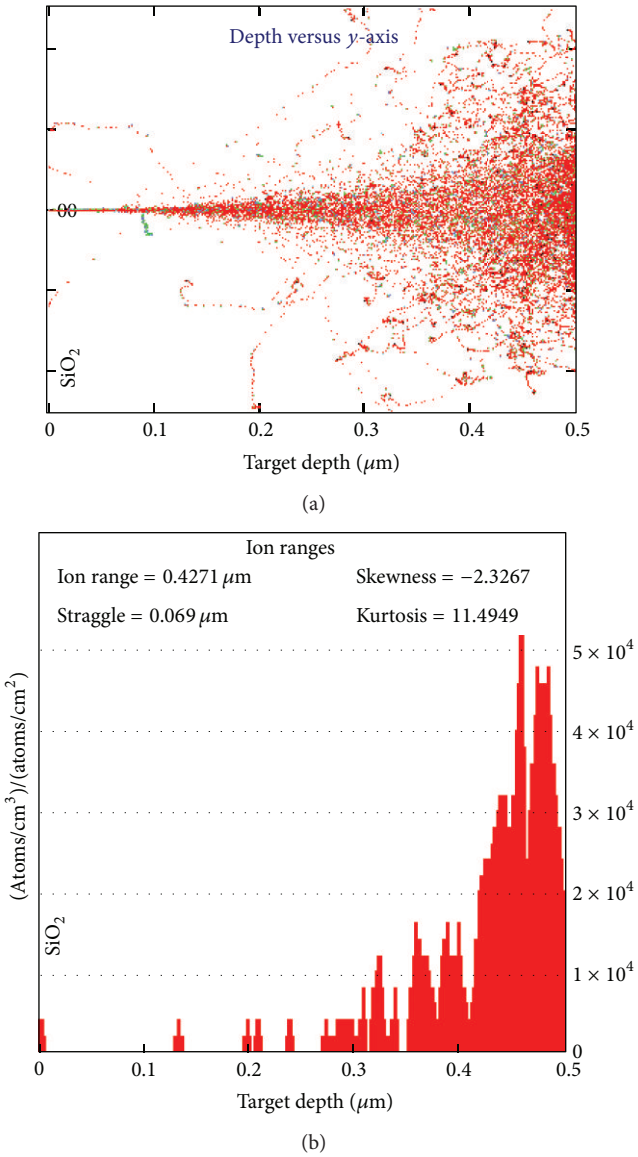

FIGURE 3: The simulation of 50 keV protons passing through 0.5 μm thick layer of SiO_2 (500 events). (a) Trajectory of protons in xOy plane. (b) Distribution of stopped protons along the oxide depth.

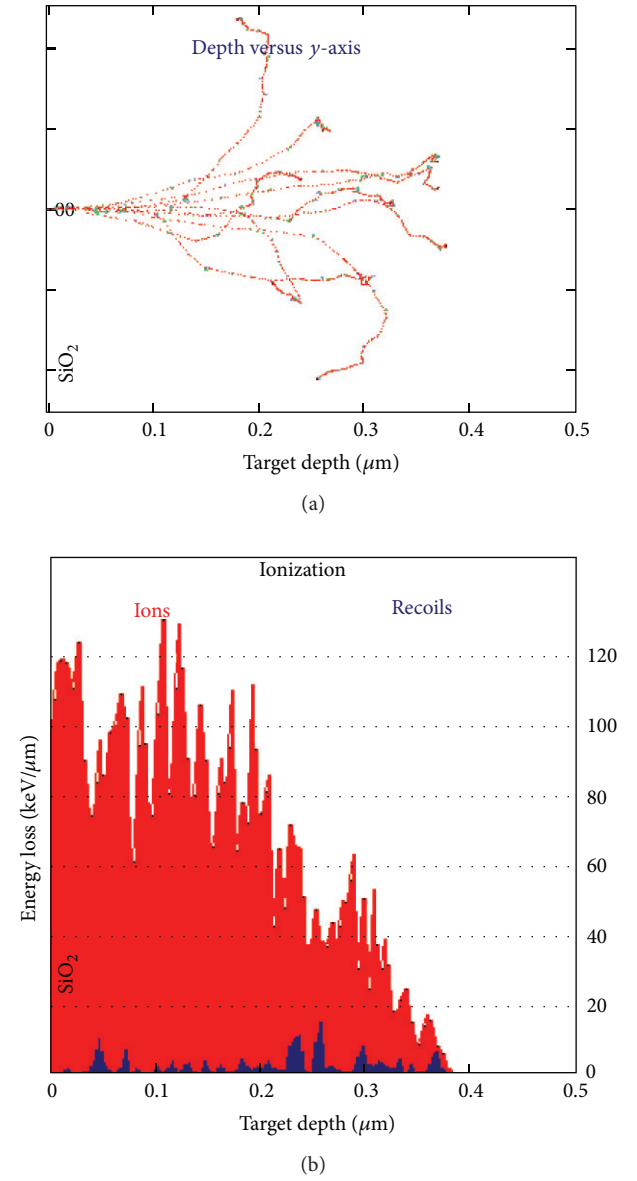

FIGURE 4: The simulation of 30 keV alpha particles passing through 0.5 μm thick layer of SiO_2 (10 events). (a) Trajectory of alpha particles in xOy plane. (b) The ratio of specific ionization (linear transfer of energy) of incident alpha particles and displaced Si and O atoms along the oxide depth.

the insulator, thus changing and disrupting characteristics of an electronic memory device which the insulator is part of [17].

6. Conclusion

Based on analysis of data gathered from performed experiments, the exposure of semiconductor memories to gamma radiation causes three effects: holes being captured in trapping sites of an oxide, injection of holes from oxide into FG, and emission of electrons through FG-oxide interface.

The generation of electron-hole pairs leads to trapping of positive-charged carriers (holes) in insulator, causing negative shift in I_D/V_G characteristics. Namely, positive-charged carriers induced by gamma radiation require the increase of negative gate voltage to compensate the positive charge. It means that gamma radiation causes decrease in threshold voltage, being proportional to the absorbed dose of radiation. The future research of radiation compatibility of semiconductor memories can be directed towards analyzing the influence of gate oxide material and oxide thickness and examining the effects of absorbed dose rate. Monte Carlo simulations of radiation interaction with material proved to be significant and can be a good estimation tool in probing semiconductor memory behavior in radiation environment.

Acknowledgment

The Ministry of Education, Science and Technological Development of the Republic of Serbia supported this work under Contract no. 171007.

References

[1] J. L. Barth, C. S. Dyer, and E. G. Stassinopoulos, "Space, atmospheric, and terrestrial radiation environments," *IEEE Transactions on Nuclear Science*, vol. 50, no. 3, pp. 466–482, 2003.

[2] V. S. Vavilov and N. A. Ukhin, *Radiation Effects in Semiconductors and Semiconductor Devices*, Consultants Bureau, New York, NY, USA, 1977.

[3] R. Radosavljević and A. Vasić, "Effects of radiation on solar cells as photovoltaic generators," *Nuclear Technology & Radiation Protection*, vol. 27, no. 1, pp. 28–32, 2012.

[4] D. Nikolić, A. Vasić, I. Fetahović, K. Stanković, and P. Osmokrović, "Photodiode behavior in radiation environment," *Scientific Publications of the State University of Novi Pazar A*, vol. 3, no. 1, pp. 27–34, 2011.

[5] G. Holmes-Siedle and L. Adams, *Handbook of Radiation Effects*, Oxford University Press., Oxford, UK, 2nd edition, 2002.

[6] G. C. Messenger and M. S. Ash, *The Effects of Radiation on Electronic Systems*, Van Nostrand Reinhold, New York, NY, USA, 1992.

[7] M. Vujisić, N. Marjanović, I. Fetahović, K. Stanković, and P. Osmokrović, "Influence of radiation on titanium dioxide mermistors," *Scientific Publications of the State University of Novi Pazar A*, no. 1, pp. 75–82, 2012.

[8] M. Zdravković, A. Vasić, R. Radosavljević, M. Vujisić, and P. Osmokrović, "Influence of radiation on the properties of solar cells," *Nuclear Technology & Radiation Protection*, vol. 26, no. 2, pp. 158–163, 2011.

[9] K. Stanković, "Influence of the plain-parallel electrode surface dimensions on the type A measurement uncertainty of GM counter," *Nuclear Technology & Radiation Protection*, vol. 26, no. 1, pp. 39–44, 2011.

[10] Ć. Dolićanin, K. Stanković, D. Dolićanin, and B. Lončar, "Statistisal treatment of nuclear counting results," *Nuclear Technology & Radiation Protection*, vol. 26, no. 2, pp. 164–170, 2011.

[11] J. F. Ziegler, J. P. Biersack, and M. D. Ziegler, "SRIM (*The Stopping and Range of Ions in Matter*)," http://www.srim.org.

[12] J. H. Warner, S. R. Messenger, R. J. Walters, and G. P. Summers, "Displacement damage correlation of proton and silicon ion radiation in GaAs," *IEEE Transactions on Nuclear Science*, vol. 52, no. 6, pp. 2678–2682, 2005.

[13] M. Vujisic, K. Stankovic, N. Marjanovic, and P. Osmokrovic, "Simulated effects of proton and ion beam irradiation on titanium dioxide memristors," *IEEE Transactions on Nuclear Science*, vol. 57, no. 4, pp. 1798–1804, 2010.

[14] S. Stanković, B. Iričanin, D. Nikolić et al., "MSV signal processing systemfor neutron-gamma discrimination in a mixed field," *Nuclear Technology & Radiation Protection*, vol. 27, no. 2, pp. 165–170, 2012.

[15] J. R. Srour, *Basic Mechanisms of Radiation Effects on Electronic Materials, Devices and Integrated Circuits*, DNA-TR-82-20, New York, NY, USA, 1982.

[16] J. R. Schwank, M. R. Shaneyfelt, D. M. Fleetwood et al., "Radiation effects in MOS oxides," *IEEE Transactions on Nuclear Science*, vol. 55, no. 4, pp. 1833–1853, 2008.

[17] G. Cellere, A. Paccagnella, A. Visconti, and M. Bonanomi, "Ionizing radiation effects on floating gates," *Applied Physics Letters*, vol. 85, no. 3, 3 pages, 2004.

Hindawi Publishing Corporation
International Journal of Photoenergy
Volume 2013, Article ID 582819, 6 pages
http://dx.doi.org/10.1155/2013/582819

Research Article

Damage Induced by Neutron Radiation on Output Characteristics of Solar Cells, Photodiodes, and Phototransistors

Biljana Simić,[1] Dejan Nikolić,[1] Koviljka Stanković,[1] Ljubinko Timotijević,[1] and Srboljub Stanković[2]

[1] *Faculty of Electrical Engineering, University of Belgrade, Bulevar kralja Aleksandra 73, 11000 Belgrade, Serbia*
[2] *Vinča Institute of Nuclear Sciences, University of Belgrade, Mike Petrovica Alasa 12-14, 11000 Belgrade, Serbia*

Correspondence should be addressed to Koviljka Stanković; kstankovic@etf.rs

Received 27 March 2013; Accepted 9 May 2013

Academic Editor: Predrag Osmokrovic

This study investigates the effects of neutron radiation on *I-V* characteristics (current dependance on voltage) of commercial optoelectronic devices (silicon photodiodes, phototransistors, and solar panels). Current-voltage characteristics of the samples were measured at room temperature before and after irradiation. The diodes were irradiated using Am-Be neutron source with neutron emission of 2.7×10^6 n/s. The results showed a decrease in photocurrent for all samples which could be due to the existence of neutron-induced displacement defects introduced into the semiconductor lattice. The process of annealing has also been observed. A comparative analysis of measurement results has been performed in order to determine the reliability of optoelectronic devices in radiation environments.

1. Introduction

Optoelectronics is at the crossroads of electronics and optics. Using optical and electronic means, it generates, manipulates, and converts light. Photonic devices process, store, transmit, and display information for applications such as communications, displays, imaging, memory, biophotonics, energy generation, and lighting. Photonics is an essential part of a country's information infrastructure, which, in turn, plays a key role in its domestic economy and national defense. Solid-state devices like sensors, IR emitters, and laser emitters are used for optoelectronic applications. Optoelectronic devices can be classified into photoconductive and photovoltaic devices. Photoconductive devices such as photoresistors are widely used in counting systems, twilight switches, house security systems, and so forth. These detect variations in the light intensities and activate or deactivate electronic circuits. Photodiodes and phototransistors also fall in this category. These utilise the reverse biased junctions for generating current when illuminated. Photovoltaic devices produce a voltage when these are exposed to light. The light energy produces a potential difference across the p-n junction depending on the intensity of the incident light. Solar cells and photovoltaic cells are widely used in various applications to generate electricity.

One of the most specific fields of application of optoelectronic devices is the space. Possibilities of application of optoelectronic devices in this area are countless (photonic communications, photonic signal processing, photonic sensing, speciality applications, etc.). The use of optoelectronic technologies in space applications has shown an important increase in the last years due to the multiple applications and their advantages compared with standard technologies. A complete evaluation of the technology has to be performed in advance in order to select the best components and to reduce the risk of using devices that have not been designed to work in space environmental conditions. Experience shows that the evaluation of the most critical aspects reveals that not all the commercial devices that are available in the market are suitable for space use [1].

A number of researchers and institutions work hard to produce new and improve existing optoelectronic devices to be reliable and effective in specific circumstances such as space. In the space environment, optoelectronic devices

are exposed to different types of radiation, such as protons, alpha particles, heavy ions, neutrons, gamma rays, electrons, and positrons. In previous papers, the behavior of various optoelectronic devices in terms of neutron radiation has been observed [2–9].

There are free neutrons everywhere in nature, in small amounts. Their main source is cosmic rays. They also occur in nuclear reactions of natural alpha radiation and spontaneous fission of heavy nuclei. In many ways, neutron is a unique particle—with no electric charge, it has a relatively large mass, subject to radioactive decay. Neutrons build each atomic nucleus except that of hydrogen, that is, they are the constituents of all matter. For the practice of nuclear reactions, neutrons are much more important than any other particles. Neutron, as a neutral particle, does not possess the ability for direct ionization of materials. The basic mechanism of the neutron interaction with the environment is through the elastic collision with the atomic cores of that environment. Interaction with the electrons, although exists, is negligible. Energy transfer in these collisions is executed entirely in accordance with

$$\varepsilon_t = \varepsilon \frac{4 \cdot m_1 \cdot m_2}{(m_1 + m_2)^2} \cdot \sin^2\left(\frac{\theta}{2}\right), \quad (1)$$

where ε_t is energy, transferred in an elastic collision, ε is energy of incident particles, m_1 is incident particle mass, m_2 is struck particle mass, and θ is angle between the direction of scattering of incident particle and the direction of intrusion. Thereby, the neutron loses some of its energy and slows down, while the environment may suffer from different types of transformation.

Neutrons and other high-energy particles collide and displace lattice atoms in semiconductors, creating Frenkel defects. Primary displaced atoms typically have enough energy to create secondary defects. These vacancies may combine with dopant and impurity atoms to form stable defects, which, in turn, may serve as recombination centers, decreasing carrier lifetime. The decrease in carrier lifetimes in doped semiconductor materials after exposure to a neutron fluence has been characterized as an abrupt decrease followed by a rapid short-term anneal (on the order of a few hours) and a long-term anneal (on the order of months), in which the carrier lifetime increases [10]. Axness et al. [11] show that the lattice damage and carrier lifetime degradation are spatially dependent.

This work describes a series of measurements undertaken to try to identify the similarities and differences in behavior of solar cells, photodiodes, and phototransistors in situation when these have previously been damaged by neutron radiation and have had enough time to recover. The aim of this paper is to provide readers with a comparative overview of the processes that occur in solar cells, photodiodes, and phototransistors after neutron irradiation and to give a critical review of the effectiveness of these devices in the environment with neutron radiation, that is, space.

2. Materials and Methods

Experimental measurement in this paper was carried out on the commercially available optoelectronic devices. In this experiment, the following were used:

(1) monocrystalline silicon solar panel (maximum power voltage 4.0 V, maximum power current 100.0 mA, dimension: 70 ∗ 65 ∗ 3.2 mm);

(2) four types of silicon PIN photodiodes (BP104, BPW41N, BPW34, all manufactured by Vishay, and SFH203FA by Osram);

(3) two types of silicon NPN phototransistors (BPW40 manufactured by Telefunken electronic and LTR4206 by Liteon).

Semiconductor devices have been exposed to neutron and gamma radiation from ^{241}Am-Be source, which is housed in the Secondary Standard Dosimetry Laboratory (SSDL) Institute of Nuclear Sciences "Vinča," Belgrade. ^{241}Am-Be source emits gamma photons of low energy (60 keV and 14 keV), so that for the activity of 1 Ci, the photon equivalent dose rate is $\dot{H}_\gamma = 12$ mSv/hr are calculated, and the photon absorbed dose rate is $\dot{D}_\gamma = 12$ mGy/hr at a distance of 5 cm from the source. The intensity of the neutron emission from this source is 2.7×10^6 neutrons s^{-1}, and the mean energy of the neutrons $E_{\text{nav}} = 5.5$ MeV. Based on measurements of the quality factor for this neutron spectrum $Q_{\text{n}} = 7$, calculated the neutron absorbed dose rate $\dot{D}_{\text{n}} = 1.714$ mGy/hr and the equivalent dose rate of neutrons $\dot{H}_{\text{n}} = 12$ mSv/hr. This means that at 5 cm distance from the ^{241}Am-Be source with a total absorbed dose rate is $\dot{D}_{\text{tot}} = 13.714$ mGy/hr, while the total equivalent dose is $\dot{H}_{\text{tot}} = 24$ mSv/hr. In this experiment, the semiconductor devices were placed at a distance of 5 cm from the ^{241}Am-Be source, and the exposure period was 16.75 hr. In this interval, the material components received the radiation of the total absorbed dose in the amount of $D_{\text{tot}} = 229.71$ mGy (13.714 mGy/hr ∗ 16.75 hr), and respectively, the total equivalent dose $H_{\text{tot}} = 402$ mSv (24 mSv/hr ∗ 16.75 hr). The components were irradiated in the air at a temperature of 21°C and relative humidity of 40% to 70%.

Before and after the irradiation, current-voltage (I-V) characteristics of all optoelectronic devices were measured in highly controlled conditions at room temperature. During the measurement, the samples were removed from the experimental room after absorption of the anticipated dose of radiation. There have been undertaken three measurements of the I-V characteristics:

(1) *first measurement*: immediately before neutron irradiation,

(2) *second measurement*: immediately after neutron irradiation,

(3) *third measurement*: 1 month after neutron irradiation.

The third measurement has been undertaken one month after the irradiation, in order to give enough time for sample

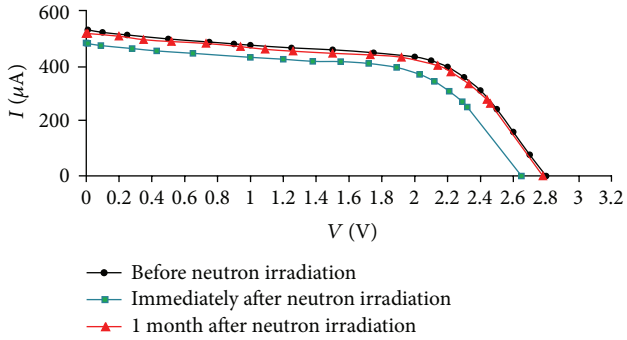

Figure 1: I-V characteristics of the solar panels before and after neutron irradiation.

recovery. For this reason, the changes occurring in the samples can be considered permanent. Standard measurement equipment was used to measure I-V curve. The professional digital multimeter Amprobe 33XR was used for the current measurement. Combined measurement uncertainty for all measurements was less than 1.2% [12–15]. Measurements of I-V characteristics have been performed for illumination levels of 10 W/m^2 (for phototransistors BPW40), 4.32 W/m^2 (for solar panels), and 0.45 W/m^2 (for phototransistors LTR4206 and all photodiodes, BP104, BPW41N, BPW34, and SFH203FA).

3. Results and Discussion

I-V characteristics of optoelectronic devices before and after the neutron irradiation are shown in Figure 1 (solar panels), Figure 2 (reverse biased photodiodes), and Figure 3 (phototransistors). They all behaved in a similar way; neutron radiation decreased their photocurrent and, after that, the annealing process increased it. The extent of their damage and efficiency of their annealing process are different from one type of devices to another. Neutron radiation had the least impact on solar panels and the most on phototransistors. At the solar panels, the recovery process was also the most effective, while it has achieved the poorest results on photodiodes (Figures 1 to 3).

The fundamental "structural" element of solar (PV—photovoltaic) systems, the solar cell, is usually based on the p-n junction device that, exposed to solar radiation, gives power as its output characteristic. Radiation damage due to neutrons is primarily connected to the displacement of silicon atoms from their lattice sites in the crystalline silicon solar cells, leading to the destruction and distortion of local lattice structure and formation of defects. If, under the influence of neutrons, stable defects are made, they could, together with impurity atoms, donors, and, for example, implanted atoms, form complex defects acting as recombination sites or traps, significantly decreasing minority carrier lifetime. This lifetime decrease produces the degradation of the electrical parameters of the cell, such as series resistance (R_s), output current, and finally efficiency (μ). The interaction between vacancies, self-interstitials, impurities, and dopants in Si leads to the formation of undesirable point defects such as recombination and compensator centers which affect performance of solar cells, especially in space. The introduction of radiation-induced recombination centers reduces the minority carrier lifetime in the base layer of the p-n junction increasing series resistance. Factors that influence the internal parameters of solar cells such as series and parallel resistance lead to changes in efficiency and maximum generated power in a solar cell [16].

High-energy particles like neutrons create much more displacement damages than gamma radiation. When an atom is ejected from its position, it creates a vacancy in the lattice. The ejected atom may recombine with a vacancy or stay in an interstitial position in the lattice. The vacancies are mobile and combine with other vacancies or with impurities of the semiconductor [17, 18]. Sporea et al. [19] have calculated that the major degradation of the photodiode responsivity, for the total gamma dose of 1.23 MGy and to the neutron fluence of 1.2×10^{13} n/cm^2, occurs in the case of neutron irradiation (37.5%) as compared to the gamma irradiation (7.2%).

Phototransistors are susceptible to neutron radiation. Neutron radiation affects phototransistors performance primarily by creating lattice defects, which can dramatically increase carrier recombination rate. In turn, the increase in recombination rate degrades the current gain. Many studies of displacement damage mechanisms in bipolar transistors have indicated that the common-emitter current gain degrades through the introduction of recombination centers. Measurement data of phototransistors before and after radiation indicate that the effect of neutron damage is most pronounced on the base current of the transistors. The phototransistor is a light-controlled device in which the base current, that is, light controls the output collector current. Fast neutrons primarily cause cluster defects and are the dominant radiation-induced damage mechanism in phototransistor. The number of atomic displacements caused by neutrons is very large. The result is the formation of recombination-generation centers. Electron-hole recombination causes reductions in current gain and switching times. Electron-hole generation causes an increase in leakage current. Majority carrier removal and decreases in carrier mobility cause increases in forward collector-emitter voltage. The current gain is determined by the fraction of majority carriers emitted by the emitter that pass through the base as minority carriers and collected as majority carriers by the collector. An increase in recombination-generation center density due to radiation-induced defects causes a decrease in minority carrier lifetime so that the rate of electron-hole recombination increases in the base. Thus, the current gain decreases as the fraction of emitter-injected carriers reaching the collector decreases so that photocurrent decreases [20].

For this research, the long-term isothermal annealing at room temperature was used. The vacancies and interstitials are quite mobile in silicon at room temperature and hence, are referred to as unstable defects. After vacancy introduction by irradiation, vacancies move through the lattice and form more stable defects, such as divacancies and vacancy-impurity complexes. When electrical properties

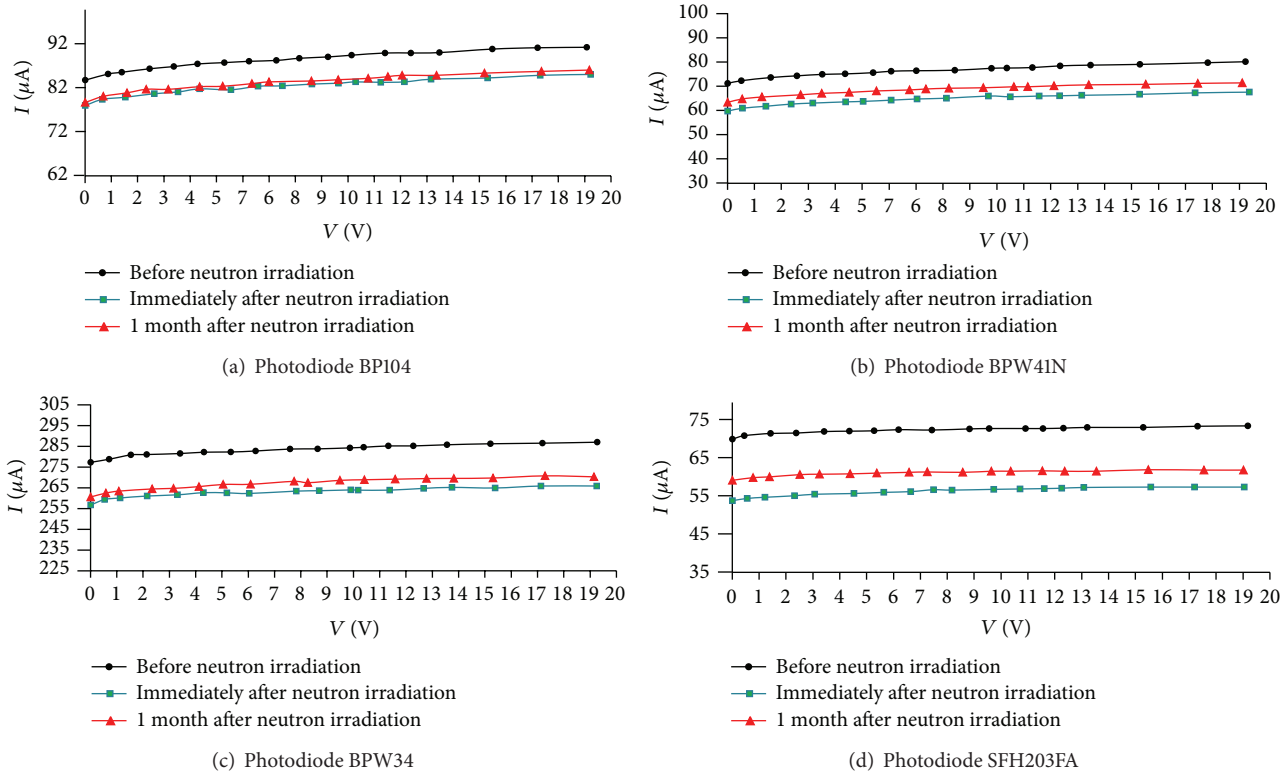

(a) Photodiode BPI04

(b) Photodiode BPW41N

(c) Photodiode BPW34

(d) Photodiode SFH203FA

Figure 2: *I-V* characteristics of the reverse biased photodiodes before and after neutron irradiation.

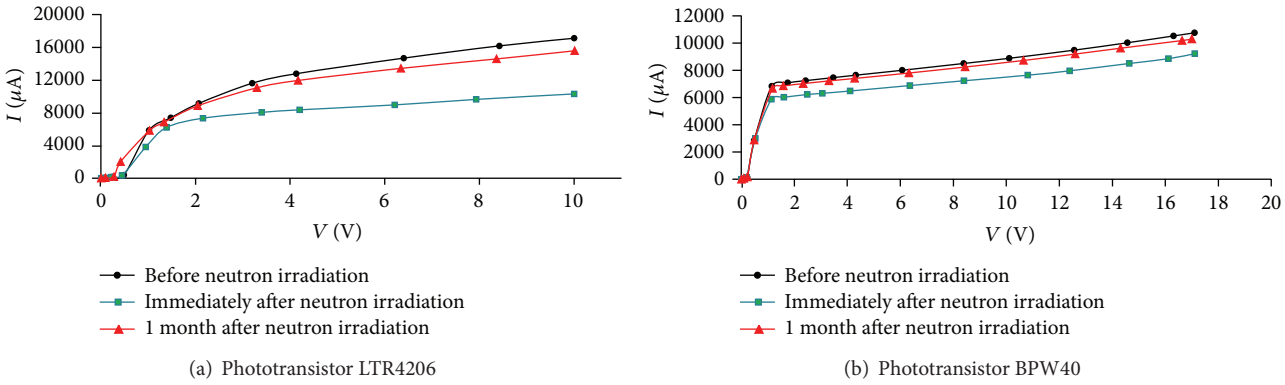

(a) Phototransistor LTR4206

(b) Phototransistor BPW40

Figure 3: *I-V* characteristics of the phototransistors before and after neutron irradiation.

are monitored during this defect rearrangement (or annealing) process, a decrease in the effectiveness of the damage with increasing time is typically observed [10]. Moll [21] describes the enhancement of the effective doping concentration for the longer annealing times. Feick [22] observed this phenomenon at room temperature. During the process of annealing, defects cluster and some electrical inactive defects become active in a cluster. From the standpoint of the photocurrent intensity before irradiation and after annealing process, best results have been achieved in the solar panels. Radosavljević and Vasić [23] observed an increase of the maximum power for lower values of irradiation. They proposed the following explanation that small doses of radiation may produce a decrease in series resistance. Subsequently, this will lead to a lowering of the noise level and an increase in the output current since, as is well known, high series resistance of a solar cell is one of the main limiting factors of its efficiency. Since the rate of damage recovery from annealing in solar panels is almost the same as the rate of damage creation (Figure 1), for lower values of neutron irradiation, it is possible to use annealing as a part of a hardening method [17, 18, 24, 25].

Solar cells have attracted much attention as good candidates for low cost, good stability, and high efficiency. There are many researches in this emerging technology in order to investigate the behavior of solar cells in various working conditions [26–29]. Solar cells have proved to be very reliable devices regardless of the environment in which they exist.

This experiment showed that, even under conditions of increased neutron radiation, solar cells were able to recover their characteristics almost to the level before the radiation and that makes them dominant over conventional optoelectronic devices.

4. Conclusion

The effect of neutron radiation on optoelectronic devices, solar panels, and photodiodes phototransistors has been observed in this paper. Neutron radiation is considered to be one of the most severe of all types of radiation experienced in space as it can cause biological damage. It represents approximately 30% of the total exposure for those aboard the ISS. In space, neutrons are produced when charged particles collide with physical matter, such as the walls and equipment on the ISS. Therefore, it is important to give a review of the effectiveness of optoelectronic devices in the enviroment with neutron radiation, that is, space. According to current theories, neutron irradiation in all samples caused degradation of their structure and deterioration of the output characteristics. Solar panels have proved to be most resistant to the effects of neutrons. And annealing process for them had the best effect. The reason for that could be the construction of a solar panel. To obtain the maximum power voltage of panels (4 V), a large number of individual cells are used in series and parallel combinations. According to the degree of recovery in the annealing process, one can conclude that, for working in the environment of increased neutron radiation, solar panels and phototransistors preferable than photodiodes.

Acknowledgment

The Ministry of Education, Science and Technological Development of the Republic of Serbia supported this work under Contract 171007.

References

[1] H. Johnston, "Radiation damage of electronic and optoelectronic devices in space," in *Proceedings of the 4th International Workshop on Radiation Effects on Semiconductor Devices for Space Application*, Tsukuba, Japan, October 2000.

[2] S. J. Watts, J. Matheson, I. H. Hopkins-Bond, A. Holmes-Siedle, A. Mohammadzadeh, and R. Pace, "A new model for generation-recombination in silicon depletion regions after neutron irradiation," *IEEE Transactions on Nuclear Science*, vol. 43, no. 6, pp. 2587–2594, 1996.

[3] M. B. El-Mashade, M. Ashry, S. M. Eladl, and M. S. Rageh, "Experimental measurements of some optoelectronic devices before and after gamma irradiation," *Journal of Microwaves and Optoelectronics*, vol. 3, no. 6, pp. 1–12, 2004.

[4] Z. D. Kovalyuk, V. N. Katerynchuk, O. A. Politanska, O. N. Sydor, and V. V. Khomyak, "Effect of gamma radiation on the properties of InSe photodiodes," *Technical Physics Letters*, vol. 31, no. 5, pp. 359–360, 2005.

[5] M. Vujisić, K. Stanković, N. Marjanović, and P. Osmokrović, "Simulated effects of proton and ion beam irradiation on titanium dioxide memristors," *IEEE Transactions on Nuclear Science*, vol. 57, no. 4, pp. 1798–1804, 2010.

[6] M. Vujisić, K. Stanković, E. Dolićanin, and P. Osmokrović, "Radiation hardness of COTS EPROMs and EEPROMs," *Radiation Effects and Defects in Solids: Incorporating Plasma Science and Plasma Technology*, vol. 165, no. 5, pp. 362–369, 2010.

[7] D. R. Alexander, "Transient ionizing radiation effects in devices and circuits," *IEEE Transactions on Nuclear Science*, vol. 50, no. 3, pp. 565–582, 2003.

[8] B. D. Iričanin and D. M. Gvozdić, "The analytic approach in the modelling of one-dimensional electron concentration distribution in some two-valley semiconductor electron devices," *Journal of Physics A*, vol. 31, no. 13, pp. 2997–3017, 1998.

[9] S. Stanković, B. Iričanin, D. Nikolić et al., "MSV signal processing system for neutron-gamma discrimination in a mixed field," *Nuclear Technology and Radiation Protection*, vol. 27, no. 2, pp. 165–170, 2012.

[10] J. R. Srour, C. J. Marshall, and P. W. Marshall, "Review of displacement damage effects in silicon devices," *IEEE Transactions on Nuclear Science*, vol. 50, no. 3, pp. 653–670, 2003.

[11] C. L. Axness, B. Kerr, and E. R. Keiter, "Analytic 1-D pn junction diode photocurrent solutions following ionizing radiation and including time-dependent changes in the carrier lifetime from a nonconcurrent neutron pulse," *IEEE Transactions on Nuclear Science*, vol. 57, no. 6, pp. 3314–3321, 2010.

[12] K. D. Stanković, "Influence of the plain-parallel electrode surface dimensions on the type a measurement uncertainty of GM counter," *Nuclear Technology and Radiation Protection*, vol. 26, no. 1, pp. 39–44, 2011.

[13] Ć. Dolićanin, K. Stanković, D. Dolićanin, and B. Lončar, "Statistisal treatment of nuclear counting results," *Nuclear Technology and Radiation Protection*, vol. 26, no. 2, pp. 164–170, 2011.

[14] K. Stanković, M. Vujisić, D. Kovačević, and P. Osmokrović, "Statistical analysis of the characteristics of some basic mass-produced passive electrical circuits used in measurements," *Measurement*, vol. 44, no. 9, pp. 1713–1722, 2011.

[15] M. Vujisić, K. Stanković, and P. Osmokrović, "A statistical analysis of measurement results obtained from nonlinear physical laws," *Applied Mathematical Modeling*, vol. 35, no. 7, pp. 3128–3135, 2011.

[16] M. Zdravković, A. Vasić, R. Radosavljević, M. Vujisić, and P. Osmokrović, "Influence of radiation on the properties of solar cells," *Nuclear Technology and Radiation Protection*, vol. 26, no. 2, pp. 158–163, 2011.

[17] A. Holmes-Siedle and L. Adams, *Handbook of Radiation Effects*, Oxford Science, 1993.

[18] G. C. Messenger and M. S. Ash, *The Effects of Radiation on Electronic Systems*, Van Nostrand Reinhold, New York, NY, USA, 2nd edition, 1991.

[19] D. G. Sporea, R. A. Sporea, C. Oproiu, and I. Vată, "Comparative study of gamma-ray, neutron and electron beam irradiated index-guided laser diodes," in *Proceedings of the 8th European Conference on Radiation and Its Effects on Components and Systems (RADECS '05)*, pp. PA31–PA39, September 2005.

[20] G. E. Schwarze and A. J. Frasca, "Neutron and gamma irradiation effects on power semiconductor switches," in *Proceedings of the 25th Intersociety Energy Conversion Engineering Conference (IECEC '90)*, vol. 6, pp. 30–35, August 1990.

[21] M. Moll, *Radiation damage in silicon particle detectors—microscopic defect and macroscopic properties [Ph.D. thesis]*, University of Hamburg, Hamburg, Germany, DESY-THESIS-1999-040.

[22] H. Feick, *Radiation tolerance of silicon particle detectors for high-energy physics [Ph.D. thesis]*, University of Hamburg, Hamburg, Germany, 1997, Internal Report, DESY F35D-97-08.

[23] R. Radosavljević and A. Vasić, "Effects of radiation on solar cells as photovoltaic generators," *Nuclear Technology and Radiation Protection*, vol. 27, no. 1, pp. 28–32, 2012.

[24] D. Nikolić, A. Vasić, I. Fetahović, K. Stanković, and P. Osmokrović, "Photodiode behavior in radiation environment," *Scientific Publications of the State University of Novi Pazar A*, vol. 3, no. 1, pp. 27–34, 2011.

[25] M. Vujisić, N. Marjanović, I. Fetahović, K. Stanković, and P. Osmokrović, "Influence of radiation on titanium dioxide mermistors," *Scientific Publications of the State University of Novi Pazar A*, vol. 4, no. 1, pp. 75–82, 2012.

[26] M. J. Jeng, Y. L. Wung, L. B. Chang, and L. Chow, "Particle size effects of TiO_2 layers on the solar efficiency of dye-sensitized solar cells," *International Journal of Photoenergy*, vol. 2013, Article ID 563897, 9 pages, 2013.

[27] Y. Yamamoto, Y. Aoyama, S. Shimizu, J. Kano, F. Saito, and S. Ito, "Influence of titania dispersivity on the conversion efficiency of dye-sensitized solar cells," *International Journal of Photoenergy*, vol. 2011, Article ID 234931, 7 pages, 2011.

[28] H. Boo, J. Lee, M. G. Kang et al., "Effect of high-temperature annealing on ion-implanted silicon solar cells," *International Journal of Photoenergy*, vol. 2012, Article ID 921908, 6 pages, 2012.

[29] M. I. Kabir, S. A. Shahahmadi, V. Lim, S. Zaidi, K. Sopian, and N. Amin, "Amorphous silicon single-junction thin-film solar cell exceeding 10% efficiency by design optimization," *International Journal of Photoenergy*, vol. 2012, Article ID 460919, 7 pages, 2012.

Hindawi Publishing Corporation
International Journal of Photoenergy
Volume 2013, Article ID 843174, 6 pages
http://dx.doi.org/10.1155/2013/843174

Research Article

Comparative Study of Gamma Radiation Effects on Solar Cells, Photodiodes, and Phototransistors

Dejan Nikolić,[1] Koviljka Stanković,[1] Ljubinko Timotijević,[1] Zoran Rajović,[2] and Miloš Vujisić[1]

[1] *Faculty of Electrical Engineering, University of Belgrade, Bulevar kralja Aleksandra 73, 11000 Belgrade, Serbia*
[2] *Electric Power Industry of Serbia, Masarikova 1-3, 11000 Belgrade, Serbia*

Correspondence should be addressed to Koviljka Stanković; kstankovic@etf.rs

Received 27 March 2013; Accepted 9 May 2013

Academic Editor: Predrag Osmokrovic

This paper presents the behavior of various optoelectronic devices after gamma irradiation. A number of PIN photodiodes, phototransistors, and solar panels have been exposed to gamma irradiation. Several types of photodiodes and phototransistors were used in the experiment. *I-V* characteristics (current dependance on voltage) of these devices have been measured before and after irradiation. The process of annealing has also been observed. A comparative analysis of measurement results has been performed in order to determine the reliability of optoelectronic devices in radiation environments.

1. Introduction

Optoelectronics is an interesting branch of electronics that combines both electronics and optics. Optoelectronic devices find varied applications in telecommunications, military services, medical field, and automatic control systems. These devices produce electrical energy when exposed to incident light energy. In this paper, solar cells, photodiodes, and phototransistors have been observed.

Photoelectric transducers generate electric current when exposed to light. A photovoltaic cell consists of many p-n junctions connected in series. One of the junctions is very thin, so light can easily pass through it. When light passes, charge carriers such as holes and electrons are produced proportional to the incident light. Photovoltaic cells are used in various applications to generate electricity where main power is not available. Examples include solar cells and solar batteries, which are used in satellites. The solar energy incident on the p-n junction of the solar cell collides with the valence electrons. This causes the formation of electron-hole pairs, which cross the p-n junction in an opposing manner and create a voltage across the p-n junction. The voltage generated per cell is approximately 0.6 V. Large arrays of solar cells are used in series and parallel combinations to produce a large voltage.

Photodiodes are high-impedance devices that are usually reverse biased for improved performance. These are high-speed sensors which generate a tiny current (in μA) proportional to the amount of incident light. The photodiode consists of a relatively large silicon p-n junction, which is illuminated by the incident light. Light photons impinging on the junction have sufficient energy to rupture a number of covalent bonds in the junction, thereby producing electron-hole pairs. This causes the flow of current in the diodes. As the illumination increases, additional electron-hole pairs are released and the diode current increases.

Phototransistors employ the principle of photodiodes, but the amplifying action of the transistor makes these devices more sensitive. Phototransistors are duo diodes having two junctions in the same device separated by a wide base region, thus forming an n-p-n junction. The n-p junction is slightly forward biased and the p-n junction is reverse biased. Light energy striking the n-p junction liberates electron-hole pairs. The released electrons diffuse out of the p region towards the junction. The holes, however, are trapped in the p region and

form a positive surface charge. This causes an increase in forward bias of n-p junction, increasing the current flow. Phototransistor is usually connected in common-emitter configuration with an open base. Photons are focused to the junction through a lens system. Only two leads (collector and emitter) of the phototransistor are usually used in circuit connections. The base current is created by the photons falling on the base-collector junction. The current in the phototransistor depends on the intensity of incident light and is less affected by the voltage in the circuit.

During the previous decades many researchers tested various optoelectronic devices and published the results of their researches [1–7]. Two types of radiation damage effects occur in solid-state electronic products: displacement damage and ionization effects. Displacement damage is the movement of atoms from their normal position in the lattice to another placement, causing a defect in the lattice material. Ionization effect is the generation of electron-hole pairs within the material that causes radiation effects.

When gamma rays interact with material, they create two effects. The first effect is ionization. Photoelectric effect, Compton scattering, and pair production eject electrons from the atoms of the material. These ejected electrons can create secondary reactions. The result is a track of ionized atoms in the bulk of the material. The second effect is atomic displacement. Sometimes the atom receives so much kinetic energy at the site of interaction that it leaves its initial location in the material. This displacement creates additional atomic movement on its track that may result in a cluster of defects into the atomic lattice. The immediate and long-term results of ionization and atomic displacement strongly depend on the material. After electron-hole generations, electrons and holes travel in the bulk under the influence of the local electric field. The mobility of electrons is much higher than the mobility of holes, but both charge carriers may get into defects of the lattice called traps. Charge carriers accumulate around traps and create a local charge build-up. These traps can be single point defects or a mismatch of interface surfaces [8, 9].

High-energy photons give rise to clusters of defects and low-energy photons only produce single point defects. The interstitial atoms are not such electrically active as a complex of defects. Defects introduce intermediate energy levels in the gap between the conducting band and the valence band. These band-gap defects disturb the transport of electrical charges by several reactions [10]. First, generation and recombination of electron-hole pairs degrade the minority carrier lifetime. Second, the trapping and compensation effects change the majority carrier density and decrease the carrier mobility [11]. The results show that, under the influence of these effects, the reduction of photocurrent is significant.

This work describes a series of measurements undertaken to try to identify the similarities and differences in behavior of solar cells, photodiodes, and phototransistors in situation when these have previously been damaged by gamma radiation and have had enough time to recover. The aim of this paper is to provide readers with a comparative overview of the processes that occur in solar cells, photodiodes, and phototransistors after gamma irradiation and to give a critical review of the effectiveness of these devices.

2. Materials and Methods

Experimental measurement in this paper was carried out on the commercially available optoelectronic devices. In this experiment the following were used:

(1) four types of silicon PIN photodiodes (BP104, BPW41N0, BPW34 all manufactured by Vishay, and SFH203FA by Osram),

(2) two types of silicon NPN phototransistors (BPW40 manufactured by Telefunken electronic and LTR4206 by LITEON),

(3) monocrystalline silicon solar panel (maximum power voltage 4.0 V, maximum power current 100.0 mA, dimension: $70 * 65 * 3.2$ mm).

Devices were irradiated with Co^{60} gamma source with dose of 2000 Gy, the energy of 1.25 MeV, and half-life time of 5.27 years (this energy is sufficient for the creation of electron-hole pairs). The dose rate was 100 Gy/h at a distance of 150 mm away from the radioactive source. Irradiation was performed through glass in controlled environment. The dose rate was measured by electrometer UNIDOS with ionization chamber TW 30012-0172, produced by PTW, Germany. Measurement uncertainty of the system is less than 1.2%. The components were irradiated in the air at a temperature of 21°C and relative humidity of 40% to 70%. Irradiation was performed in professional laboratory at the Department of Radiation and Environmental Protection of the Vinča Institute of Nuclear Sciences in Belgrade, Serbia.

Before and after the irradiation, current-voltage (I-V) characteristics of all optoelectronic devices were measured in highly controlled conditions at room temperature. During the measurement, the samples were removed from the experimental room after absorption of the anticipated dose of radiation. Three measurements of the I-V characteristics have been undertaken:

(1) first measurement: immediately before gamma irradiation,

(2) second measurement: immediately after gamma irradiation,

(3) third measurement: 1 month after gamma irradiation.

The third measurement has been undertaken one month after the irradiation, in order to give enough time for sample recovery. For this reason, the changes occurring in the samples can be considered as permanent. Standard measurement equipment was used to measure I-V curve. The professional digital multimeter AMPROBE 33XR was used for the current measurement. Combined measurement uncertainty for all measurements was less than 1.2% [12–16]. Measurements of I-V characteristics have been performed for illumination levels of 10 W/m^2 (for phototransistors BPW40), 4.32 W/m^2 (for solar panels), and 0.45 W/m^2 (for phototransistor LTR4206 and all photodiodes: BP104, BPW41N, BPW34, and SFH203FA).

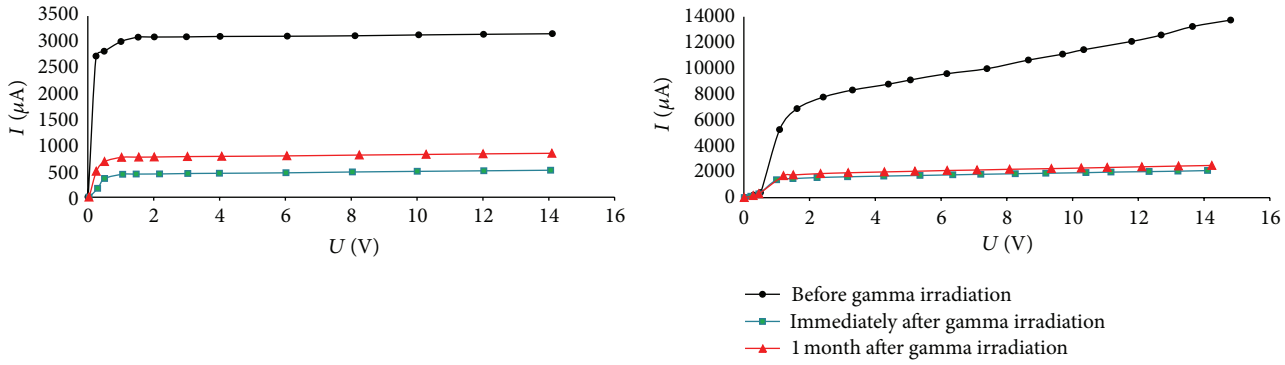

(a) Phototransistor BPW40

(b) Phototransistor LTR4206

FIGURE 1: I-V characteristics of the phototransistors before and after gamma irradiation.

3. Results and Discussion

Gamma rays lightly ionize and penetrate deeply into the matter. For low-energy photons (<0.5 MeV) the photoelectric effect is the dominant interaction. Photon scattering is by definition the scatering of an incoming photon by an electron. This scattering can be coherent (the photon energy is conserved) or incoherent (the photon energy is partially transferred to the electron). In both cases the photon has its trajectory modified and the electron is ejected from the atom. The most common scattering is Compton scattering. Pair production is dominant interaction at high energy and occurs only if the photon energy is greater than 1.022 MeV. In the electric field of a nucleus or an electron, a photon is spontaneously annihilated and converted into an electron-positron pair. The positron and the electron have a total kinetic energy equal to the difference of the initial photon energy and 1.022 MeV. Since the energy of the photon in this experiment is 1.25 MeV, the dominant effect that occurs is pair production. All three types of optoelectronic devices used in this experiment consist of p-n junction. Because of that, after gamma irradiation they all behaved in a similar way (Figures 1 to 3). Gamma radiation decreased their photocurrent and, after that, the process of annealing increased it. Figures 1 to 3 show that gamma radiation caused the greatest damages in phototransistors and the smallest in solar panels.

Vukić [17] shows that the measured values of the forward emitter current gain decreased by 20–40% after the absorption of a total dose of 500 Gy. The gain of the phototransistor is directly proportional to the minority carrier lifetime in the base region, and since this is strongly affected by radiation, these devices are comparatively radiation sensitive. Gain degradation and leakage are the most striking and common effects of radiation on bipolar transistors. One cause of gain degradation is atomic displacement in the bulk of a semiconductor. This bulk damage produces an increase in the number of recombination centers and therefore reduces minority carrier lifetime. The other main cause of gain degradation is ionization in the oxide passivation layer, particularly that part covering the emitter-base junction region [1]. Mechanisms of hole injection into the emitter and surface electron depletion

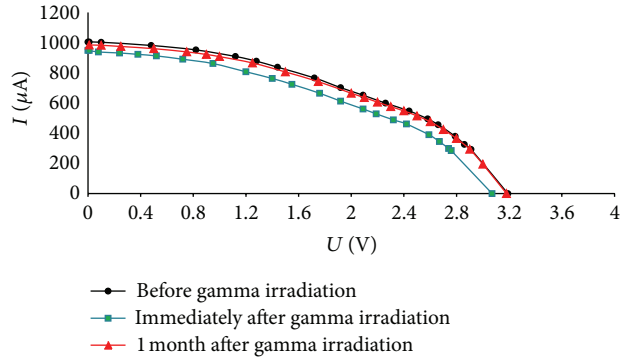

FIGURE 2: I-V characteristics of the solar panels before and after gamma irradiation.

would have significant influence on the serial transistor's forward emitter current gain. Enhanced hole injection into the emitter is manifested through the accumulation of the surface of the base, caused by the negative oxide charge trapped in the oxide over the emitter-base junction. Forward bias of the base junction would cause many holes to be injected into the emitter, thus increasing the base current [17]. The collector current changes significantly with the total dose. Since the base current increases, reduction of a collector current (Figure 1) has a strong impact on the current gain degradation. Vukić and Osmokrović [18] show that two effects cause the decrease of collector current in the heavily doped emitter devices: the recombination in the neutral base region and the reduction of the emitter injection efficiency.

The permanent damage in solar cell materials is caused by the collisions of incident radiation particles with atoms in the crystalline lattice, which are displaced from their positions. These defects degrade the transport properties of the material and particularly the minority carrier lifetime. The interaction between vacancies, self-interstitials, impurities, and dopants in Si leads to the formation of undesirable point defects such as recombination and compensator centers which affect performance of solar cells, especially in space. The introduction of radiation-induced recombination centers reduces the minority carrier lifetime in the base layer of the p-n junction

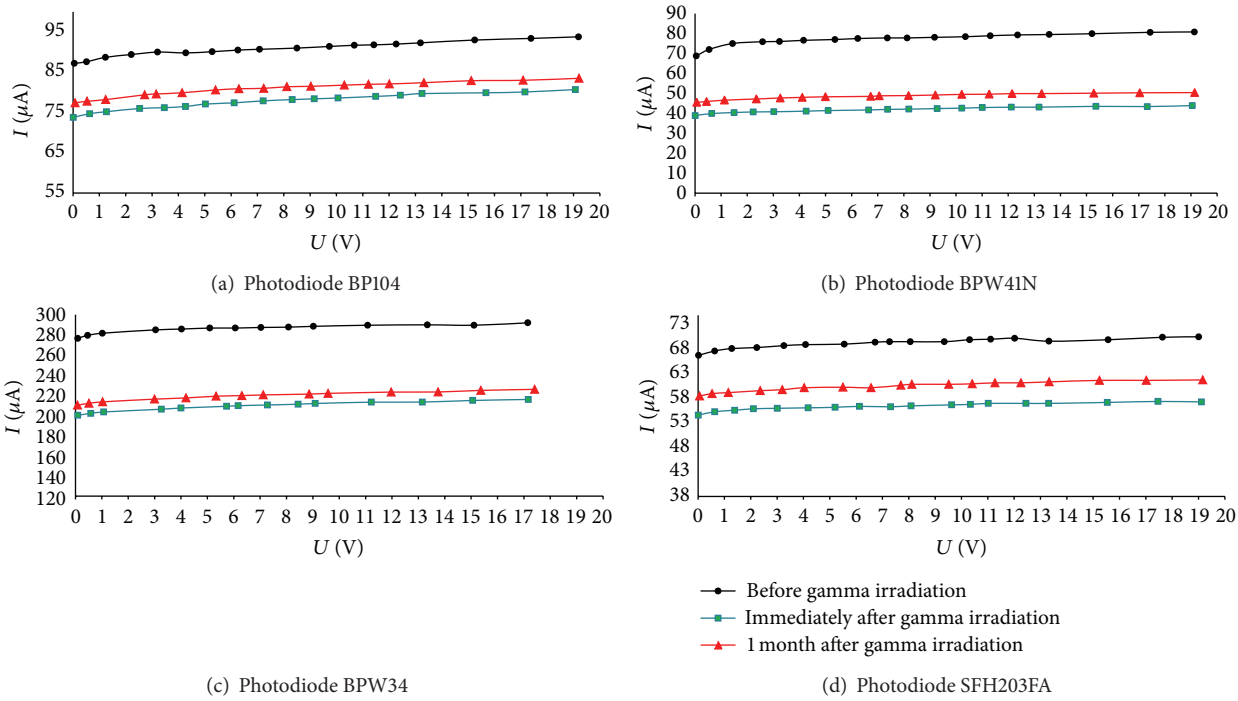

Figure 3: I-V characteristics of the reverse-biased photodiodes before and after gamma irradiation.

increasing series resistance [19]. Radosavljević and Vasić [20] show that the generation of electron-hole pairs due to ionization effects usually results in the generation and increase of noise and the minimum signal that can be detected. All of these effects lead to the decrease of the output current, as can be seen in Figure 2.

PIN photodiodes interpose a lightly doped i-region between the P and N layers. The PIN detector operates with a sufficiently high reverse bias to completely deplete the central region. Consequently, all of the charge is collected by drift. Although light collection efficiency in PIN diodes is less affected by radiation damage, leakage current in the lightly doped intrinsic region is sensitive to displacement damage [21]. Displacement damage within the silicon material results from incident radiation, causing crystal lattice defects. These defects (vacancies, divacancies, interstitials, and defect clusters) generate energy levels in the forbidden bandgap of the material lattice, causing the reduction of the minority carrier lifetime. The final result is the decreasing of the photocurrent (Figure 3).

For this research, the long-term isothermal annealing at room temperature was used. The vacancies and interstitials are quite mobile in silicon at room temperature and hence are referred to as unstable defects. After vacancy introduction by irradiation, vacancies move through the lattice and form more stable defects, such as divacancies and vacancy-impurity complexes. When electrical properties are monitored during this defect rearrangement (or annealing) process, a decrease in the effectiveness of the damage with increasing time is typically observed [22–24]. Moll [25] describes the enhancement of the effective doping concentration for the longer annealing times. This phenomenon Feick [26] observed at room temperature. During the process of annealing defects cluster and some electrical inactive defects become active in a cluster. The best results annealing process has achieved are in the solar panels and the worst are in phototransistors (Figures 1 to 3). The rate of damage recovery from annealing in solar panels is almost the same as the rate of damage creation (Figure 2), so it is possible to use annealing as a part of a hardening method [8, 9]. Probable cause is the construction of solar panels. To obtain the maximum power voltage of panels (4 V), a large number of individual cells are used in series and parallel combinations. The effect of gamma irradiation on the single cell is similar to the effect on photodiode but a combination of a number of cells that affected the panel would be more resistant to the influence of gamma radiation and the process of annealing would be more efficient.

In recent papers the efficiency and properties of solar cells in terms of various conditions have been observed [27–30]. Those researches show that development, innovation, and new devices concepts in silicon solar cells are taking place to bring down the cost of solar technologies and make them even more effective and competitive with conventional optoelectronic devices. Experimental measurements applied in this paper also confirm that solar cells, even in the area of reliability in gamma radiation environments, are superior to conventional optoelectronic devices such as phototransistors and photodiodes.

4. Conclusion

Degradation of the main parameters of the optoelectronic devices and their improvement, as a consequence of

annealing, were observed for all used samples. The results confirm that gamma irradiation leads to degradation of the I-V characteristics and then annealing improves these characteristics. Due to their amplifying action, the phototransistors are the most sensitive to radiation effects. On the other hand, the solar panels are the least sensitive to gamma radiation. Its characteristics, in annealing process, managed to recover to a value near the initial (the one before the irradiation). The combination of cells in the panel construction is a possible cause of this.

Acknowledgment

The Ministry of Education, Science, and Technological Development of Serbia supported this work under Contract 171007.

References

[1] M. B. El Mashade, M. Ashry, M. Sh. Eladl, and M. S. Rageh, "Experimental measurements of some optoelectronic devices before and after gamma irradiation," *Journal of Microwaves and Optoelectronic*, vol. 3, no. 4, pp. 1–12, 2004.

[2] Z. D. Kovalyuk, V. N. Katerynchuk, O. A. Politanska, O. N. Sydor, and V. V. Khomyak, "Effect of gamma radiation on the properties of InSe photodiodes," *Technical Physics Letters*, vol. 31, no. 5, pp. 359–360, 2005.

[3] M. Vujisić, K. Stanković, N. Marjanović, and P. Osmokrović, "Simulated effects of proton and ion beam irradiation on titanium dioxide memristors," *IEEE Transactions on Nuclear Science*, vol. 57, no. 4, pp. 1798–1804, 2010.

[4] M. Vujisić, K. Stanković, E. Dolićanin, and P. Osmokrović, "Radiation hardness of COTS EPROMs and EEPROMs," *Radiation Effects and Defects in Solids*, vol. 165, no. 5, pp. 362–3369, 2010.

[5] D. R. Alexander, "Transient ionizing radiation effects in devices and circuits," *IEEE Transactions on Nuclear Science*, vol. 50, no. 3, pp. 565–582, 2003.

[6] B. D. Iričanin and D. M. Gvozdić, "The analytic approach in the modelling of one-dimensional electron concentration distribution in some two-valley semiconductor electron devices," *Journal of Physics A*, vol. 31, no. 13, pp. 2997–3017, 1998.

[7] S. J. Stanković, B. D. Iričanin, D. Nikolić et al., "MSV signal processing system for neutron-gamma discrimination in a mixed field," *Nuclear Technology and Radiation Protection*, vol. 27, no. 2, pp. 165–170, 2012.

[8] A. Holmes-Siedle and L. Adams, *Handbook of Radiation Effects*, Oxford Science, 1993.

[9] G. C. Messenger and M. S. Ash, *The Effects of Radiation on Electronic Systems*, Van Nostrand Reinhold, New York, NY, USA, 2nd edition, 1991.

[10] G. C. Messenger, "Summary review of displacement damage from high energy radiation in semiconductors and semiconductor devices," in *Proceedings of the 1st European Conference on Radiation and Its Effects on Devices and Systems (RADECS '91)*, pp. 35–40, September 1991.

[11] J. R. Hauser and S. E. Kerns, "Circuit related issues due to radiation in hostile environments," *Journal of Electronic Materials*, vol. 19, no. 7, pp. 671–688, 1990.

[12] K. D. Stanković, "Influence of the plain-parallel electrode surface dimensions on the type a measurement uncertainty of gm counter," *Nuclear Technology and Radiation Protection*, vol. 26, no. 1, pp. 39–44, 2011.

[13] Ć. Dolićanin, K. Stanković, D. Dolićanin, and B. Lončar, "Statistical treatment of nuclear counting results," *Nuclear Technology & Radiation Protection*, vol. 26, no. 2, pp. 164–170, 2011.

[14] K. Stanković, M. Vujisić, D. Kovačević, and P. Osmokrović, "Statistical analysis of the characteristics of some basic mass-produced passive electrical circuits used in measurements," *Measurement*, vol. 44, no. 9, pp. 1713–1722, 2011.

[15] M. Vujisić, K. Stanković, and P. Osmokrović, "A statistical analysis of measurement results obtained from nonlinear physical laws," *Applied Mathematical Modeling*, vol. 35, no. 7, pp. 3128–3135, 2011.

[16] K. Stankovic, M. Vujisic, and Lj. Delic, "Influence of tube volume on measurement uncertainty of GM counters," *Nuclear Technology & Radiation Protecion*, vol. 25, no. 1, pp. 46–50, 2010.

[17] V. Vukić, "Minimum dropout voltage on a serial PNP transistor of a moderately loaded voltage regulator in a gamma radiation field," *Nuclear Technology & Radiation Protection*, vol. 27, no. 4, pp. 333–340, 2012.

[18] V. Vukić and P. Osmokrović, "Impact of forward emitter current gain and geometry of PNP power transistors on radiation tolerance of voltage regulators," *Nuclear Technology & Radiation Protection*, vol. 27, no. 2, pp. 152–164, 2012.

[19] M. Zdravković, A. Vasić, R. Radosavljević, M. Vujisić, and P. Osmokrović, "Influence of radiation on the properties of solar cells," *Nuclear Technology & Radiation Protection*, vol. 26, no. 2, pp. 158–163, 2011.

[20] R. Radosavljević and A. Vasić, "Effects of radiation on solar cells as photovoltaic generators," *Nuclear Technology & Radiation Protection*, vol. 27, no. 1, pp. 28–32, 2012.

[21] H. Johnston, "Radiation damage of electronic and optoelectronic devices in space," in *Proceedings of the 4th International Workshop on Radiation Effects on Semiconductor Devices for Space Application*, Tsukuba, Japan, October, 2000.

[22] J. R. Srour, C. J. Marshall, and P. W. Marshall, "Review of displacement damage effects in silicon devices," *IEEE Transactions on Nuclear Science*, vol. 50, no. 3, pp. 653–670, 2003.

[23] D. Nikolić, A. Vasić, I. Fetahović, K. Stanković, and P. Osmokrović, "Photodiode behavior in radiation environment," *Scientific Publications of the State University of Novi Pazar Series A*, vol. 3, no. 1, pp. 27–34.

[24] M. Vujisić, N. Marjanović, I. Fetahović, K. Stanković, and P. Osmokrović, "Influence of radiation on titanium dioxide mermistors," *Scientific Publications of the State University of Novi Pazar Series A*, vol. 4, no. 1, pp. 75–82, 2012.

[25] M. Moll, *Radiation damage in silicon particle detectors—microscopic defect and macroscopic properties [Ph.D. thesis]*, University of Hamburg, Hamburg, Germany, DESY-THESIS-1999-040, December 1999.

[26] H. Feick, *Radiation tolerance of silicon particle detectors for high-energy physics [Ph.D. thesis]*, University of Hamburg, Hamburg, Germany, DESY F35D-97-08, August 1997.

[27] C. M. Lee, S. P. Chang, S. J. Chang, and C. I. Wu, "High-efficiency Si solar cell fabricated by ion implantation and inline backside rounding process," *International Journal of Photoenergy*, vol. 2012, Article ID 670981, 7 pages, 2012.

[28] C. H. Tai, C. H. Lin, C. M. Wang, and C. C. Lin, "Three-terminal amorphous silicon solar cells," *International Journal of Photoenergy*, vol. 2011, Article ID 813093, 5 pages, 2011.

[29] T. T. Chow, G. N. Tiwari, and C. Menezo, "Hybrid solar: a review on photovoltaic and thermal power integration," *International Journal of Photoenergy*, vol. 2012, Article ID 307287, 17 pages, 2012.

[30] M. Herman, M. Jankovec, and M. Topič, "Optimal I-V curve scan time of solar cells and modules in light of irradiance level," *International Journal of Photoenergy*, vol. 2012, Article ID 151452, 11 pages, 2012.